DOKUZ EYLÜL UNIVERSITY

GRADUATE SCHOOL OF NATURAL AND APPLIED SCIENCES

ESTIMATION OF LOOSENING RATES OF FASTENERS UNDER CERTAIN TRANSVERSE VIBRATION CONDITIONS BY USING COMPUTATIONAL INTELLIGENCE TECHNIQUES

by

Aysel BIYIK

June, 2017

İZMİR

ESTIMATION OF LOOSENING RATES OF FASTENERS UNDER CERTAIN TRANSVERSE VIBRATION CONDITIONS BY USING COMPUTATIONAL INTELLIGENCE TECHNIQUES

A Thesis Submitted to the

Graduate School Of Natural And Applied Sciences of Dokuz Eylül University

In Partial Fulfilment of the Requirements for the Degree of Master of Science in Industrial Engineering, Industrial Engineering Program

by

Aysel BIYIK

June, 2017

İZMİR

THESIS EXAMINATION RESULT FORM

We have read the thesis entitled **"ESTIMATION OF LOOSENING RATES OF FASTENERS UNDER CERTAIN TRANSVERSE VIBRATION CONDITIONS BY USING COMPUTATIONAL INTELLIGENCE TECHNIQUES"** completed by **AYSEL BIYIK** under supervision of **PROF. DR. ADİL BAYKASOĞLU** and we certify that in our opinion it is fully adequate, in scope and in quality, as a thesis for the degree of Master of Science.

Prof. Dr. Adil BAYKASOĞLU

Supervisor

Prof.Dr. M.Fatih Taşgetiren

(Jury Member)

Prof. Dr. M. Evren TOYGAR

(Jury Member)

Prof. Dr. Emine İlknur CÖCEN

Director

Graduate School of Natural and Applied Sciences

ACKNOWLEDGEMENTS

First, I would like to express my gratitude and thanks to my graduate thesis advisor, Prof. Dr. Adil BAYKASOĞLU, whose support; advice and encouragement that helped me overcome challenges during my studies.

I am also grateful to my colleague Emre ERBİL and would like to thank him for being helpful and understanding towards me throughout my studies.

Finally, I would like to thank my beloved family; my mother Fatma BIYIK, my father Zekeriya BIYIK, my sister Özlem BIYIK, Yasemin BIYIK and my brother Tuncay BIYIK for their continuous support, patience and encouragement through all my life.

Aysel BIYIK

ESTIMATION OF LOOSENING RATES OF FASTENERS UNDER CERTAIN TRANSVERSE VIBRATION CONDITIONS BY USING COMPUTATIONAL INTELLIGENCE TECHNIQUES

ABSTRACT

Fasteners have many advantages such as providing high clamping load, reusability, ease of manufacturability and being cheap, but loosening under vibration is an important problem. Several methods have been developed to ensure safety against the risk of loosening of fasteners. These methods are not preferred in most cases as generally cause an increase in weight and cost of the final product, also due to the limits of their use. As an efficient solution to these problems, special bolt under-head profiles are arisen. However, it is also known that none of the under-head profiles are verified by any kind of simulation and optimization methods and most of them are not producible by cold forging method. It is also seen in feasibility studies and literature survey that this situation cannot give efficient results by means of performance/cost ratio. In this study, loosening mechanism is modeled by using numerical simulation methods, experimental setup is prepared within parameters which are observed in the Junker vibration tests that they have effects on the process, then numerical simulations are run. Results are obtained for ten different *objective criteria* by using simulation model. Second model representing the simulation model is constructed by using *genetic programming* method. So-called method has not been used before, to estimate the loosening behavior of fasteners under dynamic and transversely vibrational loading conditions. Clamp loss is the criterion that describes *loosening rate* best within the ten objective criteria which are used in the estimation model. *Genetic programming*-based *symbolic regression* method is used for estimating the *clamp loss*.

Keywords: Self-loosening in fasteners, vibration resistance, bolt under-head profiles, genetic programming

YATAY TİTREŞİM KOŞULLARI ALTINDA BAĞLANTI ELEMANLARININ ÇÖZÜNME ORANLARININ BİLİŞSEL ZEKÂ YÖNTEMLERİ KULLANILARAK TAHMİN EDİLMESİ

ÖZ

Bağlantı elemanları, yüksek kilitleme kuvveti sağlamaları, tekrarlı kullanılabilmeleri, kolay üretilebilmeleri ve ucuz olmaları gibi avantajlara sahiptir, ancak titreşim altında gevşemeleri önemli bir sorundur. Cıvataların gevşeme riskine karşı emniyet sağlamak için çeşitli yöntemler geliştirilmiştir. Bu yöntemler genellikle son üründe ağırlık ve maliyet artışına neden olmakta, ayrıca kullanım kısıtlarından dolayı pek çok durumda tercih edilmemektedir. Bu sorunlara bir çözüm olarak titreşim direnci sağlayan özel cıvata kafa altı profilleri verimli çözümler olarak ortaya çıkmaktadır. Bununla birlikte, piyasadaki kafa altı profillerinin herhangi bir simülasyon ve optimizasyon tekniği ile tasarlanıp doğrulanmadığı ve pek çoğunun da soğuk dövme yöntemi ile üretilebilir olmadığı bilinmektedir. Bu durumun fayda maliyet açısından verimli sonuçlar sağlamadığı fizibilite ve literatür araştırması çalışmalarında da görülmüştür. Bu çalışmada gevşeme mekanizması sayısal simülasyon yöntemi ile modellenerek, Junker titreşim testi ile sürece etkisi olduğu görülen parametreler dahilinde deney seti hazırlanmış, sonrasında simülasyonlar koşturulmuştur. Simülasyon modeli kullanılarak on farklı *amaç kriteri* için sonuçlar alınmıştır. Simülasyon modelini temsil eden ikinci bir model *genetik programlama* yöntemi kullanılarak kurulmuştur. Söz konusu yöntem daha önce dinamik ve yatay titreşimli yüklemeler altında çalışan bağlantı elemanlarının gevşeme davranışını tahmin etmek için kullanılmamıştır. Tahmin modelinde kullanılan on farklı *amaç kriterinden* gevşeme oranını en iyi ifade eden kriter *kilitleme yükü kaybı* olmuştur. *Gevşeme hızını* tahmin etmede kullanılan *kilitleme yükü kaybı* için *genetik programla* tabanlı *sembolik regresyon* yöntemi kullanılmıştır.

Anahtar kelimeler: Bağlantı elemanlarında gevşeme, titreşim direnci, cıvata kafa altı formu, genetik programlama

CONTENTS

Page

THESIS EXAMINATION RESULT FORM ii

ACKNOWLEDGEMENTS iii

ABSTRACT iv

ÖZ v

LIST OF FIGURES viii

LIST OF TABLES xiii

CHAPTER ONE – INTRODUCTION 1

1.1 Literature Review 2

1.2 Aim of This Study 12

CHAPTER TWO – VIBRATION AND SELF-LOOSENING OF FASTENERS 14

2.1 Definition of Screw Loosening 15

2.2 Vibration Loosening of Nut And Bolt 20

2.3 Prevention of Loosening by Means of Design 24

2.4 Conclusion 34

CHAPTER THREE – FINITE ELEMENT ANALYSIS OF FASTENING AND JOINING 35

3.1 Analysis Method 35

3.2 Analysis Results 40

3.3 Conclusion 49

CHAPTER FOUR – AN OVERVIEW OF GENETIC PROGRAMMING 50

4.1 Genetic Algorithm 50
4.2 Genetic Programming 52
4.3 Genetic Programming-Based Symbolic Regression 53
4.3.1 Symbolic Regression 54
4.3.2 Data Analysis in Symbolic Regression 55

CHAPTER FIVE – CASE STUDIES 59

5.1 Experimental Study 59
5.1.1 Determination of Friction Coefficient 60
5.1.2 Transverse Vibration Tests 66
5.1.3 Penetration Depth 69
5.2 Data Set & CAD Model 71
5.3 Simulation Model 74
5.4 Genetic Programming Model 79

CHAPTER SIX – CONCLUSION 96

REFERENCES 98

APPENDICES 107

LIST OF FIGURES

Page

Figure 1.1 Comparison of loosening for Metric High Tension Steel Bolt (M10) with different nuts 2

Figure 1.2 Thread slip regions under head surface (a) and between threads (b). Slip-stick conditions at certain position of transverse vibration (top right corner of b-1, b2 and b3) 3

Figure 1.3 Vibration test machine (left) and general features of hysteresis curve (right)..... 4

Figure 1.4 Contact normal stresses between contact pairs 4

Figure 2.1 Endurance limits of a bolt 14

Figure 2.2 Vibration in fastener systems (*'k'* is the stiffness, *'x'* is the displacement) 15

Figure 2.3 Stiffness of a bolt (spring model) 15

Figure 2.4 Stress distribution inside the joint members and the fastener 17

Figure 2.5 Preloaded (a), vibrated (b 18

Figure 2.6 Preloaded (a), loose (b) bolt 18

Figure 2.7 Micro-slip mechanism between bolt and nut thread surfaces 19

Figure 2.8 Self-loosening mechanism..... 19

Figure 2.9 Preload versus average vibration life data for different, initial preload (a), thread pitch (b) and prevailing torque level (c) 20

Figure 2.10 Typical Junker Test Machine 21

Figure 2.11 Bolt-nut orientation during transverse vibration conditions, slip-stick (a, d), stick (b), complete slip (c) 22

Figure 2.12 Bolt-Nut couple design elements..... 23

Figure 2.13 Simplified thread profile..... 24

Figure 2.14 Junker's test results for 12.5 kN of clamping force [eccentric nut (a), hexagon nut (b), spring washer (c), toothed washer (d), plate spring washer (e), hexagon nut with flange (f), double nut (g), nylon insert nut (h), Nord-lock® washer (i), slotted nut (j), steel plate insert nut (k), anaerobic adhesive (l)] 25

Figure 2.15 The effect of clamp length 26
Figure 2.16 The effect of bearing friction coefficient on loosening-rate 27
Figure 2.17 Effect of preload on loosening-rate 27
Figure 2.18 Lead or helix angle of a thread 28
Figure 2.19 Effect of thread friction coefficient on loosening-rate 28
Figure 2.20 Effect of total friction (a) and clamp length (b) on loosening-rate.. 29
Figure 2.21 21 Hard-lock eccentric nut (Patent # US6609867B2) 29
Figure 2.22 Aerotight® (a), Turret® (b), axial locking fastener (c) 30
Figure 2.23 Self-locking split-nut designs; split nut (a), Unalock® (b), DIN 980 (c), beveled nut (d) 30
Figure 2.24 Spiralock®, ShakeproofTM, Dynathread® and SinulocTM locking fasteners 31
Figure 2.25 Mechanical locking solutions 31
Figure 2.26 Nordlock® (a) and Heicolock® (b) anti-loosening washers 32
Figure 2.27 Common washer types; first line plain and spring washers, second line toothed washers, third line serrated, beveled and anti-loosening washer (Starlock®) 32
Figure 2.28 Patented serrations; EP0187244A1 - Vibration resistant fastener for soft joint surfaces (a), US3605845 A - GB1326380 A - self-locking fastener (b), US752628 - nut lock (c), US5302066A - locking fastener (d), US2959204 A - GB866556A - vibration resistant fastener for soft joint surfaces (e), US2003077143A1 - washer and threaded fastener assembly incorporating same (f) 33
Figure 2.29 Chemical solutions for vibrational conditions 33
Figure 3.1 Junker test mechanism 35
Figure 3.2 Bolt-Nut assembly details 36
Figure 3.3 Velocity parameters 37
Figure 3.4 Vibration progress: Unloaded (a), Clamped [Preload Stage] (b), Transversely displaced [- 45 mm (c), + 45 mm (d), +45 mm (e), -45 mm (f)] (Labels are referenced to Figure 3.3) 37
Figure 3.5 Displacement verification planes 38

Figure 3.6 Finite elements mesh details. Initial step (a, c and e-top), re-meshed (b, d and e-bottom). (e) is the *'Washer'* 39
Figure 3.7 Material data 40
Figure 3.8 Vibration mechanism 41
Figure 3.9 Change in transverse shear force against transverse displacement 41
Figure 3.10 Clamp force and the bending moment – transverse displacement relation 42
Figure 3.11 Pressure (contact normal stress) distribution on washer part. (Labels are referenced to Figure 3.3) 43
Figure 3.12 Relative displacements in joint members 43
Figure 3.13 Round-ribbed pattern simulation results 44
Figure 3.14 Serrated bolt under-head form clamp-loss analysis 44
Figure 3.15 Flake-type serrations under the head of the bolt 45
Figure 3.16 Circularly placed inclined small protrusions under the head of the bolt 45
Figure 3.17 Circularly placed small protrusions and pits under the head of the bolt 46
Figure 3.18 EP0187244A1 patented form results 46
Figure 3.19 US 3605845 A and GB1326380A patented form 47
Figure 3.20 US5302066A patented form 47
Figure 3.21 US2003077143A1 and US752628 patented forms 48
Figure 3.22 [US2003077143A1] (left) and [US 2959204 A - GB866556A] (right) patented forms 48
Figure 4.1 Schematic representation of EA-based symbolic regression as applied in Eureqa® software package. As the search progress, Eureqa® attempts to find a simpler solution with better fit (per the selected error metric) and discard more complicated and less accurate 57
Figure 5.1 Specimen technical drawing 60
Figure 5.2 Torque and friction coefficient formulas 61
Figure 5.3 Schatz friction coefficient testing machine 62
Figure 5.4 Test specimens; flat plain washers are used in experiments 63

Figure 5.5 Test platform; bolt under-head (a), nut fixture-fixed (no rotation allowed for nut) (b, c) 63
Figure 5.6 Atlas CopCo. test platform (a), electric torque wrench controller (b), test specimen (c), clamp condition (d), nut-driven torque application (e) 65
Figure 5.7 Surface conditions after experiments; flat under-head (AtlasCopCo) (a), nut seating surface (AtlasCopCo) (b), washer (c), serrated bolt under-head before test (d), serrated bolt under-head after test (e) 65
Figure 5.8 Bi-axial vibration testing machine 66
Figure 5.9 Load-cell and vibration mechanism 67
Figure 5.10 Clamp and transverse loading mechanism 67
Figure 5.11 Vibration test results (flat under-head form) 68
Figure 5.12 Vibration results (serrated under-head form) 68
Figure 5.13 Vibration results (mean values of flat vs serrated) 69
Figure 5.14 Rib depth under the head of the bolt, after friction and vibration tests; depth of ribs (A), rip radius (B), pitch of ribs (C). All measurements are taken by using Mahr Perthometer device 69
Figure 5.15 Rib conditions; before (Schatz) friction test (a-c), after Schatz test (b-d), before vibration test (e-g), after test (f-h) 70
Figure 5.16 Indention depth after friction tests (Atlas CopCo.) measured by Mitutoyo SJ-401 surface roughness measurement device. Flat washer coupled with flat under-head bolt (a), serrated under-head bolt (b) and measurement results (d) 70
Figure 5.17 Parametric CAD model 71
Figure 5.18 Overlapping issue for large-number-of-ribs case 72
Figure 5.19 CATIA CAD design stages: solid body (a), surface model (b), STL model (c), STL tetrahedral mesh that is used directly as a finite element initial mesh (d) 74
Figure 5.20 Contact Friction Stress: preload (a), displaced in the +x direction (b), overlapped (c) 75
Figure 5.21 Penetration Index (δ) 76

Figure 5.22 Penetration depth (z distance) and contact pressure distribution for flat and serrated under-head forms.flat - δx = 0 (a-e), flat - δx = 5 mm (b-f), serrated - δx = 0 mm (c-g), serrated - δx = 5 mm (d-h)..... 77
Figure 5.23 Clamp load-case for serrated under-head form 77
Figure 5.24 Transverse displacement of serrated under-head form (vibration load-case) δx = 0 (a), δx = + 5 mm (b), δx = - 5 mm (c), δx = 0 (d)..... 78
Figure 5.25 Flat and serrated comparison..... 78
Figure 5.26 Distribution of the input data (a) (A, B, C and D) and output data (b, c, d, e, f, g, h, I ,j and k) (Fshear at bolt head (kN) [FSBH], Fshear at nut surface (kN) [FSNS], Fshear (min) (kN) [FSMI], Fshear (max) (kN) [FSMA], clamp loss (kN) [CL], relative slip distance to the left-hand side (mm) [RSDLH], relative slip distance to the right-hand side (mm) [RSDRH], relative maximum slip distance (position at the end of the cycle) (mm) [RMAS], relative maximum slip distance (magnitude) (mm) [RMAS_M], Z displacement up to preload or penetration index (larger value penetrates most) (mm) [DZ_P])..... 83
Figure 5.27 Improved and detailed estimation models for CL without outliers. 91
Figure 5.28 Simulation results vs estimation results 93
Figure 5.29 Eureqa®: Accuracy-complexity for predicting modelling of Clamp Loss 95

LIST OF TABLES

Page

Table 1.1	Objective criteria	12
Table 5.1	Friction test parameters	64
Table 5.2	Schatz friction test results	64
Table 5.3	Friction test results (Atlas CopCo.)	65
Table 5.4	Vibration test parameters	66
Table 5.5	Design variables	72
Table 5.6	Parameters and their limits	73
Table 5.7	Full factorial (filtered) experimental design table 4^4-152	73
Table 5.8	Input and output criteria	79
Table 5.9	Eureqa® Mathematical building block	82
Table 5.10	Estimation models for 10 objective criteria	88
Table 5.11	Filtered data set with Clamp Loss results (2 outliers are omitted)	89
Table 5.12	Improved estimation models with 2 outliers omitted	90
Table 5.13	Sensitivity analysis report	93
Table 5.14	Simulation results and the estimated model results	94

CHAPTER ONE
INTRODUCTION

In the industry, engineers have been overcoming assembly problems by using various types of fasteners for years. The main purpose of using a fastener is to combine two or more components together by producing clamping load by means of applied torque. There are many environmental effects decreasing clamping load such as vibration, temperature, humidity, lubrication, and so on. There are many types of fasteners in the market for several purposes. General purpose of use relies on stability under the most problematic effects, the vibration and temperature. The loss of clamping load should cause or trigger crucial problems that some of them might cause injuries or deaths in reality. Engineers have to prevent harmful effects of vibration by making some changes in the assembly design. Washers, special bolts, nuts, studs and rivets should be useful against vibration. There are so many types of special bolts having special features in distinct part of their bodies. They can withstand excessive lateral vibrations with their specialized thread, head or under-head form. In this thesis, most common under-head form is chosen for analysis because of its several advantages. A modification in the under-head form does not cause an increase in weight and it does not increase the cost, too much. This form is geometrically modeled in a parametric structure. Parameters are justified in the range of adequate values for finite elements analyses. Ten outputs are gathered from FEA simulations that represents the loosening rate of the bolt-nut assembly under controlled transverse vibrational environment. These outputs are used in genetic programming study to find a relation between the most effective parameters and the outputs aiming to fit objective function, loosening rate. Genetic programming study is carried out to obtain a second model which provides a robust searching opportunity that helps gaining more time by speeding up the analyses without the need of numerical simulations. Genetic programming method has not been used before to predict the loosening rate, in this context, this thesis is a unique study in the field.

1.1 Literature Review

In this section, an overview of literature studies related to self-loosening of fasteners under transverse vibrations and genetic programming methods. Scientific studies related to the subject of this thesis are summarized to guide the reader in the following sections.

Firstly, self-loosening of fasteners under transverse vibrations is explained. Reiff (2005) introduced basic equations to calculate tightening torque and prevailing torque specifications for bolted joints.

Bhattacharya, Sen, & Das (2010) investigated the anti-loosening ability of various locking screw fasteners (Figure 1.1).

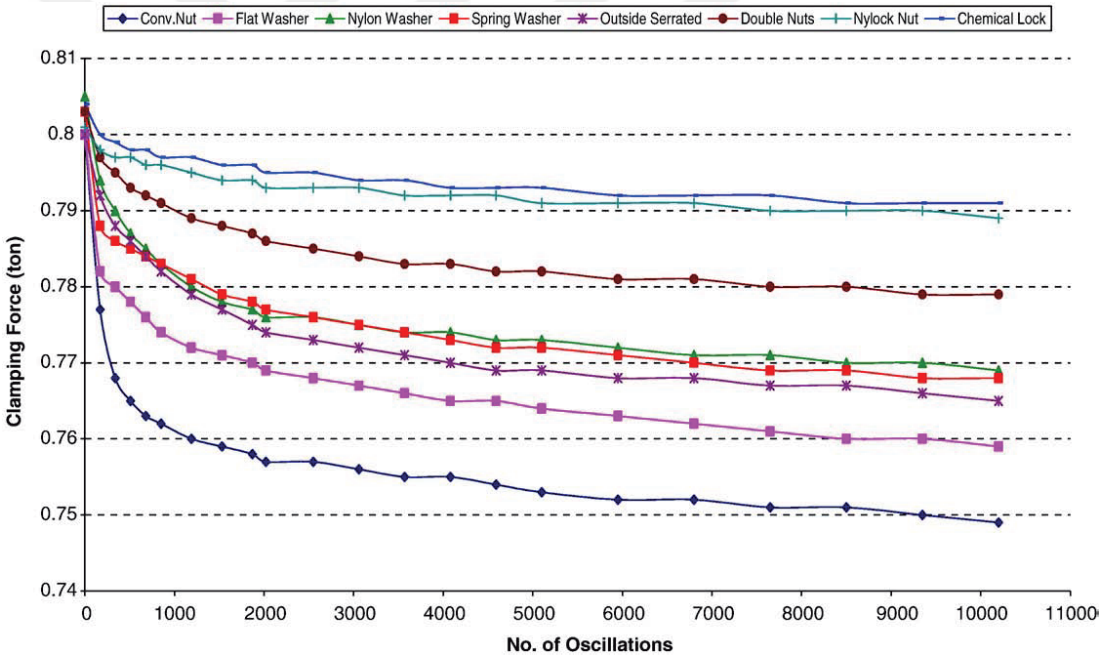


Figure 1.1 Comparison of loosening for Metric High Tension Steel Bolt (M10) with different nuts (Bhattacharya, Sen, & Das, 2010).

They found that chemical locking decreases loosening rate more than nylock and aerotight, respectively. If properly applied, double nut tightening method decreases self-loosening behavior close to aerotight and cleveloc. They also observed that above a specific threshold value of preload, loosening rate decreases dramatically. Threshold of preload value is smaller in British Standard Whitworth (BSW) threads than metric

threads due to the smaller flank angle in BSW. They found that spring washers decrease loosening rate, but flat and nylon washers do not prevent self-loosening indeed. Serrated washers provide considerable loosening resistance, but they got damage after single use.

Self-loosening is a crucial phenomenon that triggers several damage mechanisms. The evaluation of loosening mechanism can be influenced by transverse displacement, clamp length, transverse shear loads, preload, coefficient of friction, flank and lead angle, stiffness of the clamped materials, geometrical properties of seating surface at both bolt and nut interfaces, thermal loads, and even vibration frequency due to the inertia effects. Guggolz, Manoharan, Friedrich (2015) investigated these effects analytically by using the numerical formulations in literature. There are several methods describing critical displacement that initiates self-loosening event. They stated a finite element model in their study and developed an equation which increases the robustness of calculations.

Hess & Pai (2002) studied on a three-dimensional Finite Element (FE) model to investigate sub events of self-loosening. They used a test set-up as given in Figure 1.3 in their study. They divide loosening process into four stages; localized head slip with localized thread slip, localized head slip with complete thread slip, complete head slip with localized thread slip and complete head slip with complete thread slip (Figure 1.2).

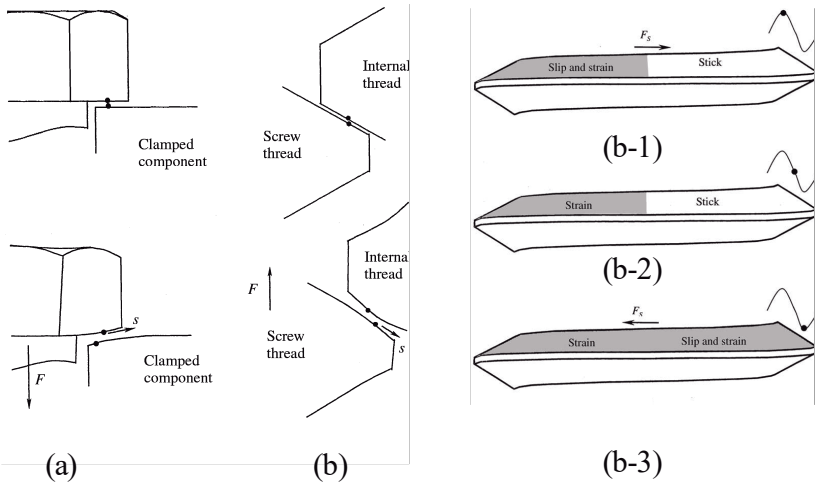


Figure 1.2 Thread slip regions under head surface (a) and between threads (b). Slip-stick conditions at certain position of transverse vibration (top-right corner of b-1, b2 and b3) (Pai & Hess, 2002a).

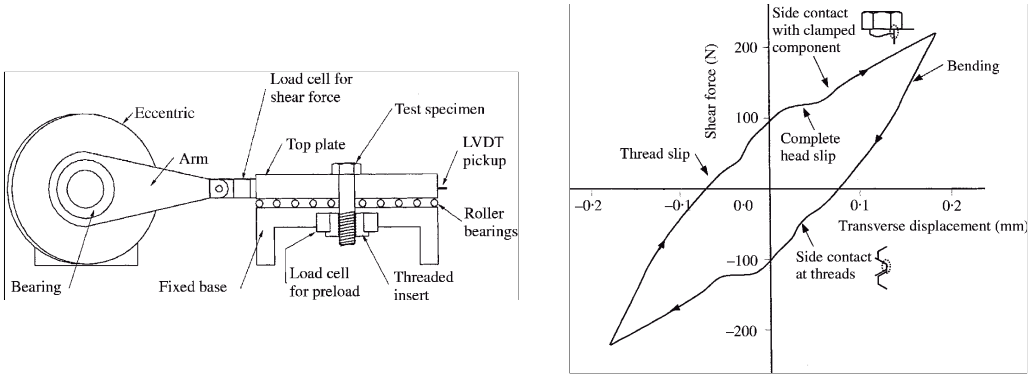


Figure 1.3 Vibration test machine (left) and general features of hysteresis curve (right) (Pai & Hess, 2002a).

Another study of Pai & Hess (2002a, 2002b) reveals that, loosening rate increases dramatically as soon as complete head slip occurs, however, local slip occurs at lower transverse loads and leads up to complete slip insidiously. They implemented more parameters to their model regarding with their further studies.

Dinger (2015); Dinger & Friedrich (2011) investigated the slip and stick condition deeply by focusing on friction condition under the head surface or bearing surface and thread seating surface. They mapped friction ratios on interference layers of bearing and thread contact surfaces and they presented clearly visible plots of complete slip,

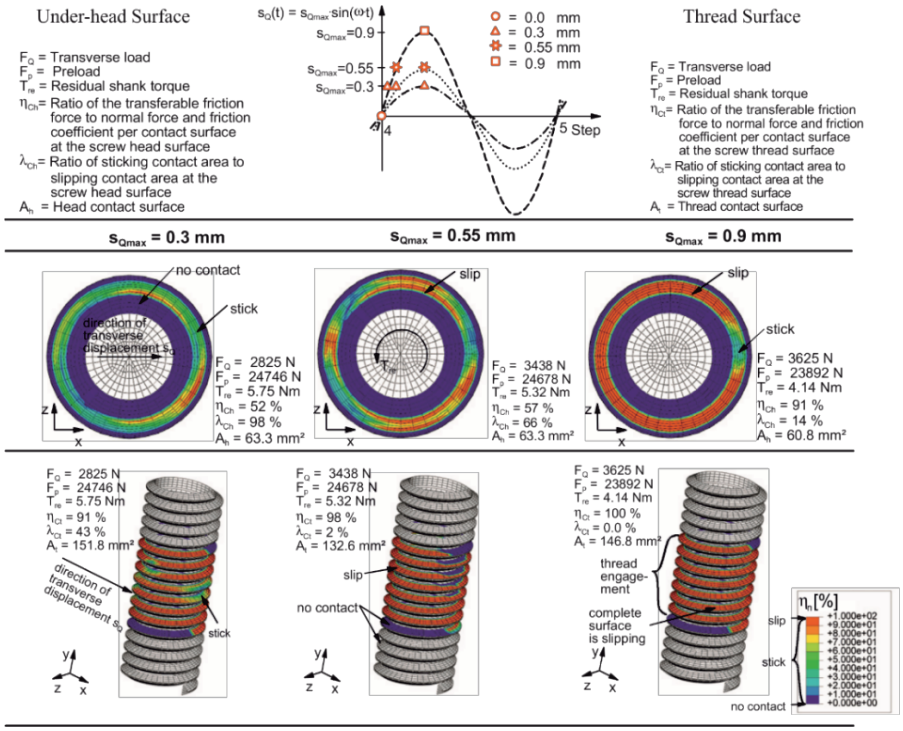


Figure 1.4 Contact normal stresses between contact pairs (Dinger & Friedrich, 2011).

stick and partial slip regions (Figure 1.4).

Fernando, Hons, & Masi (ud) studied self-loosening mechanisms theoretically and listed the effects of several parameters such as vibration excitation frequency, thread and bearing coefficients, thread pitch and flank angle. They tested the most common anti-loosening items like serrated flanged nuts, nyloc, serrated washers, and etc. Kumar (2013) suggested general methods to prevent self-loosening effect similar to the study presented by Fernando, Hons, & Masi (ud).

Fujioka (2008) figured out the loosening behavior of a washer along an arc. He clearly expressed the movement of washer under vibration effect and he plotted the distribution of friction force under the head and between threads. He investigated the effect of relative movement of washer-seating surface under the bolt head. It is obvious to see that washer moves relative to the bolt head which expedites self-loosening effect.

Ganeshmurthy & Nassar (2014); Housari & Nassar (2007); Nassar & Housari (2006); Nassar & Yang (2009) presented several articles in literature about self-loosening of bolts. They expressed valuable equations which describe self-loosening threshold and partial and local slip-stick conditions.

Ganeshmurthy & Nassar (2014) investigated the effect of tightening process in non-parallel contact condition. They also investigated the bolt hole clearance effect in this study and they found that an increase in the ratio of bolt hole by bolt shank diameter results in the loos of clamp force at a certain torque value. Three of torque application methods that Torque-Only, Torque-Turn and Torque-Angle are investigated against torque-clamp force clarity. They found that Torque-Only strategy is the most reliable strategy on both parallel and non-parallel contact surfaces up to 4° wedge angle.

Gong, Liu, & Ding (2016) studied on the precise tightening of bolts by using the calculation procedure of the effective contact radius. They expressed a calculation method integrated with Finite Element Analysis (FEA) which is more precise for lower ratio of the maximum to minimum bearing clearance.

Hattori, Yamashita, Mizuno, & Naruse (2010) investigated the loosening and sliding behavior under transverse loading conditions. They proposed a model that represents the calculation of critical relative slippage for bolt loosening under transverse loads by implementing newly introduced reaction moments based on the bolt-nut joint model.

Hess, Keifer, & Moody (2014) studied the effects of washers on loosening event of aviation threaded fasteners. They tested five combinations of the joint as they are lock washer only, lock washer on plain washer, plain washer only, and lock washer on hardened plain washer configurations. They set up the Junker-type test machine at excessive vertical displacement to observe loosening rate at a certain number of cycle obviously. Test were performed at 15 Hz with an 3mm of vertical displacement for 2400 cycles at 4000 and 2000 lbs of preload. They found that internal teeth lock washer on plain washer provides the best locking performance all over the tests. Besides, only lock washer and lock washer on hardened plain washer have the worst locking performance on tests. This study shows that the hardness of the plain washer effects the loosening performance and that can be explained with the geometrical locking effect due to the penetration of textures under the washer or bolt.

Housari & Nassar (2007) investigated the effect of thread and bearing friction coefficients on self-loosening effect. They proposed a detailed mathematical model to predict loosening rate. The model is verified experimentally in their studies, however some important points are misspelled or generalized in mathematical formulations, so researcher cannot verify calculations and simulate loosening rate as described in the article. Similarly, Nassar & Housari (2006); Nassar & Yang (2009) studied thread pitch and initial tension effects on self-loosening event, then described a mathematical model for vibration-induced loosening of fasteners. Like their previous studies, it is not clear to build a standalone calculator by using their articles. Yokoyama, Izumi, & Sakai (2009) introduced a detailed mathematical model to express displacement relations on the contact surfaces at thread and bearing contact area.

Izumi, Yokoyama, Iwasaki, & Sakai (2005) composed a FE model to simulate initiation and evolution mechanism of bolt/nut loosening event. They expressed the nonlinearity of the relation between preload and tightening torque describing the

nonuniform pressure distribution on the contact interfaces. They found different from the conventional theory that loosening due to transverse load is initiated when complete thread slip is achieved prior to bolt-head slip.

Another study of Izumi, Yokoyama, Kimura, & Sakai (2009) compares the effect of spring washer and double-nut tightening method on the self-loosening event. They clarified that if double-nut tightening method is properly applied, loosening rate decreases drastically due to the control of locking state. They stated the locking state as the reverse tightening of the bottom nut. They also found that loosening resistance increase by increasing locking force between the two of nuts. The locked double-nut remain stuck even complete slip occurs under the bearing surface. They used split-washer as a spring washer and they found that the splitting face leads to loosening before complete bearing slip. Spring washer loosens faster than bare joint as the applied transverse force reaches a critical value, hence they found spring washer to be ineffective against self-loosening, in their study.

Jeong, Lee, Park, & Kim (2015) presents the most valuable study about the anti-releasing performance of a serrated bolt. They focused on the elastic-plastic deformation of the counterpart to achieve a traction geometry in which stop rotation against the loosening direction. ABAQUS/Explicit solver is used in their FEA. They modeled only the fastener head form and they used arbitrary Lagrangian-Eulerian adaptive mesh technique to overcome convergence problems. They simulated the assembly of metal fastener to the plastic seating surface for the use of small electrical components. They calculated the joining and releasing torque values and they investigated the effect of serration depth by changing the mechanical properties of plastic counterpart. They found that the hardness of bolt has to be increased relative to the counterpart to form a residual deformation on the seating surface in which it prevents joint from loosening.

Jung, Park, Yoon, Jun, & Chung (2009) released a study comprising design optimization of the spring of a locking nut by using design of experiment (DOE) method. They implemented a two-stage optimization process. First, they used Taguchi method to optimize discontinuous parameters such as sectional shape, material and the

number of coils of the spring, second they used Response Surface Analysis method to optimize the sectional dimensions, pitch distance and the inner diameter.

Kasei (2007) investigated the effect of small slippage at bearing surface on self-loosening of bolted joints. He explained the small slippages at the bearing surface theoretically with calculations of the elastic torsion of the bolt shank.

Bommisetty & Narayanan (2014) proposed a special meshing technique for robust FE simulations. The mesh quality remains good in refinement process of FEA.

Marshall, Zainal, & Lewis (2011) investigated the influence of interfacial pressure distribution on loosening of bolted joints as Fujioka, (2008) and Izumi, Yokoyama, Iwasaki, & Sakai (2005) did. Marshall, Zainal, & Lewis (2011) used ultrasonic Non-Destructive Test methods to map the pressure distribution on the bearing contact interface. They investigated five cases of assembly, which they are no-washer, plain washer, spring (split) washer and Nordlock® washer, respectively. They found that when the stress concentration factor or the ratio between max. and min. stresses around the bolt hole are increased, loosening rate is increased. So, peak values and difference of pressure values around the bolt hole have to be minimized to decrease loosening effect. Also, bolt and nut should be harder than clamped components. This property provides more homogenous pressure distribution around the bolt hole and at that point of view, findings in their study is in good agreement with other references in this section.

Mayer & Gaul (2007) investigated the simulation parameters on contact mechanics. They used segment-to-segment contact elements on joint interfaces. They showed the advantages of segment-to-segment comparing node-to-node contact element such as the ability of modelling three-dimensional contact state in one element.

Ouyang, Oldfield, & Mottershead (2006) studied the loosening behavior under torsional dynamic loads. Their study is different from other studies in the literature by means of loading type. They used a special Jerkins-element model to calculate friction torque according to the rotation angle.

Patel & Bhatt (2016) investigated on a mathematical model to optimize weight of the chassis frame. Mathematical model express the von-Mises Stress by using three process parameters. They used hybrid methodology merging DOE and FEA methods to make statistical calculations and make regression analysis. Response Surface Methodology is used to predict response on regression model.

Friede & Lange (2010) studied the embedding effect that acts on self-loosening event. On the contrary to Ganeshmurthy & Nassar (2014) they found that there isn't any effect of fastening method such as the combination of torque and rotation control on self-loosening. They found no relation between additional axial load and self-loosening behavior in which the most common studies describe vice versa. They found that embedding effect cause more relaxation on the bolt and increase loosening rate.

Sakai (2011) investigated the self-loosening mechanism under the repeated axial loading condition. He founded that loosening rate increases as the preload decreases due to cyclic axial repetitive load due to the microslip behavior under the bearing surface and thread surface.

Sanclemente & Hess (2007) proposed a statistical method to express the effects of preload, modulus of elasticity, bolt diameter, lubrication and so on. Their study should be useful when comparing the factors assembly parameters.

Wang, Wang, Zheng, Liu, & Liu (2014) studied on self-loosening of a bolt/nut connection under thermal and transverse loads by using FEA. They found similar results with Izumi, Yokoyama, Iwasaki, & Sakai (2005) that the complete thread slip occurs prior to the complete bearing surface slip.

Yang & Nassar (2010) studied on an analytical model to predict self-loosening behavior under transverse loads. They expressed detailed calculations in their study, but the equations still do not represent the self-loosening behavior completely.

Yokoyama (2008) compared double-nut tightening method, spring and conical spring washer against loosening resistance. He found similar results with Izumi, Yokoyama, Kimura, & Sakai (2009) hat spring washer does not prevent loosening, but increase loosening rate. So, using a spring washer should not a rational choice when it

comes to self-loosening. Double-nut tightening method improves loosening resistance by decreasing loosening rate drastically if and only if the method is properly applied. Conical spring washer is investigated in two cases. First one is the low axial force condition which represents the conical state of the washer. In this case, there are two aspects. First, spring washer accelerates self-loosening behavior as because the smaller contact area generates higher contact stresses, hence the stress concentration effect near the inner diameter of the washer occurs. The second one is the higher axial force condition which represents completely flat washer case. In this case, self-loosening behavior is improved, but not depend on the use of conical spring washer. The systems acts as a flat washer condition. Yokoyama, Olsson, Izumi, & Sakai (2012) investigated the effect of rotational displacement on self-loosening behavior as Ouyang, Oldfield, & Mottershead (2006) did. They calculated a critical rotation angle that triggers loosening mechanism.

Wu & Nassar (2014) studied on the under-head design configuration to find out the most durable form under transverse loads. They compared the undercut and filleted under-head forms and they found the fillet configuration stronger than the other one.

Zhu, Hong, & Jiang (2016) compared the torque-preload formulations in literature and proposed a new model to calculate preload versus tightening torque.

Self-loosening event on bolted joints are briefly explained above, for flat under-head surface design, only. This study is focused on the effect of serrated under-head surface on *loosening rate* under cyclic transverse loading conditions. Loosening performance of flat and a standard serrated under-head form is compared. Results were so clear that serrations decrease loosening rate, dramatically. Therefore, a deeper study is initiated, but getting geometrical parameters into account. Several geometrical models are generated and simulated with FEA method, then results are investigated to find a relation between input parameters and the outputs by using *genetic programming*-based *symbolic regression* approach. Hence, this thesis is the first study in literature which uses so-called approach in such a problem. Brief information about *genetic programming* method is given in the following paragraphs.

Genetic Programming (GP) is an optimization method and it can be described as a subset of evolutionary computation targeting to generate executable programs. These small executable packages try to find the best formula solving the problem. By performing a series of operations consisting of reproduction, crossover and mutation operators, genetic programming produces only the next population in which individuals have more successful genetic material. Genetic programming re-shapes computer programs evolutionarily, just like tree structures Cramer (1985).

Symbolic regression is one of the subset of *genetic programming*. Eureqa® is a commercial software package using *symbolic regression* method to find out best equation between input and output data.

Symbolic regression is one the most popular methods of genetic programming and an appealing alternative to standard regression technique owing to its flexibility in producing freeform mathematical models from observed data without any domain data.

GP comes to front as a successful method in the field of *design optimization* and constructing *estimation models*. Cevik, Arslan, & Köroğlu (2010) modeled torsional strength of reinforced concrete beams by using GP. GP provided more accurate results when compared with other methods, in their study.

Nastran & Balic (2002) estimated metal wire behavior by using GP in their study. They studied on the wire shape after metal forming process. They estimated the curvature of wire under load.

Milfelner, Kopac, Cus, & Zuperl (2005) studied on cutting tools having special curved cutting-edge. They measured cutting force in a production process that is carried out by using this special tool. They investigated and they tried to find out the effects of best parameters on cutting force by using GP.

Ghugare & Tambe (ud) investigated the higher heating value (HHV) that indicates a coal's potential energy yield. In their study, three proximate and ultimate analysis based nonlinear correlations have been developed for the prediction of HHV of coals by utilizing the computational intelligence (CI) based GP formalism. They had

concluded that the GP-based models proposed in their study possess a significant potential to replace the existing models for predicting the HHV of coals.

For more information about this issue, *'Genetic Programming'* from Kacprzyk & Pedrycz (2015) and *'Genetic Programming Magic Bullet, Poisoned Chalice or Two-Headed Monster'* issue from Abrahart (2014) should be investigated.

1.2 Aim of This Study

In the scope of this thesis, a comprehensive estimation study is performed, comprising the loosening behavior of the bolt (a type of fastener), under transverse vibrational conditions. Preliminary studies are carried out by using an improved version of Junker vibration test machine, then a simulation model is constructed with the results gathered from tests conducted. After the literature survey, an appropriate bolt-under-head form is chosen and a parametric model is stated in CATIA V5 CAD environment. 4 effective geometrical parameters are selected and design table is generated in 4 levels by using full factorial DOE method and experiment table is set to obtain a total of 256 observations. Numerical simulations are run according to this design table in different geometrical specifications and 10 objective criteria are selected from simulation results. These 10 objective criteria are taken under evaluation in order to estimate *loosening-rate*, which are given in Table 1.1.

Table 1.1 Objective criteria

Code	Output variables
CL	Clamp loss (kN)
FSBH	$F_{shear\ at\ bolt\ head}$ (kN)
FSNS	$F_{shear\ at\ nut\ surface}$ (kN)
FSMI	$F_{shear\ (min)}$ (kN)
FSMA	$F_{shear\ (max)}$ (kN)
RSDLH	Relative slip distance to the left hand side (mm)
RSDRH	Relative slip distance to the right hand side (mm)
RMAS	Relative maximum slip distance (position at the end of the cycle) (mm)
RMAS_M	Relative maximum slip distance (magnitude) (mm)
DZ_P	Z Displacement up to preload or penetration index (larger value penetrates most) (mm)

The objective criteria are capable of describing loosening behavior of fasteners, but a mathematical closer look is required for robust calculations, so understanding the

relationship between inputs and outputs is extremely important. Therefore, a *second model* is constructed by using simulation results. The point of so-called *second model* is to achieve a less-time-consuming and robust estimation model. While estimating *loosening-rate* of the fasteners under dynamic and transversely vibrational loading conditions, the aim is to state a highly accurate model by using *genetic programming* approach.

In this thesis, vibration and self-loosening of fasteners are briefly explained in Chapter Two, principles and methods for FEA of fastening and joining issues are described in Chapter Three, generic information and main concepts of genetic programming are summarized in Chapter Four. In Chapter Five, a comprehensive case study is carried out and the results are concluded in the last Chapter.

CHAPTER TWO
VIBRATION AND SELF-LOOSENING OF FASTENERS

Vibrations are initiated when an inertia element is displaced from its equilibrium position due to an energy imparted to the system through an external source. A restoring force, or a conservative force developed in a potential energy element, pulls the element back toward equilibrium (Kelly, 2012). This is the main phenomenon of vibrational systems. In a fastener system, vibration mechanism is quite different. Repeated forces are commonly generated by other systems and they are acting as vertical and/or lateral forces. Fasteners behaves like springs in an assembly. They store energy inside, up to their endurance limit which is called the yield strength (Figure 2.1).

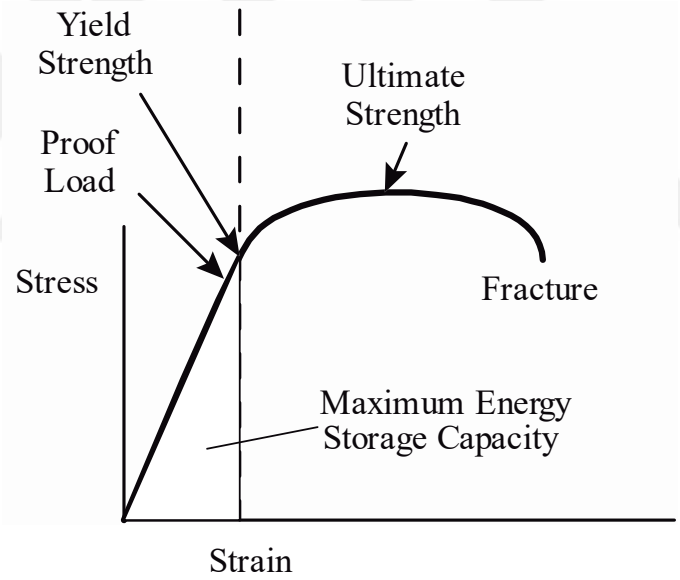


Figure 2.1 Endurance limits of a bolt

Stored energy provides a clamping force that is used for holding the assembly parts up together. When an external force is introduced, assembly parts are excited and they give response with a specific frequency to the system. Depending on the mass of the system, this frequency is generally too high and it could be neglected, in deed, when the subject is a fastener (bolt/nut). The similarity of the mechanism and the obvious relations to the issue are the matters for why ‘vibration’ term is used. In real world

examples, fasteners are exposed to random external vibrations in various and random directions. In Figure 2.2, vibration in a fastener system is described basically.

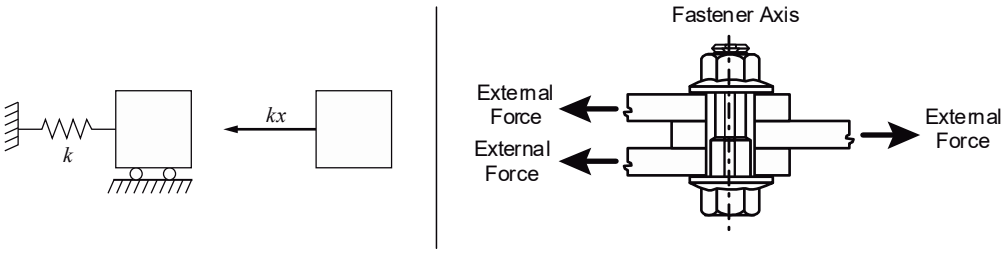


Figure 2.2 Vibration in fastener systems ('k' is the stiffness, 'x' is the displacement).

2.1 Definition of Screw Loosening

Fasteners are replaceable components in an assembly. When a fastener or bolt is failed, it can easily be changed with another bolt. Bolts are cheap and common parts, so designers use bolts and nuts frequently to combine assembly parts. Bolts, nuts or any other fasteners which have screw form in their bodies, have to be used knowing the technical definitions. When a designer decided to use a fastener in an assembly, he or she has to set adequate parameters for connection. When a bolt is tightened, an energy is pumped into it, by means of torsion (via torque wrench), tension and bending energy. Typically, 40 % of tightening torque is spent for thread friction, 50 % for bolt-head friction and 10 % for inclined plane. Inclined plane forces stand for the clamping force. The fastener can be described as a serial combination of springs (Figure 2.3). It can be loaded up by twisting, bending and pulling, up to its limits.

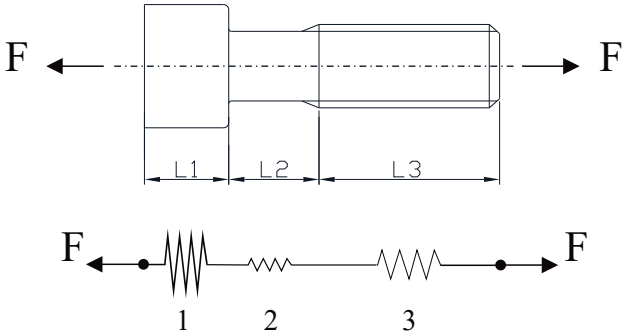


Figure 2.3 Stiffness of a bolt (spring model)

In this model, total length of the bolt is equal to *L1 + L2 + L3* at the beginning. When *F* is applied, sum of the changes in length will be:

$$\Delta L_c = \Delta L_1 + \Delta L_2 + \Delta L_3 \tag{2.1}$$

According to the Hooke's law:

$$\Delta L = \frac{FL}{AE} \tag{2.2}$$

where, ΔL is the change in length, A is the cross-sectional area, L is the length of the section, E is the modulus of elasticity and F is the clamp force. We can substitute (2.2) into (2.1) and we have:

$$\Delta L_c = F\left(\frac{L_1}{EA_1} + \frac{L_2}{EA_2} + \frac{L_3}{EA_3}\right) \tag{2.3}$$

The spring constant 'K' of each segment can be written below:

$$K = \frac{F}{\Delta L} \tag{2.4}$$

It can be seen in Figure 2.2 that the springs are serially connected, hence:

$$\frac{1}{K_T} = \frac{1}{K_1} + \frac{1}{K_2} + \frac{1}{K_3} \tag{2.5}$$

By substituting (2.2) to the (2.4), the equation (2.5) can be written as:

$$\left(\frac{1}{K_T}\right) = \frac{L_1}{EA_1} + \frac{L_2}{EA_2} + \frac{L_3}{EA_3} \tag{2.6}$$

where, K_T is the total stiffness of the bolt in the assembly.

When tightening-process is finished, spring forces inside the bolt applies a resultant force to take the bolt into its initial position. This force comes from the inclined thread shape between bolt and nut, this is called 'clamp force'.

One can see the asymmetrical stress distribution on the bolt head from the Figure 2.4. This asymmetry comes from the inclination angle of the thread surfaces, stress distribution is the result of bending moment, caused by threads.

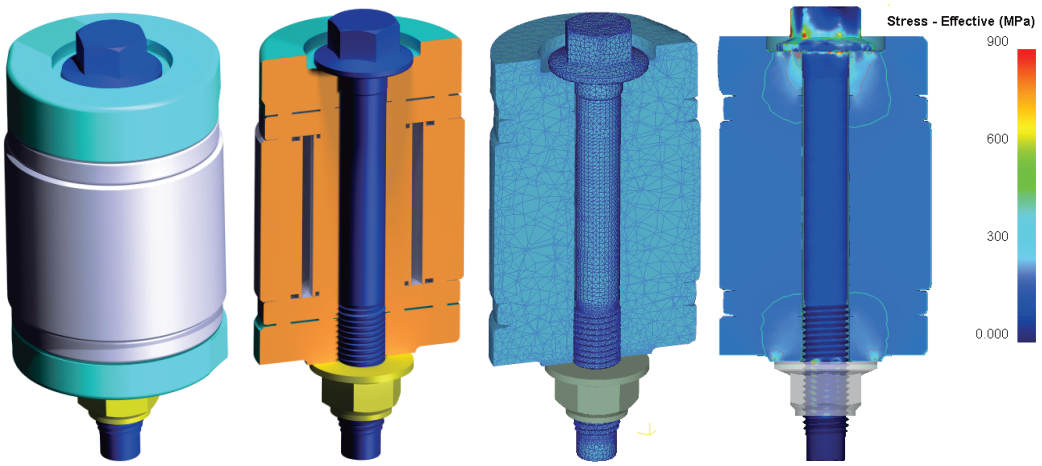
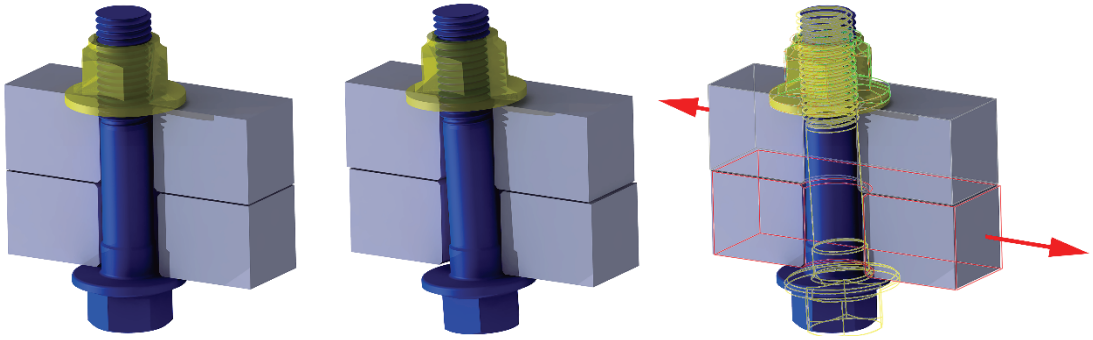


Figure 2.4 Stress distribution inside the joint members and the fastener.

Friction forces between adjacent surfaces balance torque and they prevent connection from self-loosening. For instance, when a transverse force is applied to this assembly, force equilibrium is changed to another position. External energy will be spent for friction between contact layers. Energy will be spent for relative movements between adjacent friction layers. While the layers relatively move, bolt will loosen. Certainly, if the load is continuously applied, all preload in the fastener will be lost. This can lead serious problems in the construction such as sealing problems, gas explosions, uneven bolt failures due to loss of the mean stress inside the bolt, and so on.

The main reason for self-loosening event is the instability of clamping force. Clamping force generates friction forces between adjacent planes (Figure 2.7) and they provide shear forces to resist external forces. Insufficient preload can cause transverse slip of the bolt and joint members. Self-loosening can trigger joint leakage, joint slip and fatigue failures. There are many reasons for loosing clamp force. The most effective reason is the vibration that will be investigated in this thesis, the other reasons can be thermal load cycles, embedment or softening of joint members, transverse slip, change in friction coefficient due to an oil interaction, and so on.



(a) (b) (a + b)

Figure 2.5 Preloaded (a), vibrated (b)

In Figure 2.5 and 2.6, a practical vibration-induced loosening mechanism is depicted. This example clearly shows the engagement gap between bolt and nut threads. Additionally, one can see that resulting bending moment cause a separation under the nut surface. Same separation occurs under the head of the bolt. This can lead an asymmetrical pressure distribution under the head of the bolt and nut surfaces. Excessive local contact pressure at the contact pairs creates a hinge point which cause rotations about the bolt and the nut thread axes, which initiate self-loosening chain-reaction. Figure 2.7 shows the micro-slip mechanism between bolt and thread surfaces.



(a) (b)

Figure 2.6 Preloaded (a), loose (b) bolt

There are several studies in the literature trying to explain self-loosening event. These studies reveal that there are some indicators which initiates loosening reaction. The first parameter is the transverse displacement length δ_x. Bending moment increases by increasing δ_x. After a certain value of δ_x, contact surfaces start to slip on each other.

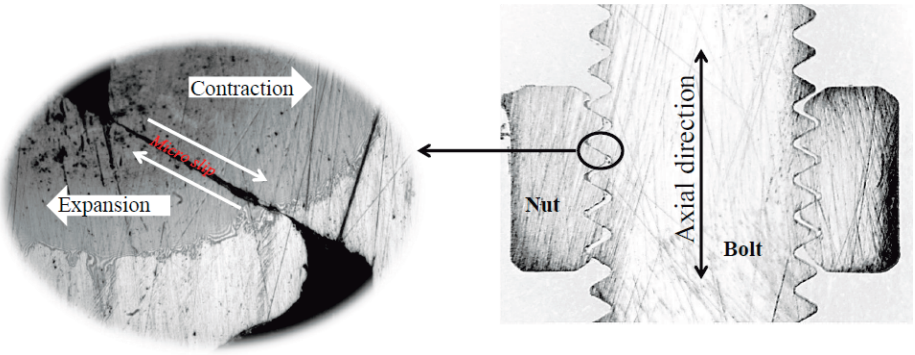


Figure 2.7 Micro-slip mechanism between bolt and nut thread surfaces (Goodier & Sweeney, 1945).

Blume & Illgner (1988) investigated self-loosening mechanism (Figure 2.8) and they had found a critical value which initiate major slippage between contact layers. They expressed an equation to predict major slippage limit. They called this limit as *'Marginal Slip'*. This equation (2.7) could shine a light to avoid self-loosening of fasteners in the assembly.

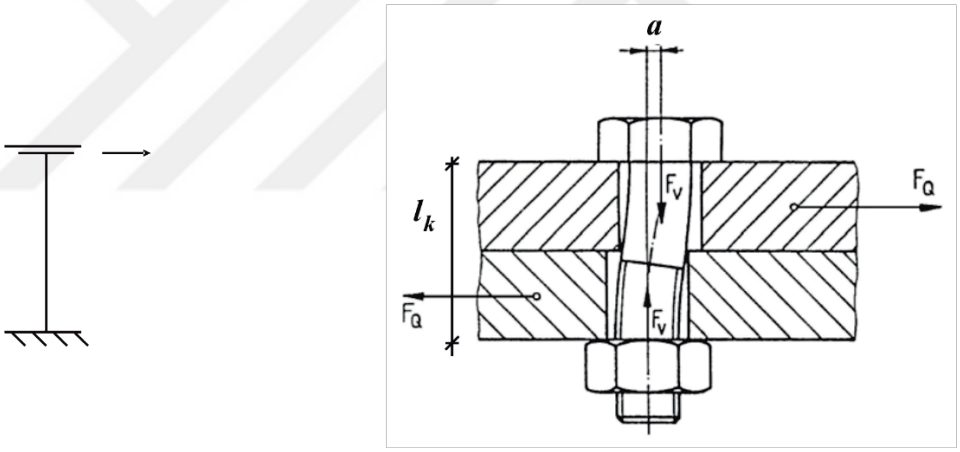


Figure 2.8 Self-loosening mechanism. (Blume, 1969; Blume & Illgner, 1988)

$$a = \frac{F_{Clamp}\mu_{br}l_k^3}{12EI} \tag{2.7}$$

where a is the *'marginal slip'*, F_{Clamp} or F_v is the 'clamp force', μ_{br} is the *'bearing surface coefficient of friction'*, l_k is the *'clamp length'*, E is the *'Young's modulus'* and I is the *'inertia moment of the bolt'*.

Friede & Lange (2009) tested equation 2.7 in their study on M20 bolts and they concluded that (2.7) gives a good approximation, but due to the fact that their experimental study is so limited, their conclusion is questionable.

Friede & Lange (2010) developed their experimental studies and make additional experiments for fasteners between M16 to M24. They found that Blume equation (2.7) gives conservative results. They expanded Blume equation as given in 2.8.

$$a = \frac{F_{Clamp}\mu_{br}l_k^3}{12EI} + \frac{F_{Clamp}\mu_{br}l_k^2}{2c_\theta} \tag{2.8}$$

where c_θ is the *'rotational stiffness of the bolt'* (Friede & Lange, 2010).

Finkelston (1972) investigated the effective parameters of self-loosening event. According to the result of his study,

- Clearance between bolt and the nut threads should be decreased. Because loosening rate of fine pitch nuts are slower than coarse pitch nuts.
- Increasing the preload on bolt leads higher loosening resistance.
- Loosening rate increase by increasing transverse displacement amplitude. However, loosening rate will be zero under a certain amplitude.

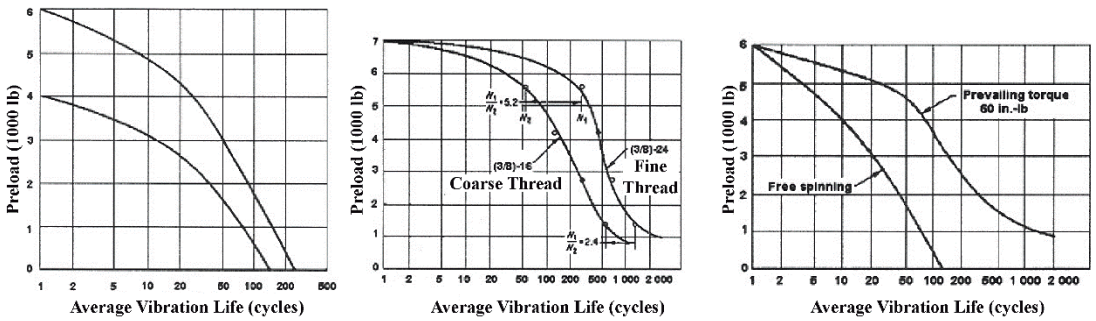


Figure 2.9 Preload versus average vibration life data for different, initial preload (a), thread pitch (b) and prevailing torque level (c) (Finkelston, 1972).

2.2 Vibration Loosening of Nut And Bolt

During the industrial revolution, steam engines were most common and powerful machines around the world. Steam generator caps were fastened with bolts and they were exposed to tension and compression stresses in uniaxial direction, generally. So,

scientists endeavored to improve fatigue and loosening resistance of bolts by investigating uniaxial loading conditions. Gerhardt Junker was working on the same problem and he had made lots of experimental studies on loosening of fasteners. Soon, he had described from his investigations that transverse loads have been far more effective than the axial loads on self-loosening of fasteners. He had made a lot of experiments to represent vibrational conditions. He invented a vibration machine (Figure 2.10) in the late 1960s and he made possible to benchmark several types of fasteners against self-loosening phenomenon.

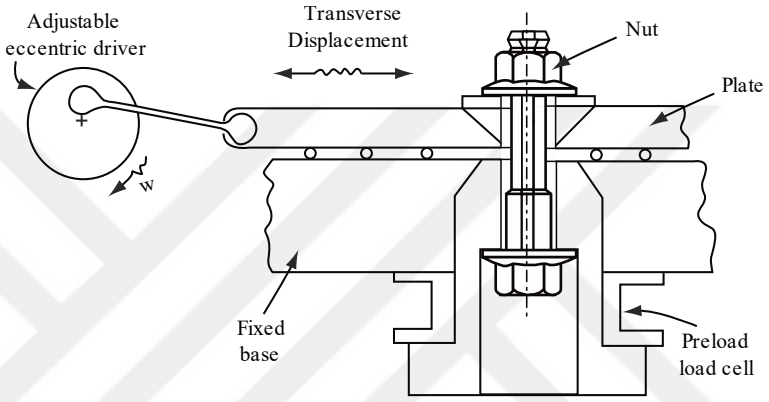


Figure 2.10 Typical Junker Test Machine

According to his invention, bolt is placed inside a bushing which creates pressure under its flange and this pressure is transmitted directly to the load-cell. Load-cell is reporting the clamp force simultaneously while bolt is vibrating. In the Figure 2.10, bolt head is locally restraint against excessive transverse displacements, but the nut-side is free to move along the horizontal or transverse axis. Adjustable eccentric driver mechanism provides a sinusoidal displacement path between the limits of $\pm\, \partial_{Transverse}$ at constant angular velocity. Plate is supported with roller bearings to minimize friction between moving parts. Clamping torque is adjusted from the nut side.

Transverse vibration triggers 4 types of behaviors on the bolt-nut assembly as given in Figure 2.11.

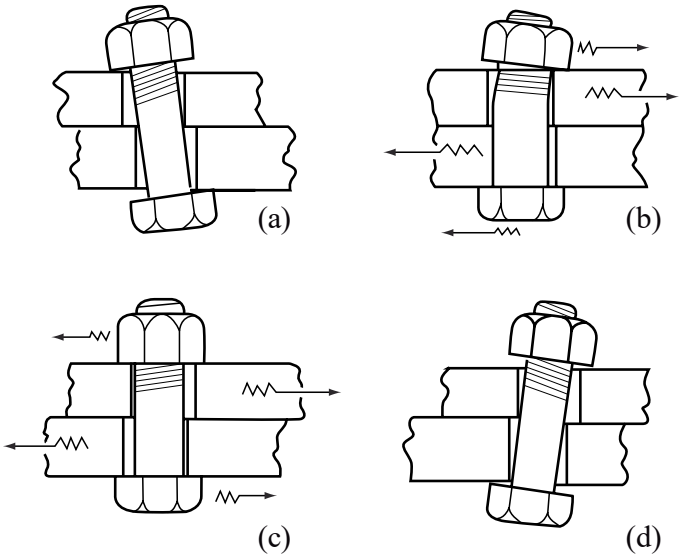


Figure 2.11 Bolt-nut orientation during transverse vibration conditions, slip-stick (a, d), stick (b), complete slip (c).

Figure 2.11 reveals some basic mechanism of vibration induced problems in the assembly. When the bending moment is too high, bolt and the nut penetrate to the counter-part at a point which have the maximum the stress-concentration factor. This point acts a hinge support and the bolt-nut couple can rotate at that points easily during the transverse movement. This condition can be seen in the Figure 2.11 (a, d). When the friction force at any location is high enough, bolt head or the nut head sticks to this area and travels at the same speed as the bonded plate (Figure 2.11 (b)). Generally, sticking condition comes from excessive bending moment, thread angle or the local embedment feature (serrations may trigger this effect). When the friction area or the friction force between moving parts, bolt head and the nut seating surface start to slip completely as given in the Figure 2.11 (c). All these conditions cause self-loosening of fastened elements in the assembly.

Clamp force is the axial force which is developed under tightening torque. While bolt is rotated around its longitudinal axis, bolt and the nut threads slip on themselves. A simple bolt-nut assembly is illustrated in Figure 2.12.

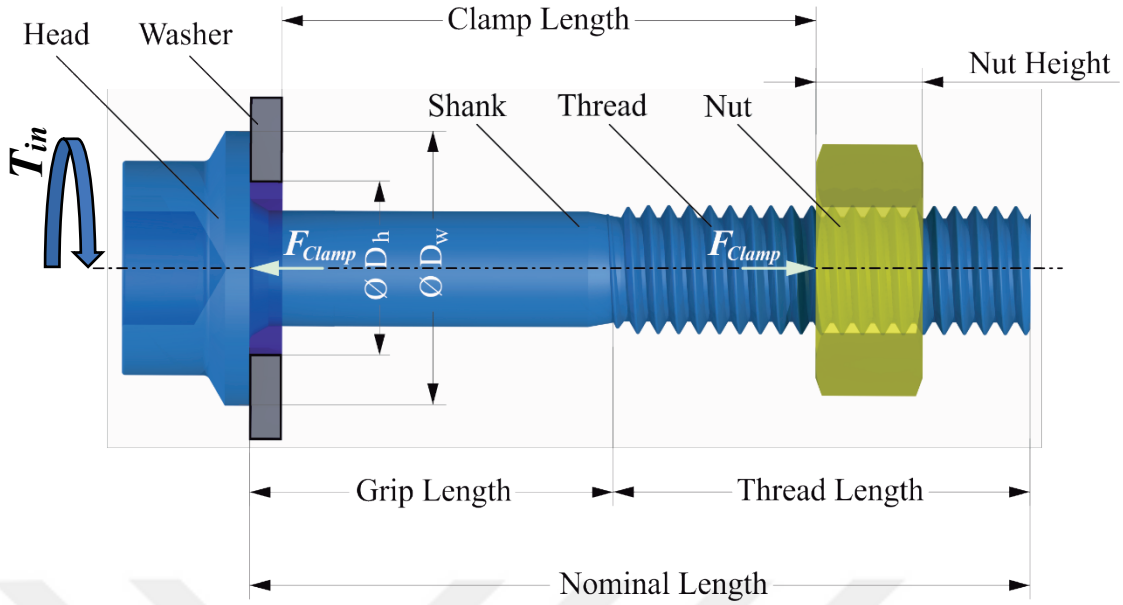


Figure 2.12 Bolt-Nut couple design elements

Tightening torque can be calculated as given in Equations 2.9-11 for different cases. In the first case, bolt and nut has the clearance between a particular geometrical tolerance such as 6g6H (6g for bolt, 6H for the nut). So, there is no *'additional'* torque in the process. So, Equation 2.9 should be used:

$$T_{in} = F_{Clamp}\left(\frac{P}{2\pi} + \frac{\mu_{Th} r_{Th}}{\cos\beta} + \mu_{br} r_{br}\right) \tag{2.9}$$

where, T_{in} is the *tightening torque*, F_{Clamp} is the clamp force, P is the *thread pitch*, β is the half of thread angle (30° in Figure 2.13), μ_{Th} is the thread friction coefficient, μ_{br} is the bearing friction coefficient (under the bolt head), r_{Th} is the *thread radius* ($\emptyset d_2/2$), r_{br} is the *bearing radius* $(\emptyset D_h + \emptyset D_w)/4$.

Prevailing Torque is the additional torque comes from the frictional forces around thread form. Usually, tight geometric tolerances cause prevailing torque. Zero clearance or pre-stressed contact between bolt and the nut threads, also increase prevailing torque. In such cases, additional prevailing torque or T_P has to be introduced in the equation as follows:

$$T_{in} = F_{Clamp}\left(\frac{P}{2\pi} + \frac{\mu_{Th} r_{Th}}{\cos\beta} + \mu_{br} r_{br}\right) + T_P \tag{2.10}$$

If one would like to calculate disassembly torque value, bearing friction and the prevailing torque should be subtracted (Equation 2.11) from the equilibrium.

$$T_{OFF} = F_{Clamp}\left(\frac{P}{2\pi} + \frac{\mu_{Th} r_{Th}}{\cos\beta} - \mu_{br} r_{br}\right) - T_P \tag{2.11}$$

Figure 2.13 shows the basic thread dimensions in the literature. $\emptyset d_2$ is the dimension known as pitch diameter which bolt-nut thread contact concentrates on this diameter.

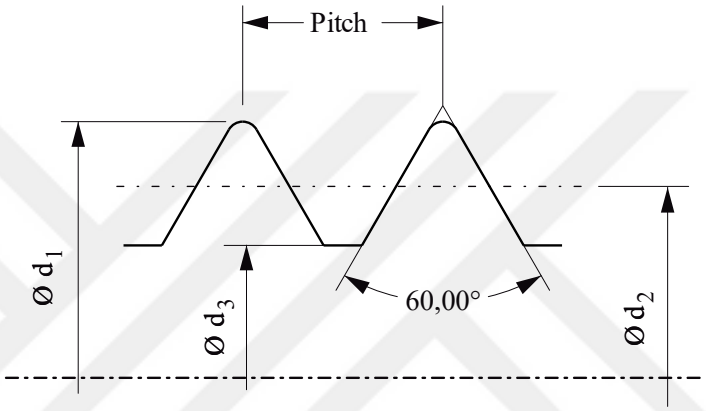


Figure 2.13 Simplified thread profile

2.3 Prevention of Loosening by Means of Design

Fastener loosening is a very common problem in the industry and scientists are still working to overcome this problem. Several studies reveal the list of parameters affecting self-loosening of fasteners, in the literature.

Engineers has been trying many things to heal self-loosening problem. They have been making modifications on the bolt threads, bolt under-head surface (serrations), on the nut threads, under the nut seating surface, on the bolt and the nut hight, or they have been trying to overcome this problem by using external elements such as special washer forms (serrated, protruded, glued, ribbed, ..) and so on. Shoji & Sawa (2011) investigated the effect of external joint parts in the assembly, such as washer, pins, chemicals and so on (Figure 2.14).

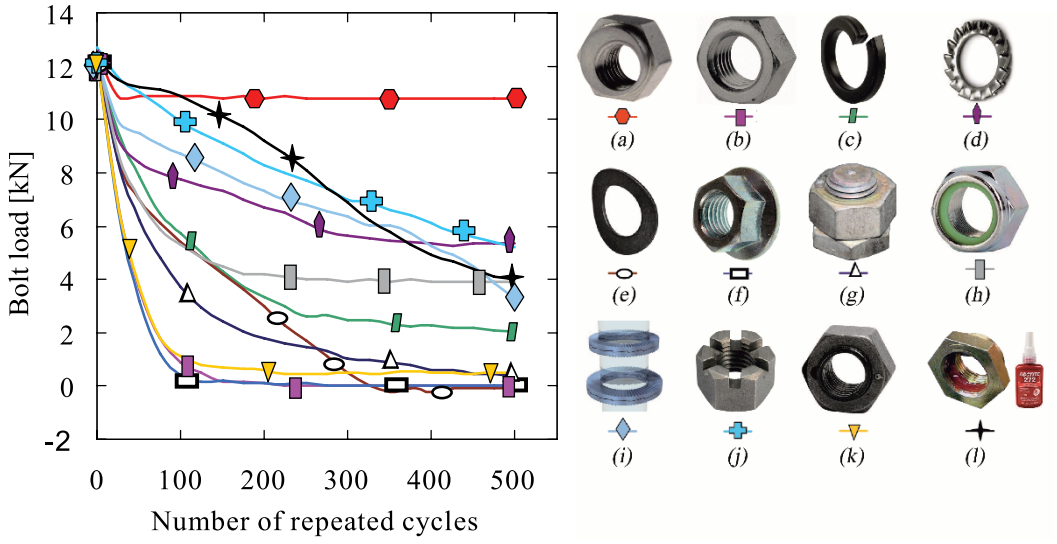


Figure 2.14 Junker's test results for 12.5 kN of clamping force [eccentric nut (a), hexagon nut (b), spring washer (c), toothed washer (d), plate spring washer (e), hexagon nut with flange (f), double nut (g), nylon insert nut (h), Nord-lock® washer (i), slotted nut (j), steel plate insert nut (k), anaerobic adhesive (l)] (Shoji & Sawa, 2011).

According to the Figure 2.14, eccentric nut provides the best anti-loosening performance of all elements. Toothed (serrated) washer provides reasonable anti-loosening performance, these results indicate that geometrical penetration should be an advantage on self-loosening phenomenon of fasteners.

Experimental studies showed that self-loosening will occur only if there exist cyclic, transverse loads, and relative slip between thread and joint surfaces. Self-loosening should be hindered by eliminating both of them. Another way to prevent self-loosening is locking bolt and the nut together with the use of special chemicals or mechanical locking systems. Commonly, self-loosening event or the *loosening-ratio* indicating the *loss of clamp force* should be improved as follows:

- *transverse displacement* should be decreased: Many scientists investigated the slip-threshold with various experimental studies. It can be found in the literature that, there is a critical slip distance value which the head or the nut completely slips on the plate. The critical value is called *marginal slip* (Figure 2.8) or *critical transverse displacement* (S_{cr}) in the literature. If the transverse displacement is below this critical value, self-loosening will not occur in the assembly.

- *clamp length* should be increased: Somehow in most cases, it is not possible to change the clamp length in the assembly. But, designers should be aware of the healing effect of *clamp length* against self-loosening. Stiffness of the bolt and the trigonometric properties are the reasons behind this effect. Longer bolt will displace more than a shorter bolt for a certain deflection angle at the free-end, so *loosening-rate* should be lower for long clamp lengths (Figure 2.15).

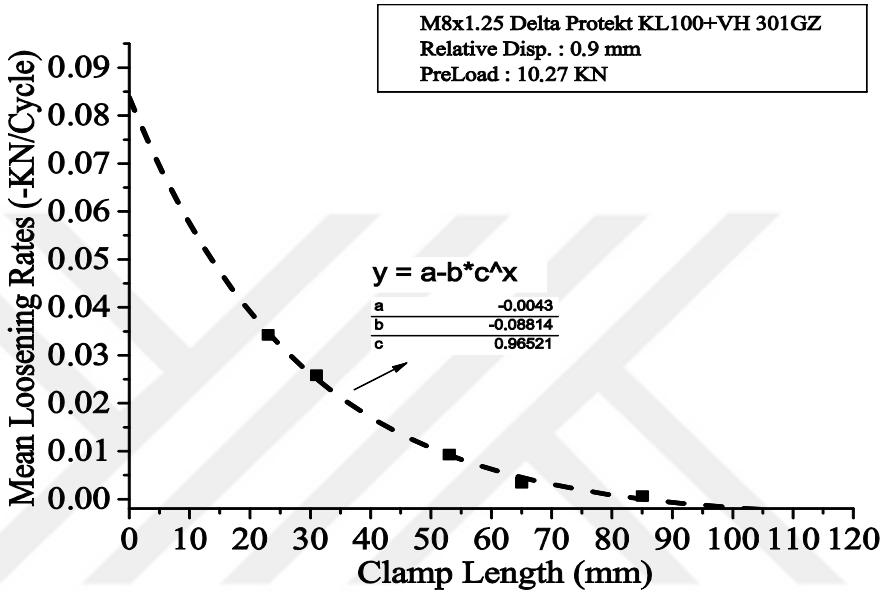


Figure 2.15 The effect of clamp length

- *bearing friction coefficient* should be increased: Increasing the friction under the head of the bolt and the nut-seating-surface will increase the *friction force* (F_{shear}), and that will increase the critical slip distance. Figure 2.16 shows the relation between *loosening-rate* and the *bearing friction coefficient*.

- *joint stiffness* should be decreased. Soft materials will deflect more than hard materials. So, larger vertical displacements could be obtained by using softer materials.

- *thread angle* should be decreased: Auto-blocking effect and the off-torque increase by decreasing thread (flank) angle. So, 55° thread angle is better than 60° in vibrational loading conditions.

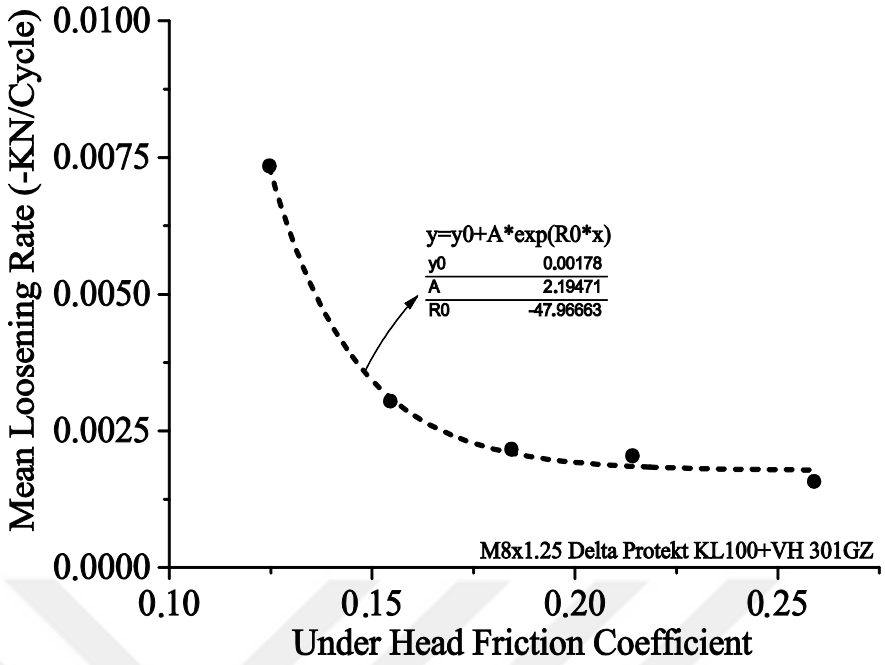


Figure 2.16 The effect of bearing friction coefficient on loosening-rate.

- *Preload* should be increased: *Preload* is the normal force acting on the moving and stationary plates. Hence, increasing *preload* will result in an increase in frictional forces, and that will reduce *loosening-rate* (Figure 2.17).

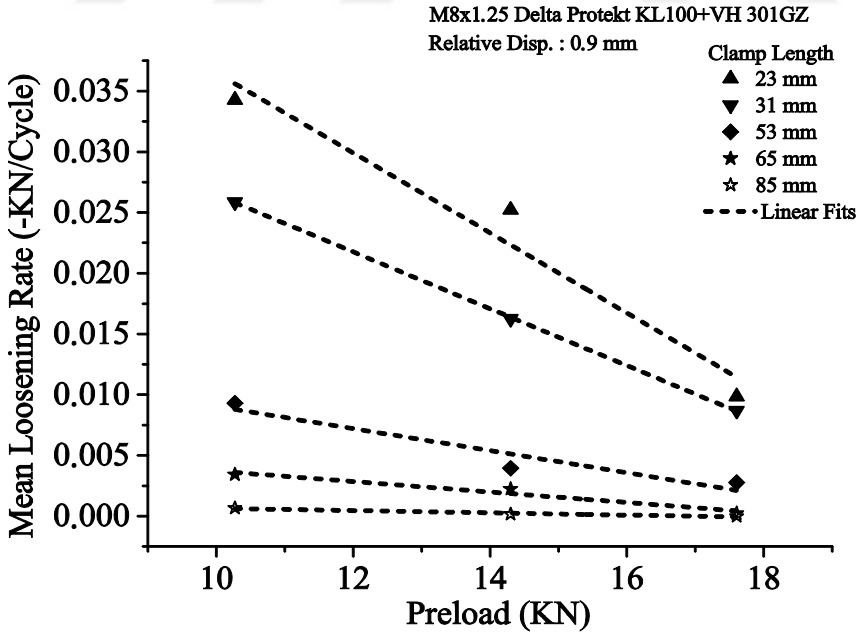


Figure 2.17 Effect of preload on loosening-rate.

- *thread pitch* should be decreased: Pitch length and pitch diameter defines the lead angle or in other words, helix angle (Figure 2.18). Fine pitch threads are more convenient in transverse loading conditions.

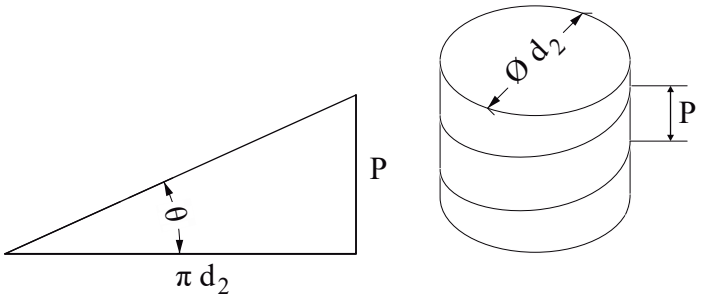


Figure 2.18 Lead or helix angle of a thread.

- *thread friction coefficient* should be increased: As described before, friction forces resist to relative displacements and they also resist self-loosening (Figure 2.19).

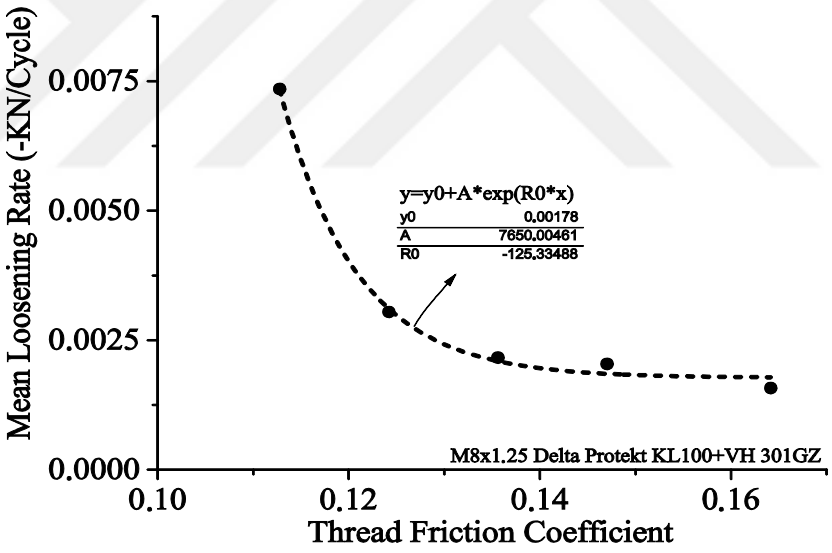
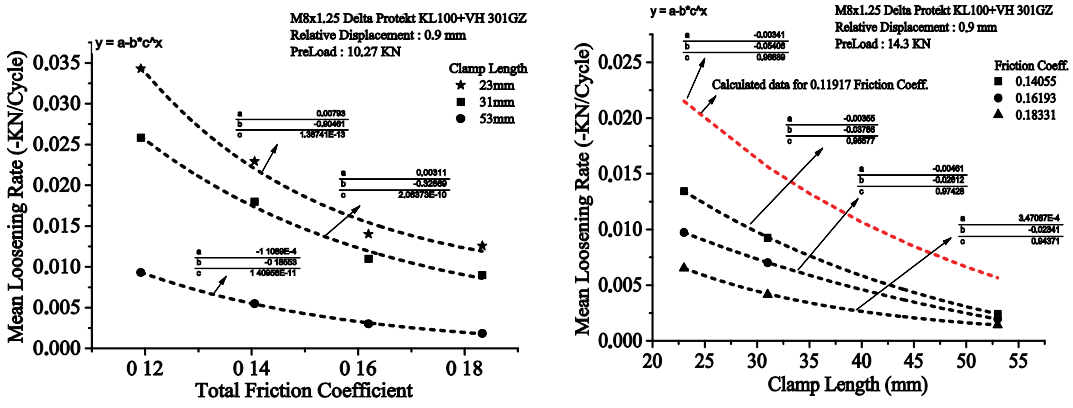


Figure 2.19 Effect of thread friction coefficient on loosening-rate.

Equation 2.7, 2.8 and 2.9 are in good agreement with the matters listed above.

Clamp length is more significant than *friction coefficient*. Figure 2.20 (a) indicates that total friction coefficient is less effective than the clamp length. Clamp length effect is getting more and more ascendant when the clamp length is increasing. It is obvious that the difference between curves of several *friction coefficients* get closer when the *clamp length* increases.



(a) (b)

Figure 2.20 Effect of total friction (a) and clamp length (b) on loosening-rate.

If all these precautions are not enough to prevent self-loosening event, another parameter, called *'off*-torque' or *'prevailing* torque' should be a remedy. *Prevailing* torque is the energy come from additional friction forces between bolt and nut threads. There are so many types of *prevailing* torque fasteners in the industry. Some of them was given in Figure 2.14.

Most common application of *prevailing torque* fasteners are: nut with locking ring of nylon, castle type locking nut, aerotight, dyna thread, eccentric nut, and so on. The principle is the same; making additional friction by reducing clearance between threads and try to generate a radially prestressed zone around the bolt and nut threads. Some of the most effective locking fasteners are given below:

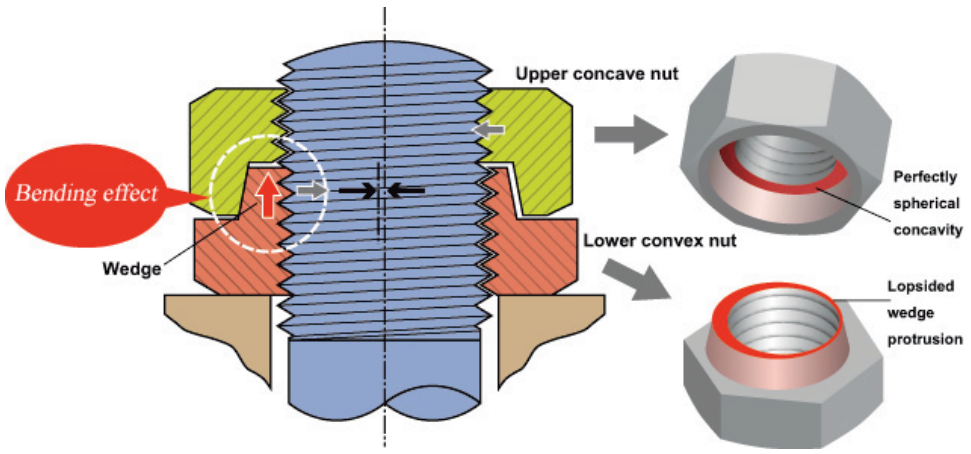
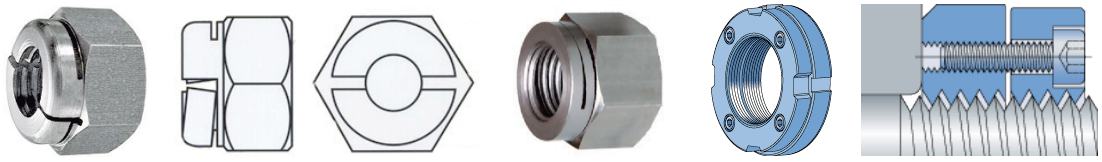


Figure 2.21 Hard-lock eccentric nut (Patent # US6609867B2).

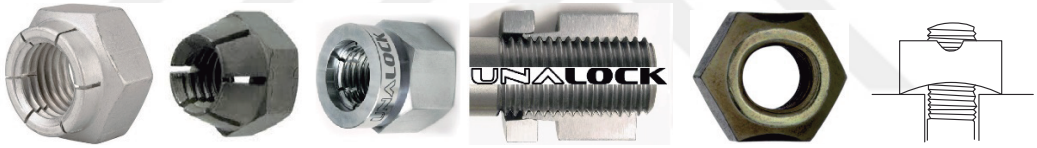
Katsuhiko Wakabayashi has been developed an eccentric nut shape (Figure 2.21) which provides additional bending moment that improves friction forces giving an advantage of anti-loosening effect to the fastener *(Patent # US6609867B2)*.



(a) (b) (c)

Figure 2.22 Aerotight® (a), Turret® (b), axial locking fastener (c).

Another solution is the *Aerotight*® which has a gap inside its thread form (Figure 2.22 (a)). The idea is to create a gap which tends to move freely rather than following the bolt and nut hole-axis. Relative inclination results in a deviation in the helix axis that results in an additional bending moment. This moment sticks the bolt and the nut threads together by generating additional frictional force and *prevailing torque*. In the Figure 2.22 (c), this moment is provided via external smaller bolts.



(a) (b) (c) (d)

Figure 2.23 Self-locking split-nut designs; split nut (a), Unalock® (b), DIN 980 (c), beveled nut (d).

Similar to the Figure 2.22 (a), there are several types of split nuts. But the point is simple and the same, creating a *prevailing torque*. In the Figure 2.23, some other split nuts and an *Unaloc*® nut are given. Figure 2.23 (b) ensures so-called *prevailing torque* by compressing the first two threads in a conical ring, then it increases the friction forces. Figure 2.23 (c) is a standard DIN 980 nut which has an elliptical hole shape that compress the bolt threads and generate an additional friction force. Figure 2.23 (d) is a beveled nut whose threads are deformed elastically (hole size gets smaller) when it is pulled down with a bolt.

Prevailing torque can be achieved by changing thread geometry as well. There are several designs about special thread forms which improve anti-loosening performance of the joint.

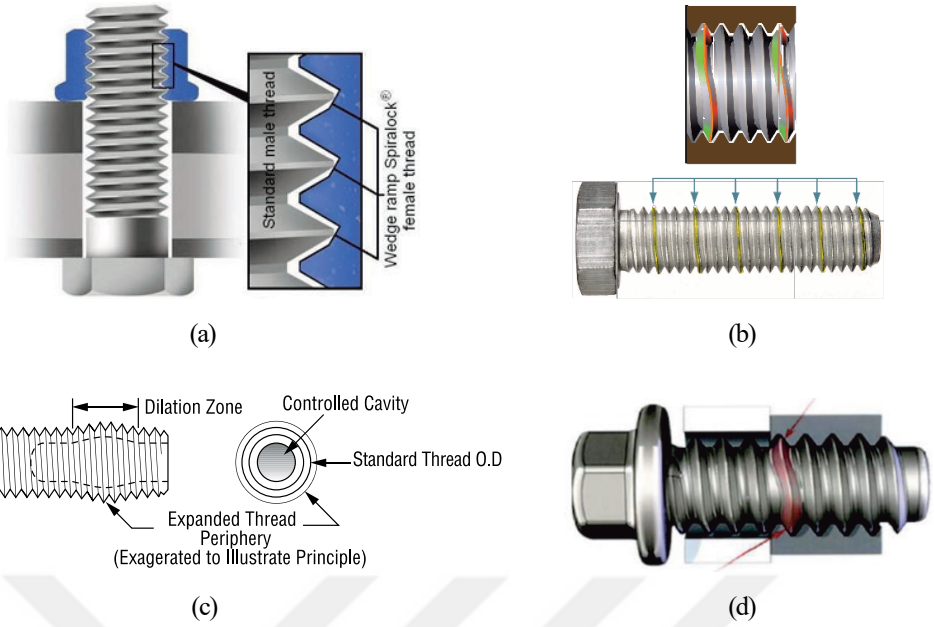


Figure 2.24 Spiralock® (a), ShakeproofTM (b), Dynathread® (c) and SinulocTM (d) locking fasteners.

In the Figure 2.24 some alternatives are given for reducing *loosening-ratio*. Some of them claim anti-loosening specification even for the zero-*clamp force*. These thread forms are very special and they are far more expensive than the traditional types.

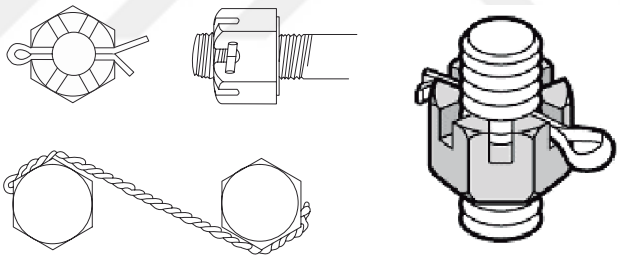
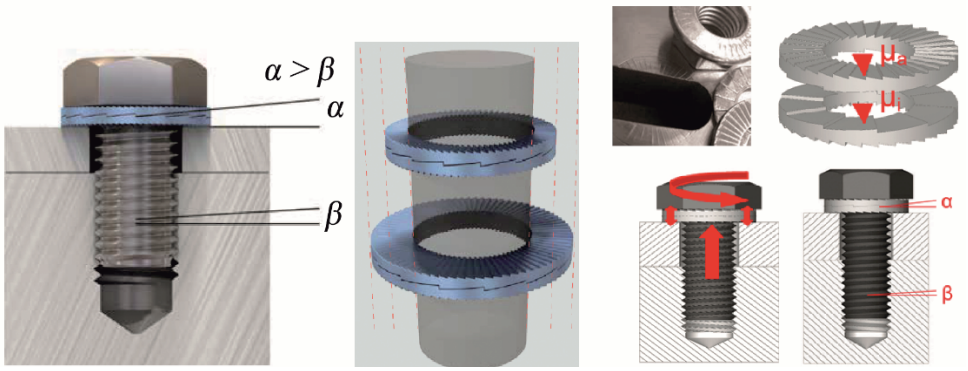


Figure 2.25 Mechanical locking solutions.

Relative motion of bolt and the nut couple can be limited by using mechanical locking techniques. Most common techniques are given in Figure 2.25. Chain method and cotter-pin methods are the most common methods in the industry.

Washers are external elements and they can provide vibration resistance to the assembly. They might be very cheap according to the design of their geometry. There are some products ruling the industry (Figure 2.26).



(a) (b)

Figure 2.26 Nordlock® (a) and Heicolock® (b) anti-loosening washers.

Nordlock® and the Heicolock® have the same principle. Washer system consists of two serrated washers, one for bolt, the other for joint element (plate). Both of the washers have serrations on both sides. Thinner serrations are in contact with the bolt and the plate. Coarse serrations contact to the washers themselves. The main principle is that, coarse serrations have the inclination angle larger than the lead angle of the bolt threads. Therefore, if bolt tends to loosen, it has to rotate axially and the head has to travel more than that of the thread pitch size and the *clamp force* will increase, because $\alpha > \beta$. Also, there is a lubricant between washer couples which reduces friction coefficient, so the movement between washers are easier than bolt head. Please consider that, serrations interacting head and plate cause an indention or embedment. This embedment is very important, so it creates a mechanical and geometrical link between mating parts (Figure 2.26 (north-east of b)).



Figure 2.27 Common washer types; first line plain and spring washers, second line toothed washers, third line serrated, beveled and anti-loosening washer (Starlock®).

In the industry, *Starlock*® is the most popular washer type in Figure 2.27 (south east corner) which clutches the fastener when it is compressed. This effect provides useful *prevailing torque* to the joint. Some other patented solutions are given in Figure 2.28.

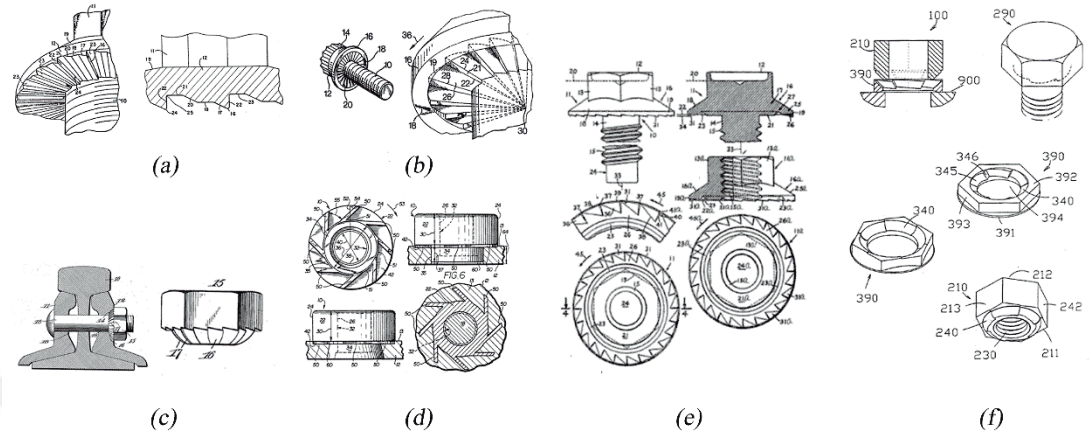


Figure 2.28 Patented serrations; EP0187244A1 - Vibration resistant fastener for soft joint surfaces (a), US3605845 A - GB1326380 A - self-locking fastener (b), US752628 - nut lock (c), US5302066A - locking fastener (d), US2959204 A - GB866556A - vibration resistant fastener for soft joint surfaces (e), US2003077143A1 - washer and threaded fastener assembly incorporating same (f).

The most cost-effective way to reduce *loosening-rate* is developing a unique and single bolt under-head form. The key-point is feasibility of design. Under-head form has to be compatible with mass-production lines, such as cold forming method.

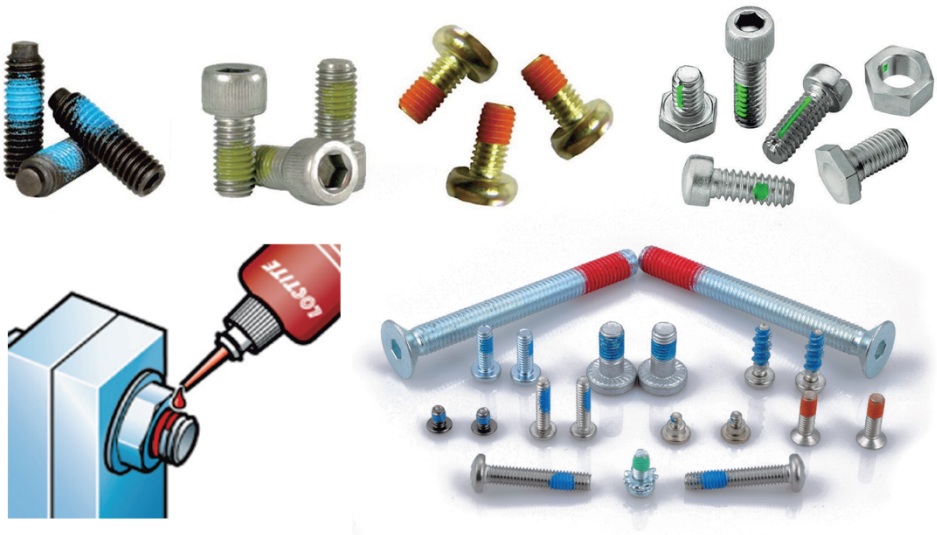


Figure 2.29 Chemical solutions for vibrational conditions.

Lastly, one of the most powerful methods for anti-loosening fasteners, is the use of chemical additives (Figure 2.29). Several chemicals should be used including acrylics

and anaerobics. Anaerobic adhesives are most powerful chemicals. They are activated under high pressure in the absence of air. They withstand very high pressure levels depending on the chemical compound, and provides a coefficient of friction of about 0.14 to 0.17, then they can be used as a lubricant. They bond bolt and the nut threads together and fill the gaps between them. This specification gives a sealing advantage to the joint. But they are very sensitive during curing operation. Fastener should be cleaned, wetted, and there should not be any oil around the application area, otherwise curing operation would not be performed properly, then all the time spent for the joint might be wasted. It could take days for curing operation and in most cases this is not an acceptable option for the contemporary production lines, racing with the time (an automobile is produced in 30 seconds in a factory).

2.4 Conclusion

There are several solutions for self-loosening problem in the industry. Most of them require an additional material(s) which increase(s) the cost and the total weight of the assembly. Additionally, chemical additives are not reusable in repeated tightening scenarios. Nut threads having reduced clearance cause peeling off the coating on the bolt thread surface which can lead early corrosion of the bolt and the nut. However, changing the bolt under-head geometry is very effective and it reduces the total cost, considerably. Also, modifying the head-seating surface of the bolt is a cost-effective method, besides it does not increase the weight of the assembly. Also, bolts having modified under-head form are completely reusable and they can withstand repeated tightening and loosening cycles. This is the main reason for why under-head form is investigated in this thesis.

CHAPTER THREE
FINITE ELEMENT ANALYSIS OF FASTENING AND JOINING

In this chapter, simulation method which is used in this thesis, is described and some important studies are also mentioned for future use.

All simulation studies are conducted in MARC/MENTAT interface of Simufact® commercial Computer Aided Engineering (CAE) software, based on Finite Elements Method (FEM). All data is gathered thought Finite Elements Analysis (FEA). CAD data is generated in CATIA V5 commercial software.

3.1 Analysis Method

As described in section two, clamp force is the product of applied torque, and the applied torque is the product of clamp force vice versa. Tightening process is a time-consuming process by means of FEA as because there is a lot of fine elements around the threads. Hence, tightening process should be eliminated by applying an axial clamp force to the fastener component. In this thesis, hundreds of simulations have to be completed via FE simulations. So, the purpose of each individual simulation has to be setting up simulation with minimum amount of finite elements mesh-count, optimum mesh size, optimum solution increments in a very short period of time.

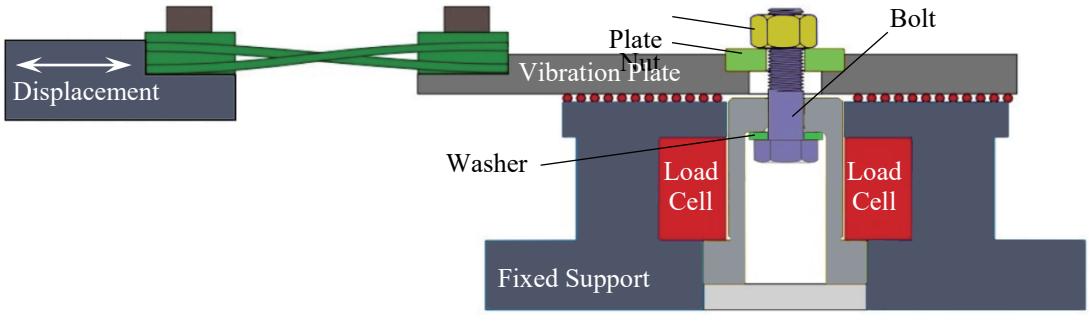


Figure 3.1 Junker test mechanism.

Simulation set-up is built under CATIA V5 software according to the Figure 3.1 and Figure 3.2.

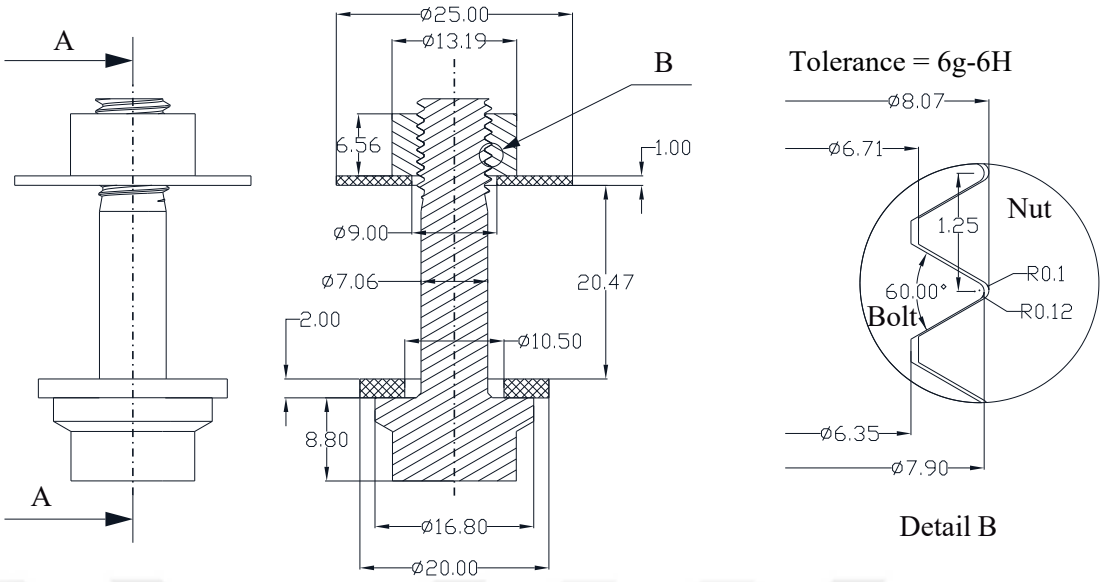


Figure 3.2 Bolt-Nut assembly details.

Bolt is made of medium carbon steel in Class 8.8 strength. That means, bolt will yield after 640 MPa of normal stress (root diameter) and it will break after 800 MPa of normal stress. Bolt-nut couple is modelled in between 6g-6H geometric tolerances as shown in Figure 3.2.

Relation between torque and clamp force was given in Chapter Two. According to the ISO 898-1 maximum axial force should not exceed the 90 % of the yield stress at the root diameter of threads. *'Proof Load'* corresponds the maximum load capacity at the smallest cross-sectional area of the threads, ($A_{s,nonimal}$). ISO 898-1 says that M8x1.25 8.8 bolts have 36.6 mm^2 $A_{s,nom}$ and these bolts can securely carry maximum of 21.2 kN axial force under the yield point. According to the automotive standards, 75 % of *'Proof Load'* should not be exceeded when calculating the nominal clamp force. So, a fastener in these specifications can carry about *21.2 x 0.75 = 15.9 kN* clamp load. One can put this value into the equation 3.1, and he has:

$$T_{in} = 15.9\left(\frac{1.25}{2\pi} + \frac{0.12\left(6.272 + 7.972\right)}{4\cos 30} + \frac{0.12\left(16.80 + 7.06\right)}{4}\right) = 28.31Nm \quad (3.1)$$

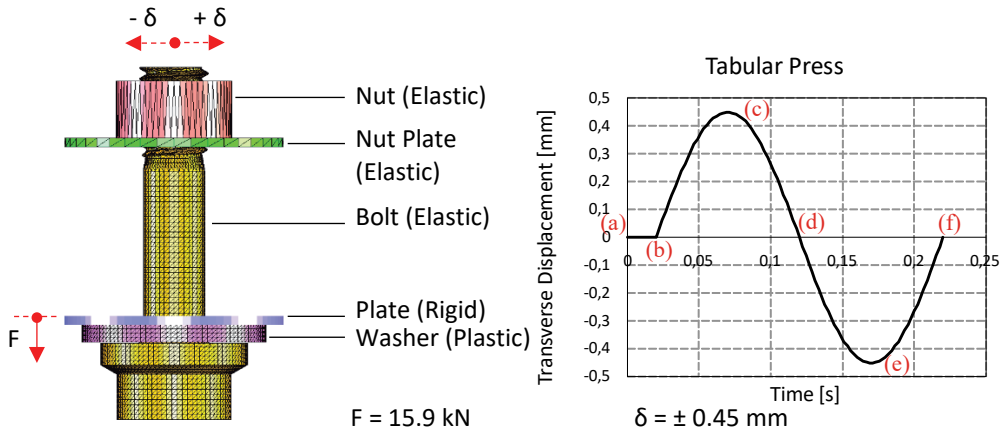


Figure 3.3 Velocity parameters.

Simulation model consists of two load cases. In the first load case, bolt is stretched as shown in Figure 3.3 up to a predefined clamp force value. Practically, bolt is clamped with 15.9 kN axial force in this case. In the second load case, *'Nut Plate'* is moved ± 0.45 mm with a sinusoidal function as shown in Figure 3.3. Total transverse displacement is completed in 0.2 seconds except for clamp time. In other words, vibration frequency is set to 5 Hz and only one cycle is simulated for each case.

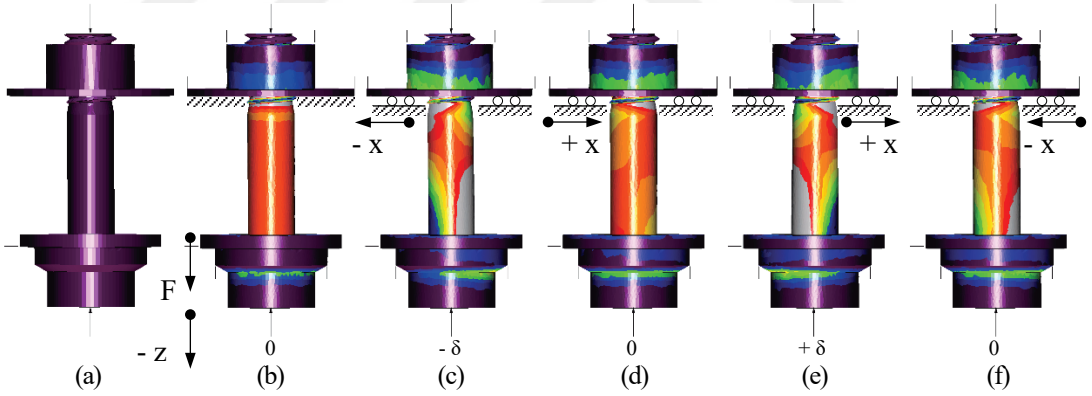


Figure 3.4 Vibration progress: Unloaded (a), Clamped [Preload Stage] (b), Transversely displaced [- 45 mm (c), + 45 mm (d), +45 mm (e), -45 mm (f)] (Labels are referenced to Figure 3.3).

Simulation steps can be seen in Figure 3.4. According to Figure 3.1, in Step (b), *'Nut Plate'* is fixed at the free nodes on the lower surface of itself in *x, y* and *z* directions. Bolt is stretched by moving the rigid plate along the bolt axis as shown in Figure 3.3-4. All the nodes under the *`Nut Plate`* are fixed in *x, y, z* directions until the force *`F`* is reached at predefined value. Step (b) is completed by using a hydraulic press at the speed of 0.1 mm/s. Automatic step increment feature is chosen for workpiece deformation, where the washer is defined as workpiece. In Step (c to f), all

the nodes under the *'Nut Plate'* are displaced on the *x-y* plane along the *x*-direction following the path as given in Figure 3.3.

All the contact elements are touching each other with a friction coefficient of 0.12, but the *'Washer'* is glued to the rigid plate to simulate *'Fixed Support'* condition in Figure 3.1. *Coulomb* contact law (bilinear, displacement) is used for frictional contacts. Automatic slip threshold with *0.05 N* force tolerance is chosen in contact parameters. Despite MARC has segment-to-segment contact, Simufact© GP (Mentat Interface) is not capable of doing this, yet. So, the mesh-sensitive node-to-segment contact method is used by ensuring that the slave contact elements have always finer mesh pattern in contact region. Dummy planes are introduced to control and validate displacements as shown in Figure 3.5.

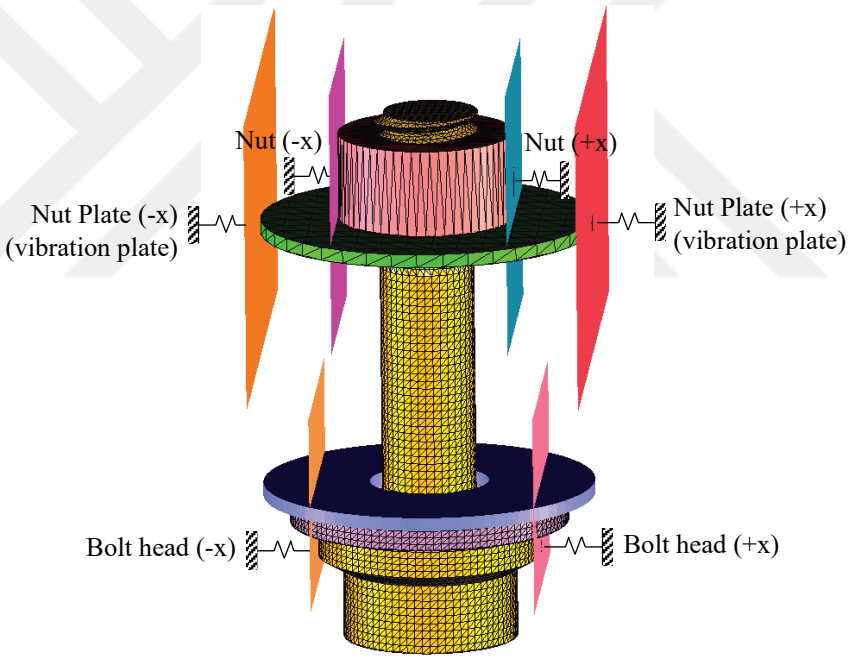
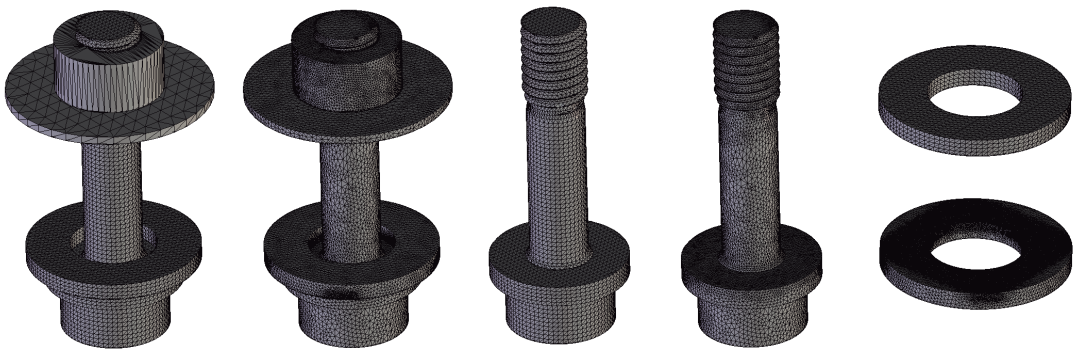


Figure 3.5 Displacement verification planes.

Dummy verification planes are acting as very soft springs (Figure 3.5). They have 0.1 N/mm stiffness with 0.1 N initial force to keep contact with the contact bodies. Max. compression length is set to 5 mm. There is a frictionless contact between dummy or verification planes. The main reason for placing those verification planes is the uniqueness of their structure. Because, if a node is tracked for displacement of an elastic or plastic body, node number and the location of the node will be changed after a re-meshing operation. There is no coordinate tracking option in MARC, so this

method should be better for tracking and reporting displacement data of individual contact members in subroutine programming environment. This method will be used effectively in Chapter Five.



(a) (b) (c) (d) (e)

Figure 3.6 Finite elements mesh details. Initial step (a, c and e-top), re-meshed (b, d and e-bottom). (e) is the 'Washer'.

All the CAD models are imported to Simufact® from STL models that are produced in CATIA *'STL Rapid Prototyping'* module. In the first increment of the load case, mesh structure is changed for all elastic and plastic elements according to MSC Patran® Tetra (tetrahedral) Global re-meshing criteria. Total number of elements for *'Washer'* is limited to 20,000 with minimum edge length of 0.05 mm's. Squared refinement box is applied onto the bolt-washer interacting surface with a level of 2, comprising the diameter of bolt's flange feature. Re-meshing criteria is set to 0.28 strain change or 0.02 tool penetration, hence the *'Washer'* is re-meshed if the plastic strain value at any element is reached to 0.28 or *'Washer'* is re-meshed if the penetration is greater than 0.02 mm at any node or contact elements pair. *'Bolt'* has a limit of 55,000 tetrahedral finite elements with a local refinement box on both under-head and thread surfaces (level 1). Min. and max. element edge length controls are disabled to eliminate re-mesh errors. *'Nut'* has 20,000 finite elements that the total number is limited, too. *Min.* and *max. edge length* controls are disabled, too and the *local refinement* feature is also disabled as because the size of the *'Nut'* is sufficiently small and 20,000 finite elements give finer edge length than the meshes on the bolt's thread surface. Lastly, *'Nut Plate'* has 10,000 finite elements (limited) with minimum edge length of 0.2 mm's and the *max. edge length* control is disabled. Local refinement

for *'Nut Plate'* is also disabled. Initial and the second increment mesh distribution is depicted in Figure 3.6.

For all elastic bodies, modulus of elasticity is set to 215,000 MPa and the *Poisson's ratio* is set to 0.29. DIN 1.0401 normalized C15 low-carbon steel is chosen for *'Washer'* material. The *Young's modulus* is set to 210,000 MPa and the *Poisson's ratio* is defined as *0.3*. Material data is entered as tabular data. C15 has an isotropic hardening rule following *von-Mises yield criterion*. Strain rates are interpolated by using *'Piecewise linear'* method. Material data is given in Figure 3.7.

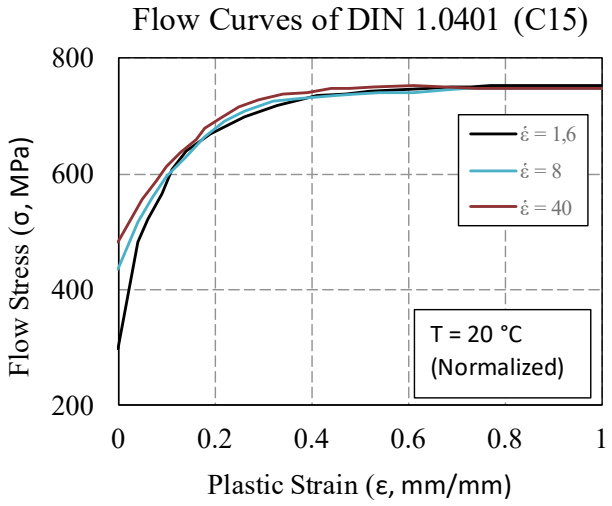


Figure 3.7 Material data.

Nonsymmetrical multifrontal sparse solver is used in computational work. Contact normal stress, force and stress components are selected as outputs for simulation.

3.2 Analysis Results

The nature of the vibration mechanism forces the assembly components to slide between interface layers of contact bodies. Sliding occurs after a certain value of shear force (Figure 3.8) that causes rotation and self-loosening problem.

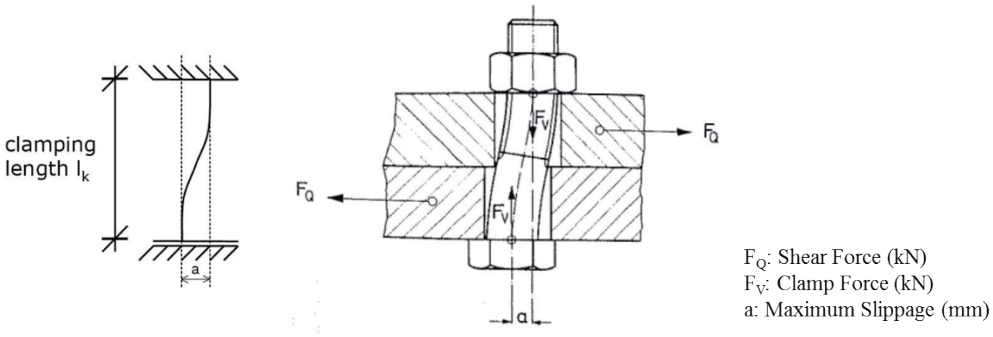


Figure 3.8 Vibration mechanism.

Self-loosening results in clamp loss in the assembly. Hence, loss of the clamp force is reported to analyze self-loosening event.

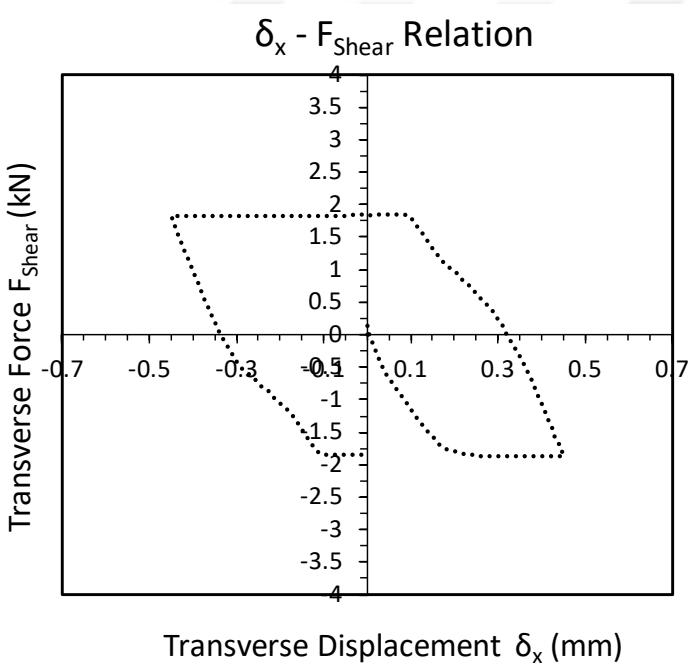


Figure 3.9 Change in transverse shear force against transverse displacement.

Figure 3.9 is a characteristic F_{shear} – *transverse displacement* plot that indicates a self-loosening or clamp-loss event. Basically, if the *clamp force* is equal to 15.9 kN and the *coefficient of friction* is 0.12, maximum *shear force* should be *15.9 x 0.12 = 1.908 kN*. If this value is lower, two mechanisms are meant to be occurred: first, clamp for is reduced, the second, friction is lowered or a lubricant is introduced. In most cases, it should be noted that the maximum value of F_{shear} can indicate clamp-loss, however, F_{shear} is influenced by bending moment! Bending moment should cause an embedment in the washer, thereby resultant moment should increase rapidly. So,

embedding should occur at any time. Let us to say that embedment is occurred just before a dramatic clamp loss and the bending moment increased the clamp force and F_{shear} value instantly. So, the maximum value of F_{shear} is increased. In such cases, the minimum value of the F_{shear} force that sliding is occurred, should be tracked and reported, rather than that of the maximum value of shear force.

In Figure 3.10, it can be clearly seen that clamp force is decreased while the joint members are in slide condition. So, F_{shear} gives the critical displacement value where complete slip occurs, but it does not give the total value of clamp-loss.

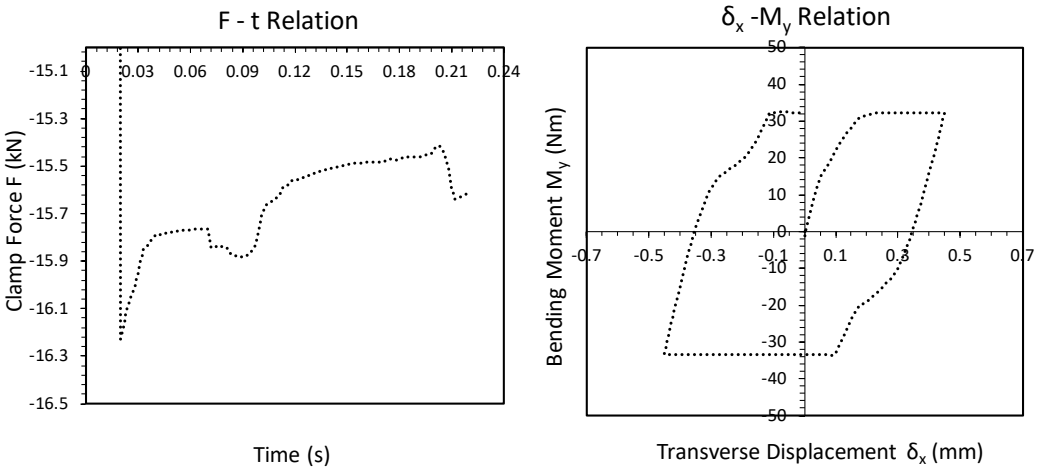


Figure 3.10 Clamp force and the bending moment – transverse displacement relation.

Pressure distribution on the washer-bolt head contact layer is shown in Figure 3.11. One can understand from this figure that (b) and (f) should be in the same position, but the patterns are different. So, slippage has to be occurred and there should be a loosening and clamp-loss.

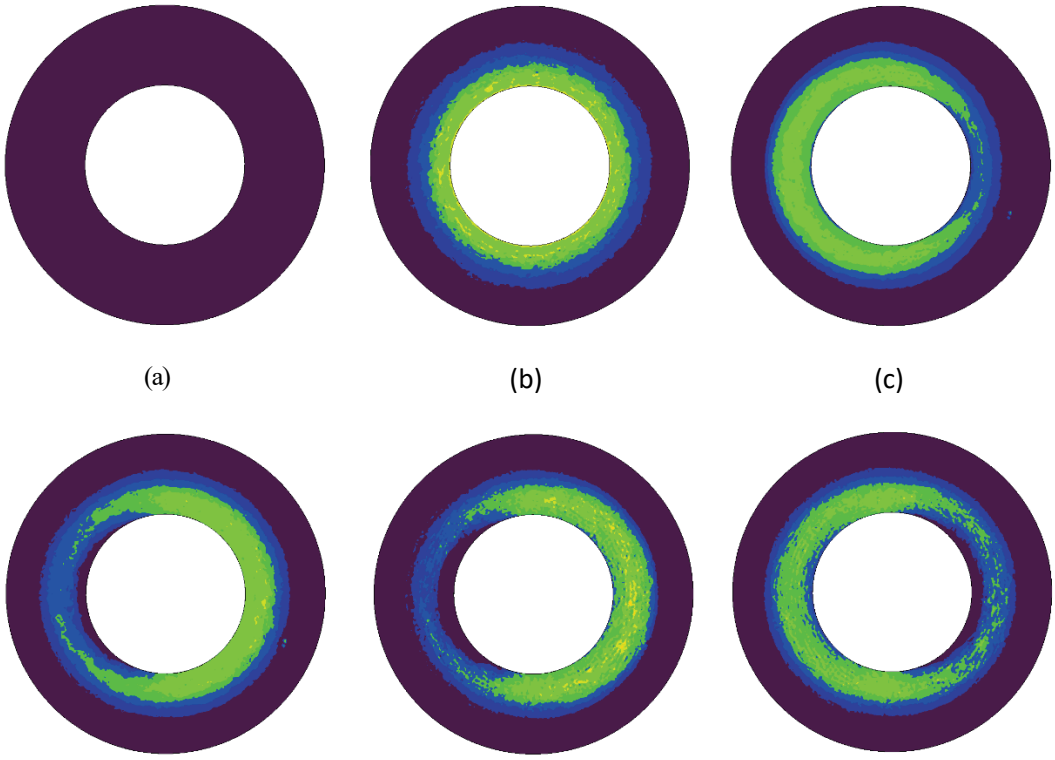


Figure 3.11 Pressure (contact normal stress) distribution on washer part. (Labels are referenced to Figure 3.3).

The result can be seen in Figure 3.12 that the slippage cause very small shift in *'Nut Plate'* which cause slightly different *transverse-displacement* – F_{shear} history.

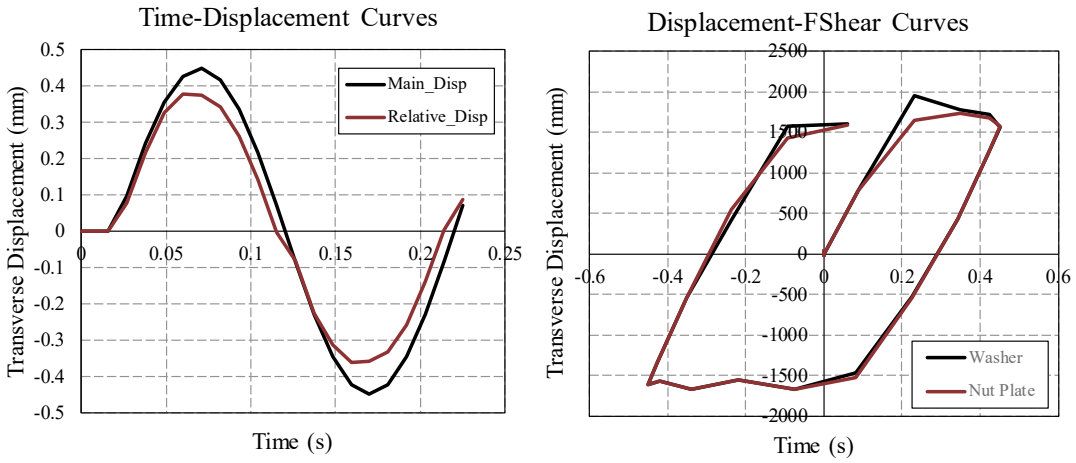


Figure 3.12 Relative displacements in joint members.

Up to this part of the Chapter, only the flat under-head form is simulated. From now on, other under-head shapes will be simulated. Maximum *clamp force* is set to 12.6

kN to eliminate excessive penetration problems. The purpose of this study is to understand if the simulation could be possible and feasible for long-term batch simulation jobs. Please see Figure A.1-2-3-4-5 in Appendices for technical drawings.

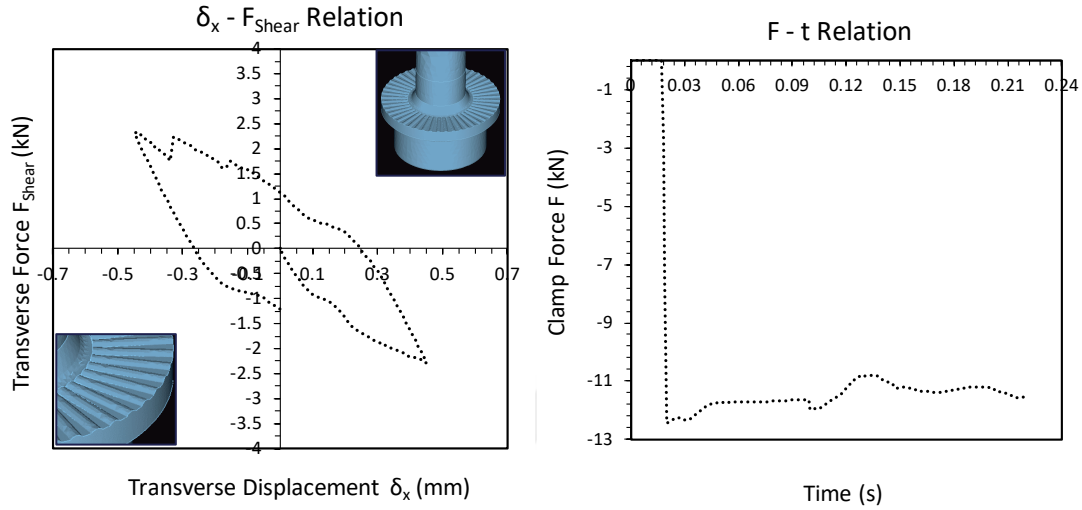


Figure 3.13 Round-ribbed pattern simulation results.

In the Figure 3.13, rounded rib shape is suitable for batch simulation cases. Noise in the F-δ_t plot can be smoothed with sensitivity analyses.

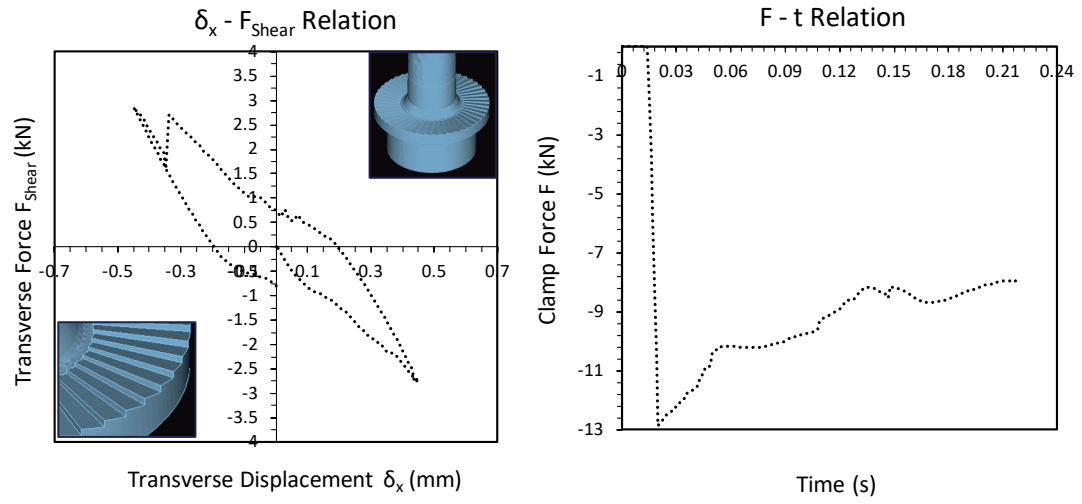


Figure 3.14 Serrated bolt under-head form clamp-loss analysis.

The under-head form given in Figure 3.14 cause more clamp-loss in the first cycle of the simulation. So, this geometry does not seem to be improved via batch simulations. The more clamp-loss simulation gives, the more error each increment produces.

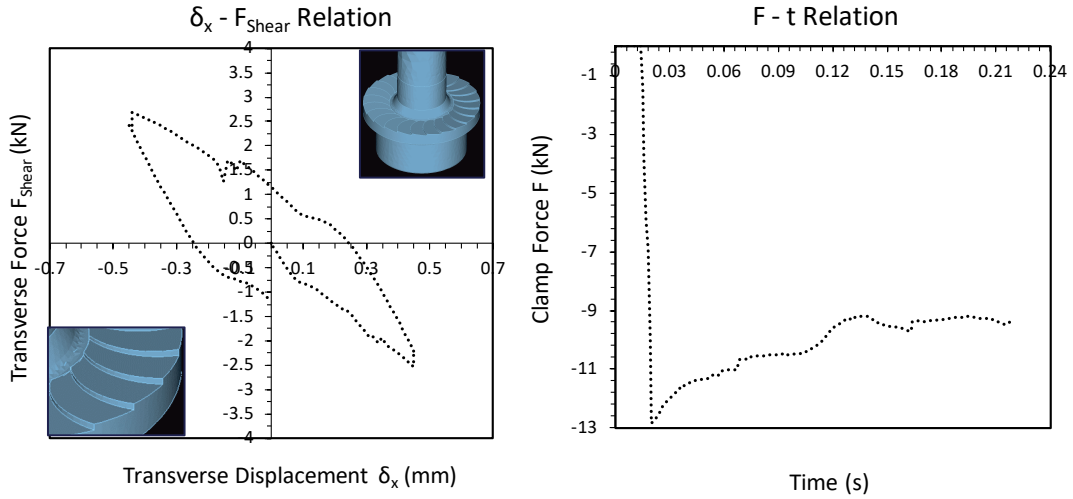


Figure 3.15 Flake-type serrations under the head of the bolt.

Flake-type (Figure 3.15) causes less clamp-loss than the one in the Figure 3.14. This form can be considered in the end of this Chapter.

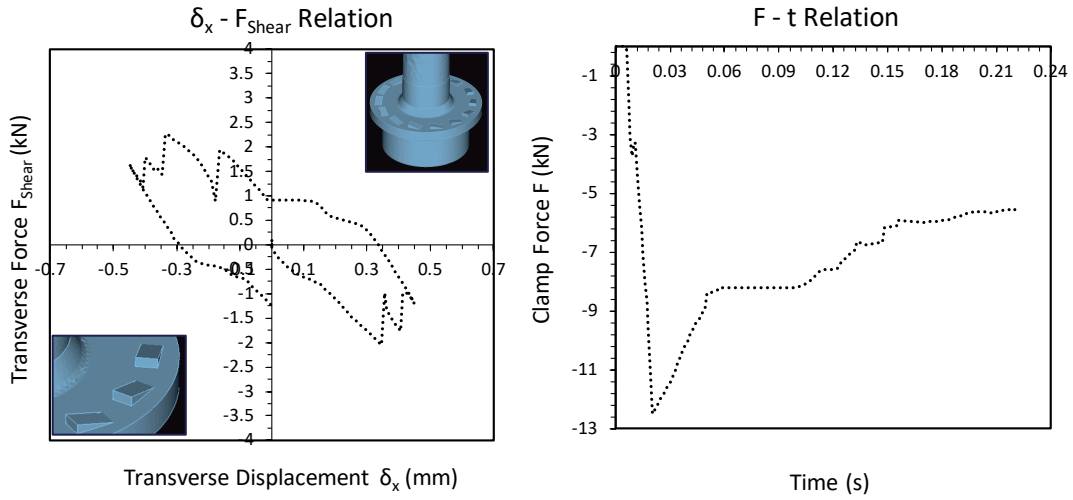


Figure 3.16 Circularly placed inclined small protrusions under the head of the bolt.

Small protrusions in the Figure 3.16 produce inconvincible clamp-loss. The main reason for clamp-loss is the inhomogeneous pressure distribution under the head of the bolt.

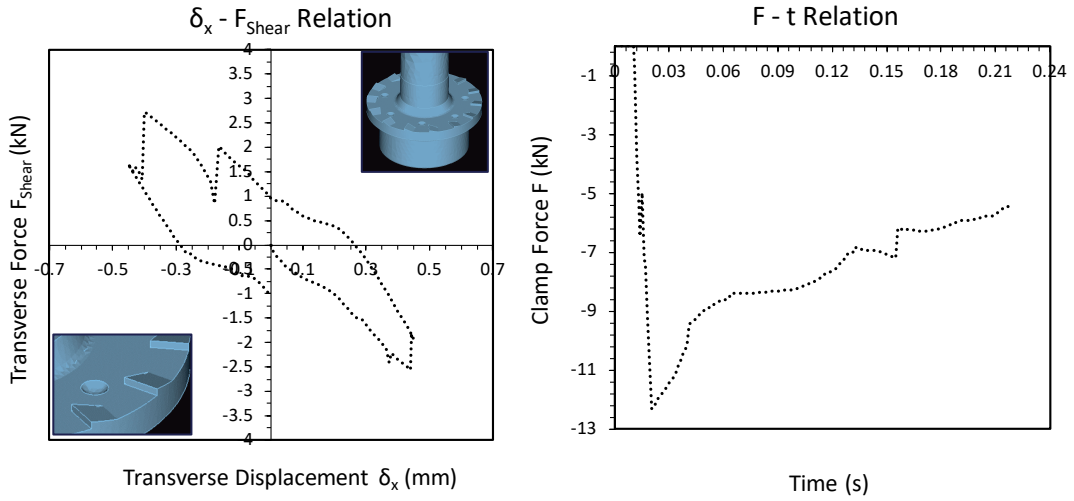


Figure 3.17 Circularly placed small protrusions and pits under the head of the bolt.

Additional small pits are added to the Figure 3.16 to restrain washer elements into these small pits (Figure 3.17). Therefore, washer and the bolt should be mechanically bonded and they will move together. Self-loosening ratio should expected to be decreased with this approach. Unfortunately, this geometrical design did not give the expected result. The model in Figure 3.17 causes too much clamp-loss in the assembly.

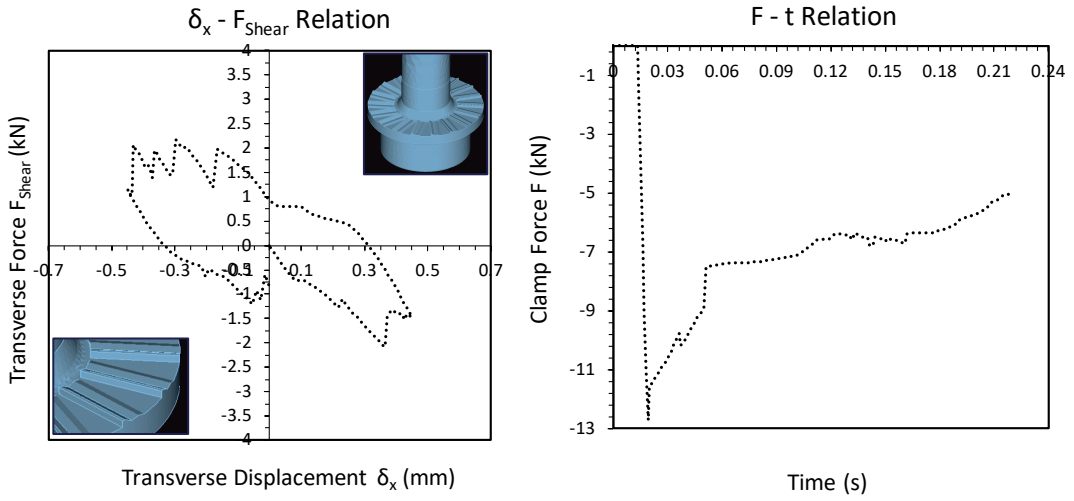


Figure 3.18 EP0187244A1 patented form results.

Stepped rip under-head form given in Figure 3.18 is even patented, but it does not seem to be useful in transverse and vibrational loading conditions.

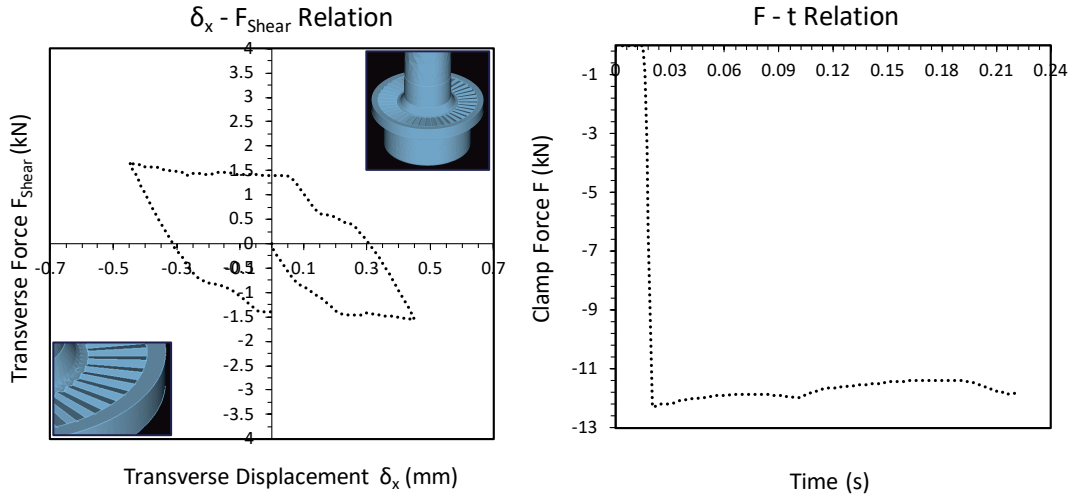


Figure 3.19 US 3605845 A and GB1326380A patented form.

In Figure 3.19, a very good under-head form is given and simulated under transverse displacements. This form produces very low clamp-loss and it should be used for optimization studies. The only thing against this form is the patent protection. So, patented forms should not be modified because of the claims of this patent. Another free-of-charge form has to be developed and improved in further studies.

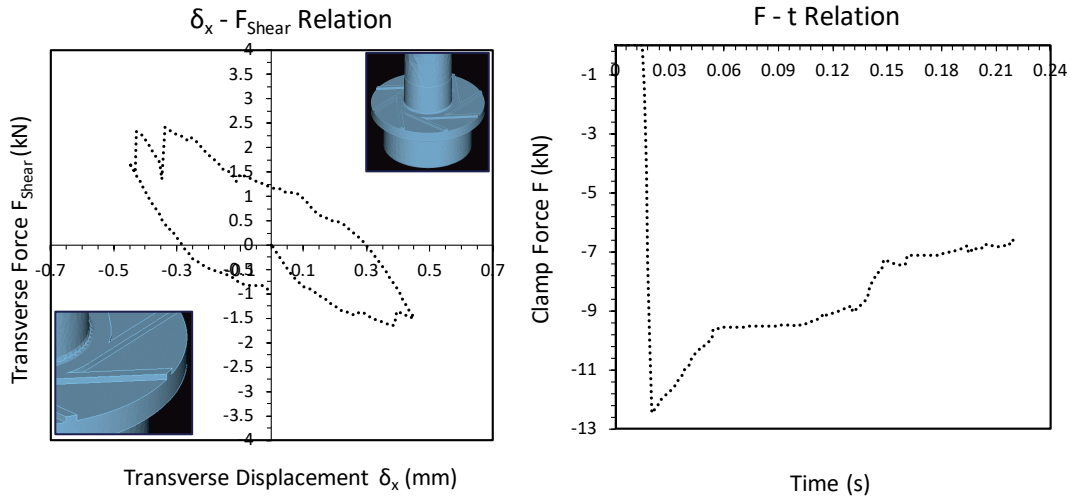


Figure 3.20 US5302066A patented form.

Figure 3.20 shows another patented under-head form that claims as if it prevents self-loosening of fasteners. Simulation results show that this form is not suitable for further studies even if it was not patented.

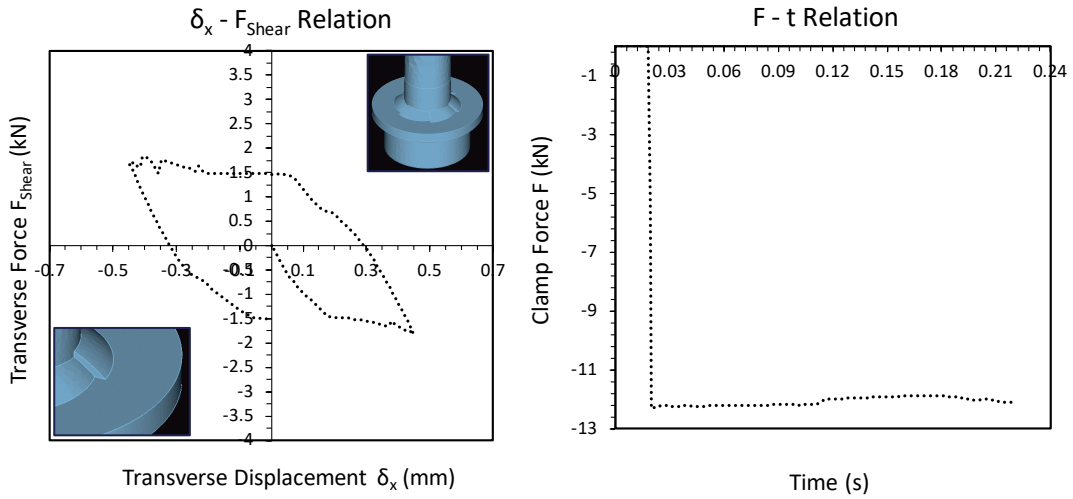


Figure 3.21 US2003077143A1 and US752628 patented forms.

The last successful under-head form is given in Figure 3.21. This form has the lowest clamp-loss value in all designs listed in this Chapter. Unfortunately, this form is also patented and it should not be modified due to the claims of patent document. Additionally, serial production and tooling costs seem like to be very high for this patented under-head design.

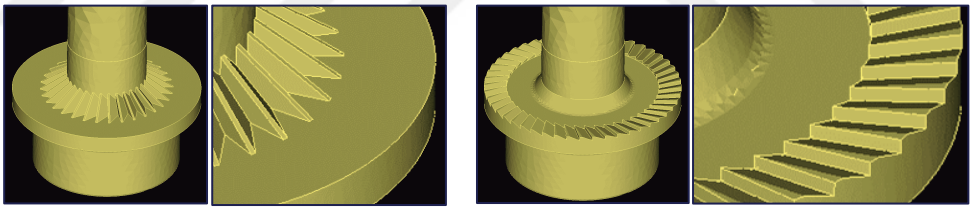


Figure 3.22 [US2003077143A1] (left) and [US 2959204 A - GB866556A] (right) patented forms.

The last two of patented vibration-resistant designs could not be listed for comparison. Unfortunately, these forms require very high concentration of mesh density. It is not feasible to work with these designs due to the excessive computational work.

Finally, only the Figure 3.13 and Figure 3.19 com to front as feasible solutions. Simulation studies will be focused on a free-of charge design around Figure 3.19. This model will be detailed in Chapter Five.

3.3 Conclusion

Vibration problem is successfully modelled and simulated in this Chapter. The following results are obtained for further use:

- Decrease in clamp force (clamp-loss) is a distinct result of self-loosening phenomenon.

- Clamp-loss is influenced by non-symmetrical or inhomogeneous pressure distribution under the head of the bolt. Sharp edges or protrusions can cause embedment on the washer surface that provides a hinged support which accelerates the rotational movement of fastener (bolt) body.

- The larger the protrusion diameter is, the higher the clamp-loss is. Hence, protrusions should be distributed homogeneously and should not be placed far from the longitudinal axis of the bolt.

- Developed simulation model can successfully predict the slip-stick condition between contact bodies. Contact bodies can be investigated separately by means of relative displacements. Further studies can purely and safely be built over this simulation model.

CHAPTER FOUR
AN OVERVIEW OF GENETIC PROGRAMMING

The problem that expressed in this thesis is a dynamic and complex problem. Genetic programming is known as fast, accurate method; it produces high quality results, and this method is widely used for solving these kinds of complex problems. Therefore, *genetic programming*-based *symbolic regression* method is used in this thesis.

4.1 Genetic Algorithm

Genetic algorithm (GA) is great method to reach solutions to complex problems. Genetic algorithms are based on the process of evolution by natural selection which has been observed in nature. They originally replicate the way that life uses evolution to find solutions to real world problems. Genetic algorithms can be used to find solutions to incredibly complicated problems.

Genetic algorithms search the solution domain by creating and developing a solution population. The greatest advantage of GAs over those based on sampling a single solution site is that they have the capacity to explore a wider area of the solution space with fewer objective function evaluations.

Genetic algorithms are search algorithms developed from the principle of natural selection. The algorithm has a population of sequences of a certain length. Each chromosome in the population represents a point in the solution space. These are also individuals who are candidates for survival through reproduction. The basic operation of the algorithm; solving unsuitable individuals, choosing more appropriate individuals to solve, and producing new individuals from selected individuals. When the operation of the algorithm is considered as a sequence, it is understood that the basic principle is elimination. The second principle is to get new solutions by using the individuals who survived from the elimination. This is achieved through exchange of information between individuals. Random information exchange between

individuals ensures that the search process continues at more appropriate points in the solution space (Telcioğlu, 2002, 2007).

The genetic algorithm, which is a heuristic method, may not find the optimum result for the problem; but it gives optimum (or very close to optimum) solutions, to the problems that cannot be solved by using known methods, or to the problems which have very long solution time if they are solved by using known methods.

Natural systems are fairly stable and robust. The best way to find out how your ability to adapt has progressed is the work on biological systems. It has been proved by theoretical and experimental studies that genetic algorithms can produce stable solutions when applied to complex search spaces. The most important reason for finding a wide range of application area in business and engineering, as well as various branches of science, is of course the simplicity it provides in calculations and the power to improve search operations (Telcioğlu, 2007).

While genetic algorithms are transformed into different forms within themselves, they differ from many traditional research and optimization methods in their basic structure. The most important differences according to Chipperfield (1997) are as follows;

- Genetic algorithms do research on the population in parallel, not single point research.
- Genetic algorithms use probability rules based on probability, but deterministic rules.
- Genetic algorithms work on a coded version of the problem, not over the parameter set itself. This does not apply to problems where real valued individuals are used.
- Genetic algorithms do not require derived information or other helpful information; they only influence from the direction of the study of the objective function and relevant relevance levels.

Genetic algorithm is a search algorithm based on parameter coding, trying to find solutions using random search techniques (Deb, 1996). The genetic algorithm gives optimum solutions when working with appropriate parameters for various problem types. In other words, the effectiveness of the genetic algorithm depends on the parameter values and methods used.

There are three operators in genetic algorithm. These are; selection operator, crossover operator and mutation operator.

4.2 Genetic Programming

Genetic programming is an extension of genetic algorithms. Genetic algorithms usually work on populations with binary sequences of fixed length. Genetic programming usually works on populations with tree structures that contain computer programs. Because genetic programming is concerned with the behavior of computer programs, the phenotype definition remains more short but to the point than genetic algorithms (Telcioğlu, 2007).

In genetic programming, mutation and crossover operators are structured in accordance with tree structure. The mutation is performed by selecting a random node. The sub-tree structure beneath the randomly selected node is deleted and a random new structure is enlarged instead (Takac, 2002).

The basic idea in genetic programming is the evolution of the "program" population. A program (an individual of a population) is usually shown as a tree with internal nodes as operators and end leaves as attributes. It is preferred over tree-type representations, graphs and other complex expressions (Gruau, 1992; Teller & Veloso, 1996).

Function and terminal cluster must contain the appropriate target problem properties. Function set; arithmetic operators, logic operators, and mathematical functions, the terminal cluster may contain problem-variables (attributes). For example, in the field of medicine, these qualities may have different definitions such

as signals, symptoms or patients (Bojarczuka, Lopesa, Freitasb, & Michalkiewiczc, 2004).

The introduction of genetic diversity is only at the tree-level, and for this reason, the formation must take place very carefully in order to bring out the appropriate structures. For example, tree-specific reproduction method is used for achieving genetic diversity in genetic programming. In this way, sub-trees can be exchanged, then the current constructions should always be produced. However, the application of other operators is not as efficient as high-occurrence mutation. And it can syntactically reveal the wrong structures. Obviously, the implementation of other operators, such as transport and sniffing, reveals various challenges. In addition, Koza has defined two separated tree structures as special operators. These are permutations and mutations. However, these operators are rarely used in genetic programming (Ferreira, 2002).

4.3 Genetic Programming-Based Symbolic Regression

Genetic programming is a strong technique to discover solutions for difficult problems. It provides an outline for the underlying concepts of GP which is reinforced by a description of a general framework for methodological stages that are associated with its implementation.

Computers are faster and more compact, modeling takes several hours or instead of days or weeks. Problems can be solved quickly and efficiently by using special software with their default parameters.

There are some more sophisticated and expert user-friendly software packages such as Eureqa® and GeneXproTools®, in the field of genetic programming. Such software packages have advantages as they are free or shareware for specific period of time, hence, they are very useful for experimentation and customization environments.

GP forms the set of equations. It works by implementing an algorithm which is embedded in the program, and it produces multiple solutions for the problem state. When the program is initiated, algorithm matches to a specific set of data, and it produces estimation equations in a very short period of time. These equations are

automatically checked by the software to see how well they perform. Then, small random changes are made to create a new solution sequence after checking the solution quality. This is a recurring process that continues until any user inter-action.

Operational controls of GP are analogous to biological evolution, the creation of populations, intergenerational evolution controlled by genetic operators, and the survival of the most powerful person. As a result, the terminology used in this section broadly reflects the terminology used to describe Darwinian evolution. Evolved equations are usually represented / stored in one or more hierarchically encoded computer codes, which function as small computer programs that can be executed using the appropriate software.

The GP now offers one of the best effort / award-winning data-driven modeling opportunities offered to researchers. Difficult and non-linear problems can be modeled without any assumptions about the mathematical form that a solution has to take and the type of relationship expected from the data in some cases.

GP is a scientific application that requires very careful application. Creates nonlinear problem solving equations quickly and robustly. Develop and report new and interesting solutions in an open and transparent manner. Depending on the difficulty of the problem, this program can sometimes produce in bad and complex models. However, bad models can be rejected and not taken into the solution set.

4.3.1 Symbolic Regression

GP is widely used to generate predictive models for a given problem with symbolic regression. This section focuses on symbolic regression.

Conventional regression is deterministic and always results in the same pattern or response when analyzed. The form of linear regression functions, the variables used to study the problem are fixed; the only part of Y that determines the regression over X_1 and X_2 is the coefficients a, b, and c as shown in the following equation:

$$Y = a + bX_1 + cX_2 \tag{4.1}$$

Koza (1990) simply suggests that the symbolic regression requires finding a function in a symbolic form that fits a specific sample of the dependent variable associated with given values.

While conventional regression is related to function fitting, symbolic regression is related to function discovery and fitting. Symbolic regression is stochastic and differs from each model produced by the latest model. All variables are dependent on the software settings and do not require any pre-setting.

The success of the symbolic regression is that it is data-driven, that the functional form of the natural system or solution is not a necessity, and these solutions are developed quasi-randomly using a data set that identifies the problem to be investigated.

In this way, some assumptions linking technical, statistical or mechanical modeling, as well as limitations related to polynomial or parametric regression and / or black box modeling, can be exceeded (Abrahart, 2014; Schmidt, Vallabhajosyula, Jenkins, Hood, Soni, & Wikswo, 2011).

4.3.2 Data Analysis in Symbolic Regression

The symbolic regression identifies the influential variables, estimates the parameters at several stages and include operator selection, model solving, and model selection (Aryadoust, 2015).

Operators: The symbolic regression initially produces a number of mathematical functions from the building blocks specified by the researcher (McRee, 2010).

These building blocks are based on a few mathematical functions or operations separated by three groups based on their complexity (Aryadoust, 2015):

1. Level 1 operators: simple functions such as addition (+), negation (-) and multiplication (*);

2. Level 2 and level 3 operators: more complex functions such as division (÷) and trigonometric and circular functions such as sine, cosine and tangential functions;

3. Level 4 and level 5 operators: highly complex functions such as exponential functions (eg, natural logarithm and square root) and inverse trigonometric functions such as arithmetic, arccosine and arctangent (Schmidt & Lipson, 2007).

Model solving: Following choice of operator, symbolic regression uses evolutionary algorithms (EA) that apply Darwin's theory of evolution, such as mating, reproduction, and selection. (Fogel & Corne, 1998; Schmidt & Lipson, 2008).

Symbolic regression starts with an initialization stage, that the first generation of mathematical functions potentially fitting the data ("solutions") is randomly generated and varied; next, the fit of each of these potential solutions is evaluated with reference to one or more fit indices (Gwiazda, 2006).

Based on the results of these fit indices, the fittest solutions are chosen as "parents," and reproduce new solutions ("offspring") for use in successive iterations ("generations").

Symbolic regression should preserve variety in successive generations of solutions; or else the process will end in "premature convergence" (Schmidt & Lipson, 2007; Schmidt, Vallabhajosyula, Jenkins, Hood, Soni, & Wikswo, 2011), immobility based on the primary convergence of solutions around a suboptimal solution point called a local optimum.

In this study, GP-based symbolic regression method is used. Eureqa® is the leading software package serving this method inside its built-in functions. Eureqa® (Nutonian, n.d.a), the software package uses three options: crossover, mutation, and age fitness Pareto optimization.

Figure 4.1 summarizes the above EA-based symbolic regression mechanisms applied in the Eureqa® software package.

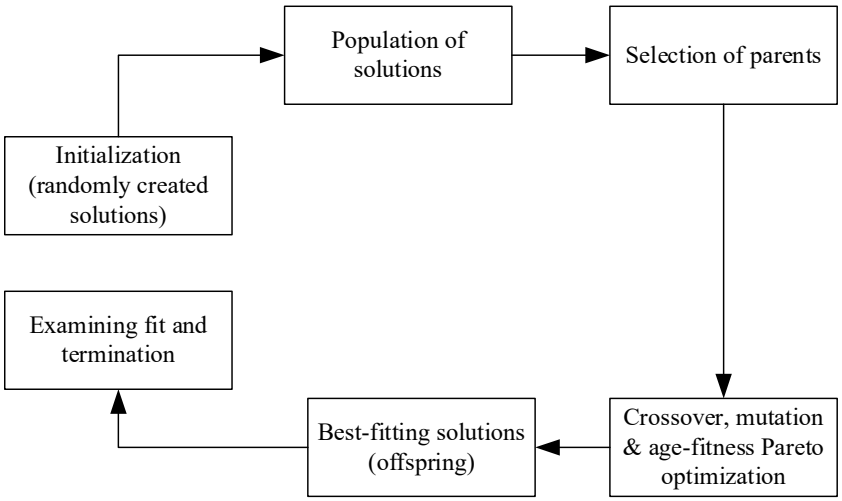


Figure 4.1 Schematic representation of EA-based symbolic regression as applied in Eureqa® software package. As the search progress, Eureqa® attempts to find a simpler solution with better fit (per the selected error metric) and discard more complicated and less accurate.

Eureqa® evaluates the solution verified in cross-validation with a second sample. The evaluation of a non-solution in a second sample that has not been tested, allows researchers to build stronger data theories because it provides more evidence for supporting a cross validation solution. In addition, this validation process can help researchers choose between competing solutions that fit equally well with test data (Zhang, Goh, & Kunnan, 2014).

Fit statistics: This issue is explained briefly in Chapter 5.4.

Each operator in the Eureqa® solutions assign a numeric value to indicate its complexity.

For example, addition and negation have a value of 1, whereas logistic and step functions have a value of 4. The total complexity of each solution is the sum of the complexity values of the operators used in that solution. As less complex models with low errors of measurement are desirable, sometimes the researcher has to make a trade-off between complexity and fit by choosing less complex models over more complex models with slightly better fit statistics (Schmidt & Lipson, 2007). The researcher can also base this decision on the sensitivity of each input variable, estimated according to its frequency of occurrence across all solutions, as well as the sensitivity or relative impact of each input variable on the output within each model.

Since *Genetic Programming* (GP) gives successful results, it is being preferred for solving complex real world problems. In this thesis, *self-loosening* behavior of fasteners under transverse vibrational loadings is investigated by using FE method, and loosening rate is estimated with a mathematical function. Simulation model is built to give ten distinct objective criteria which they are supposed to be in relationship with *loosening rate*. Simulation model is stated on the basis of a fastener (bolt) which has a ribbed under-head form having high vibration-resistance. Input parameters are selected relying on embodiment of the rib geometry under the head of the bolt, and mathematical equations for the results obtained, are investigated by using *Symbolic Regression* (SR) which is a sub branch of GP. SR is a well-studied method in GP for discovering free-form mathematical models from observed data. SR is one the most popular applications of genetic programming and an attractive alternative to standard regression approaches due to its flexibility in generating free form mathematical models from observed data without any domain knowledge. Indeed, user-friendly *genetic programming based symbolic regression* (GP-SR) tools such as Eureqa®.

CHAPTER FIVE
CASE STUDIES

In this chapter, the effect of geometrical specification of bolt under-head form is investigated by experimental studies. A special type of vibration testing machine is introduced in this chapter by which the experimental studies was carried out. CAD design systematics is given later on. Then, a detailed information about numerical simulations is given in the following section (5.3). Also, simulation section comprises the result of simulation sets, which are generated with automated macro codes. Crowning touches of genetic programming and regression modelling issues are given in section 5.4 and finally most powerful model which represents the whole experimental data is obtained by using genetic programming method. A genetic programming software tool called Eureqa® is used for detecting equations and hidden mathematical relationships in a given data set. Eureqa® works in order to reduce the error function, given by the discrepancy between the data and the generated model. Its goal is to identify the simplest mathematical formulas which could describe the underlying mechanisms that produced the data. It also allows to evidence the behavior of each solution with respect to its size. In this study, estimated models will be stated by using *genetic programming* method to represent loosening behavior of fasteners under transverse vibrational loading conditions. Simulation results will guide Eureqa® during estimation process. Full-factorial DOE method will be used in simulation studies. Simulations are run and estimation models are constructed according to this data set. At the end of this study, best objective function which is capable of estimating *loosening behavior* by using *genetic programming* method, will be obtained in the guidance of 10 different simulation outputs. More detailed explanations and all the steps carried out in this study, are given in the following pages.

5.1 Experimental Study

Experimental studies are divided into three subsections, determination of friction coefficient, measurement of penetration depth and transverse vibration tests. For both

studies, a set of bolt-nut connection is required. Hence, two types of bolts are produced for experimental studies.

M8x1.25x30 Serrated Bolt is selected for preliminary studies. Technical drawing is given in Figure 5.1. Due to the test machine limitations, product length is increased to 50 mm by adjusting ejector mechanism at the last forging station. Two versions of depicted fastener are produced, serrated (just like in drawing) and the flat under-head form, respectively. Flat version is produced by changing the serrated upsetting die with a flat upsetting die (please see Figures A.1-2-3-4-5 in Appendices).

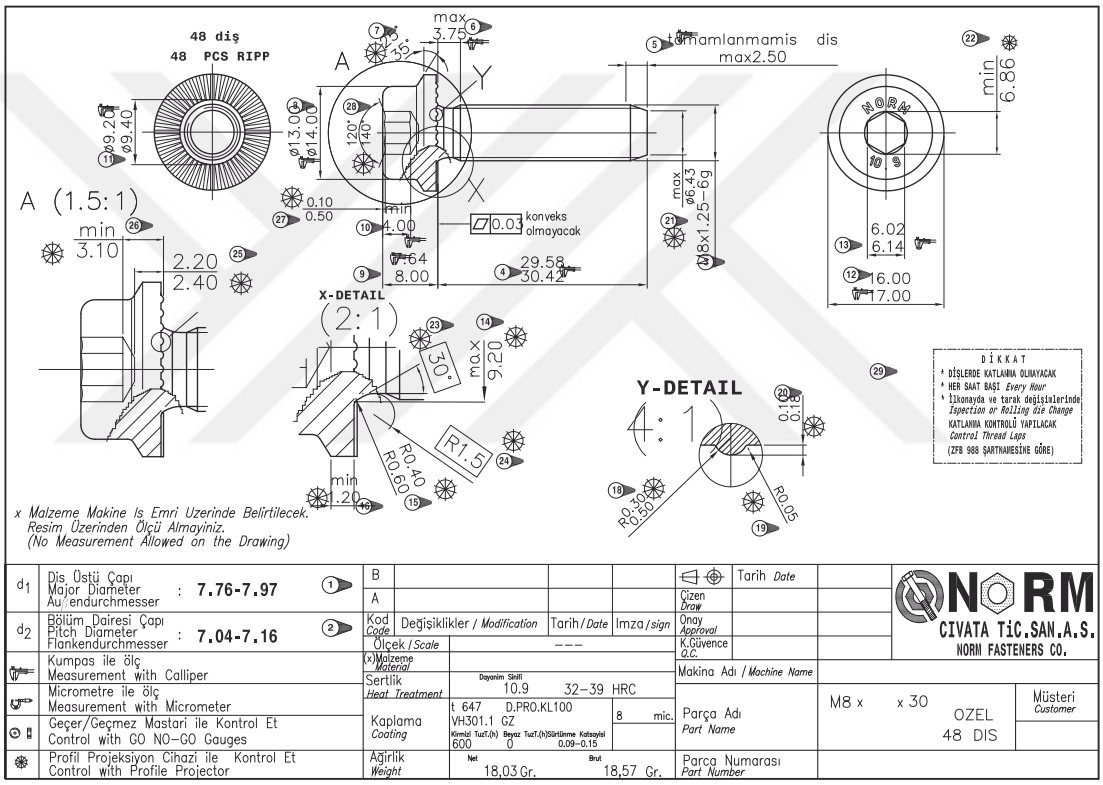


Figure 5.1 Specimen technical drawing.

5.1.1 Determination of Friction Coefficient

While tightening a bolt, a torque energy is applied to the bolt head. This energy travels through bolt body and concentrates at two main locations, under-head friction area and the thread friction area. Thread friction is the friction value between mating threads. Under-head friction is the friction value between the bearing material of the bolt and the adjacent clamping plate or, the nut and the adjacent clamping plate

depending on which is rotated for tightening; bolt or the nut. The total friction coefficient is the value describing the overall friction in the clamped assembly parts of bolt, nut and the bearing component. The equations are gathered from ISO 16047 specification – *Fasteners – Torque/clamp force testing*.

Figure 5.2 illustrates the torque components, where M_A is the '*Applied Torque'*, M_{br} is the *'Bearing Torque'*, M_{Th} is the *'Thread Torque'* in the equation (5.1). μ_{th} is the '*Thread Friction Coefficient'*, μ_{br} is the *'Bearing Friction Coefficient'*, μ_{total} is the *'Total Friction Coefficient'*, F_{Clamp} is the *'Clamp Force'*, D_{br} is the *'Bearing Diameter'*, D_h is the *'Hole Diameter'*, D_w is the *'Outer Bearing Surface Diameter'* and P is the *'Pitch Height of Threads'*. The formulation is given in the set of equations down below (5.1-5):

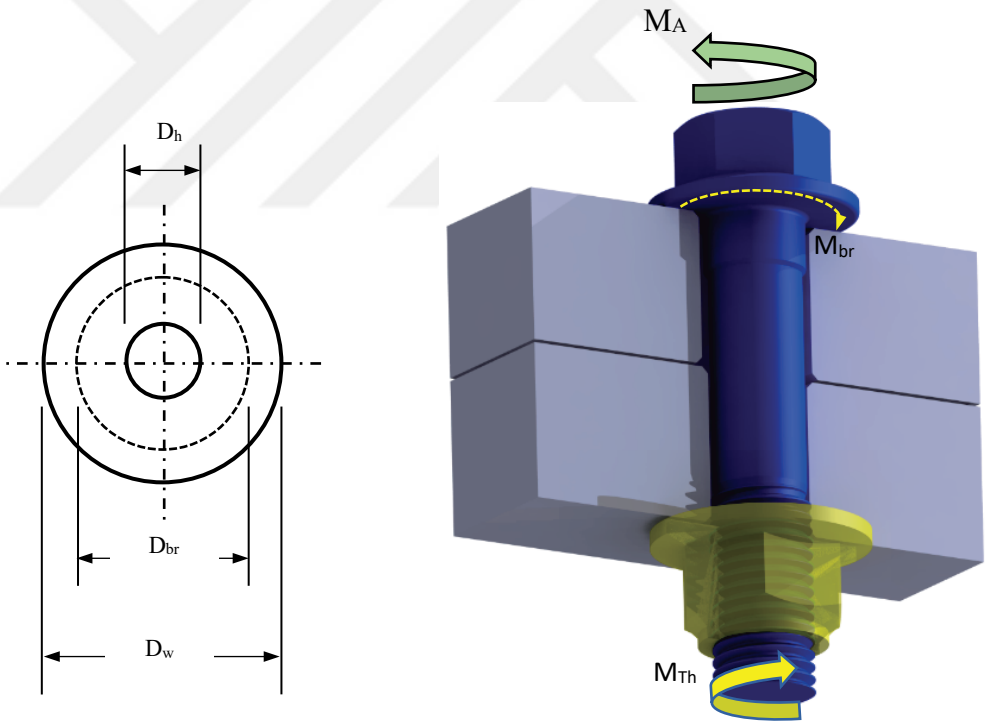


Figure 5.2 Torque and friction coefficient formulas.

$$M_A = M_{br} + M_{Th} \tag{5.1}$$

$$\mu_{th} = \frac{\left(\frac{M_{Th}}{F_{Clamp}}\right) - 0.159P}{0.578d_2} \tag{5.2}$$

$$\mu_{br} = \frac{2\left(M_A - M_{Th}\right)}{D_{br}F_{Clamp}} \tag{5.3}$$

$$\mu_{total} = \frac{\left(\frac{M_A}{F_{Clamp}}\right) - 0.159P}{0.578d_2 + \left(\frac{D_{br}}{2}\right)} \tag{5.4}$$

$$D_{br} = \frac{\left(D_h + D_w\right)}{2} \tag{5.5}$$

Coefficient of friction is determined by using two kinds of testing machines. First machine (Schatz, Figure 5.3) is able to calculate both bolt under-head friction coefficient and thread friction coefficient, separately.

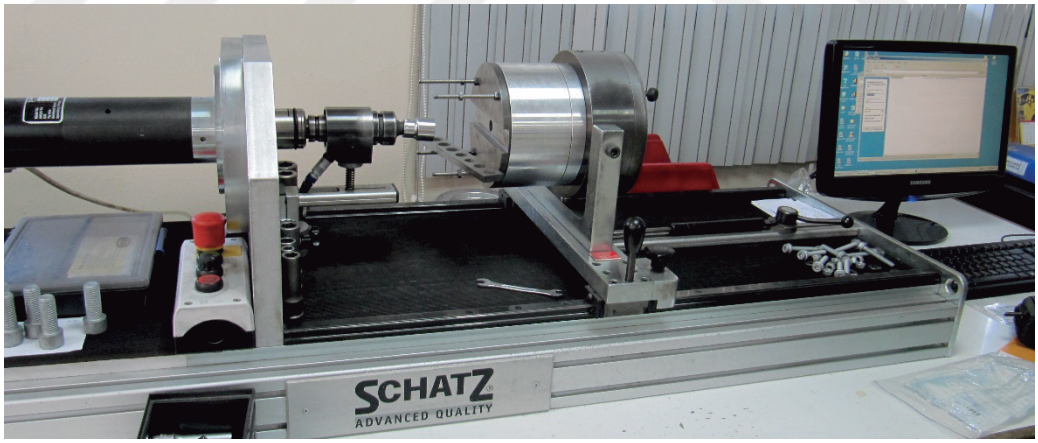


Figure 5.3 Schatz friction coefficient testing machine.

Test specimens are given in Figure 5.4.

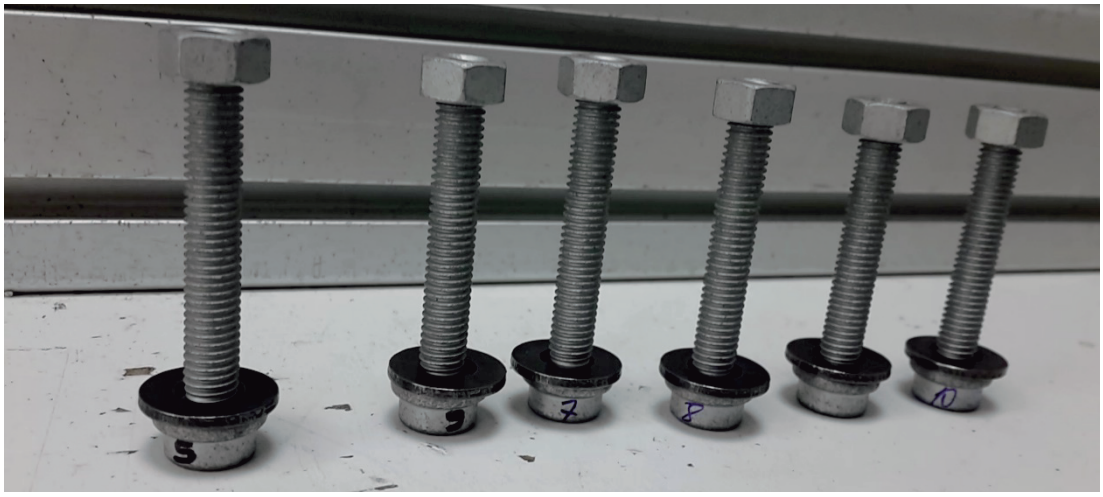
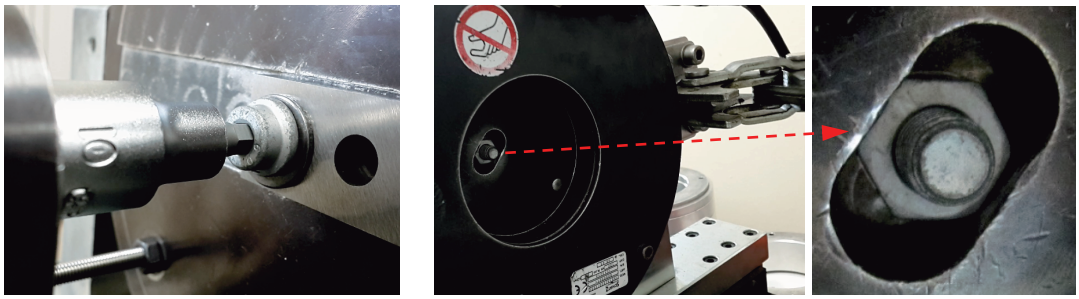


Figure 5.4 Test specimens; flat plain washers are used in experiments.

Test specimens are placed onto the test platform as shown in Figure 5.5. It is very important that nut has to be fixed to ensure fixed constraint conditions. Because, if there is a relative rotational movement on the nut-seating surface, applied torque will be divided into three sections of those bolt under-head surface friction, bolt-nut thread friction and the nut seating surface friction which the last one is not supposed to be calculated. As soon as a relative motion under the seating surface of the nut, a distinct decrease in the torque value will be observed in the driving tool. This situation should be validated thru the change in electric current of screw-driver.



(a) (b) (c)

Figure 5.5 Test platform; bolt under-head (a), nut fixture-fixed (no rotation allowed for nut) (b, c).

Test parameters are given in Table 5.1. Plain washer is used for measuring penetration depth of serrations and for understanding if there is a relation between penetration depth and self-loosening event.

Table 5.1 Friction test parameters.

Friction Test Parameters	[SERRATED]	[FLAT]
Fastener Identity	M8x1.25x50 (10.9)	M8x1.25x50 (10.9)
Coating	Delta Protekt® KL100 - VH301.1 GZ	Delta Protekt® KL100 - VH301.1 GZ
Washer Hardness [HV]	380	380
Bearing Diameter [mm]	12.35	14.65
Clamp Length [mm]	35	35

All parameters are fixed to reveal the effect of serrations against self-loosening of fasteners. The most effective parameters are the clamp length, coating material, bearing diameter and the washer hardness. Delta Protekt® is a lamellar zink-flake coating which zink-flakes are scarified for steel corrosion. VH301.1 GZ corresponds to the lack material which homogenize the coefficient of friction on the entire surface of the coated material.

Total of 12 specimens are tested for friction coefficient, 6 for flat and 6 for serrated under-head form. Friction results are given in Table 5.2 with statistical results.

Table 5.2 Schatz friction test results.

F L A T					TOTAL	Thread	Head
Sub-series #1	Ts Step 1	Tq Step 1	TqT Step 1	TqH Step 1	μ tot Step 1	μ th Step 1	μ h Step 1
Nr	kN	Nm	Nm	Nm			
Max.					0,15	0,16	0,16
Min.					0,09	0,08	0,08
1	22,83	39,3	16,41	22,89	0,13	0,13	0,14
2	22,8	38,73	17,77	20,96	0,13	0,14	0,13
3	22,8	37,25	16,8	20,45	0,13	0,13	0,12
4	22,81	38,66	18,33	20,33	0,13	0,15	0,12
5	22,82	36,98	16,1	20,88	0,12	0,12	0,12
6	22,8	37,5	16,72	20,78	0,13	0,13	0,12
Sub-series #1	Ts Step 1	Tq Step 1	TqT Step 1	TqH Step 1	μ tot Step 1	μ th Step 1	μ h Step 1
n = 6	kN	Nm	Nm	Nm			
x	22,81	38,07	17,02	21,05	0,13	0,13	0,13
s	0,01	0,95	0,85	0,94	0	0,01	0,01
Min.	22,8	36,98	16,1	20,33	0,12	0,12	0,12
Max.	22,83	39,3	18,33	22,89	0,13	0,15	0,14
R	0,03	2,32	2,23	2,56	0,01	0,02	0,02

S E R R A T E D					TOTAL	Thread	Head
Sub-series #1	Ts Step 1	Tq Step 1	TqT Step 1	TqH Step 1	μ tot Step 1	μ th Step 1	μ h Step 1
Nr	kN	Nm	Nm	Nm			
Max.					0,15	0,16	0,16
Min.					0,09	0,08	0,08
1	22,83	37,24	15,7	21,55	0,14	0,12	0,15
2	22,83	34,92	15,9	19,02	0,13	0,12	0,13
3	22,84	37,9	18,58	19,32	0,14	0,15	0,14
4	22,83	36,71	16,2	20,51	0,14	0,13	0,15
5	22,8	38,44	18,77	19,66	0,14	0,15	0,14
Sub-series #1	Ts Step 1	Tq Step 1	TqT Step 1	TqH Step 1	μ tot Step 1	μ th Step 1	μ h Step 1
n = 5	kN	Nm	Nm	Nm			
x	22,83	37,04	17,03	20,01	0,14	0,13	0,14
s	0,01	1,35	1,51	1,02	0,01	0,02	0,01
Min.	22,8	34,92	15,7	19,02	0,13	0,12	0,13
Max.	22,84	38,44	18,77	21,55	0,14	0,15	0,15
R	0,03	3,52	3,08	2,53	0,02	0,03	0,02

The second testing machine is the Atlas CopCo. friction tester. In these tests, bolt-nut connection is set–up for nut-driven application. Hence, washer and bolt is supposed to be fixed and only the nut is moveable around the bolt axis. At the end of these tests, friction coefficient will be calculated very low because of the relative motion between bolt under-head and the washer surfaces which is undesired. The purpose of this test is to determine the penetration of the serrations under the head of the bolt. This machine has two transducers, the first one is the torque sensor which measures the

twisting strain of the bushing (this is the applied torque also) and second one is the axial load-cell which measures the clamp load. This test will show-up the penetration depth at certain clamp force, that's why this machine is used for tests.



(a) (b) (c) (d) (e)

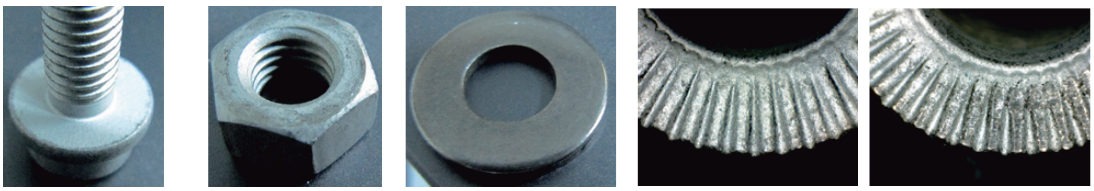
Figure 5.6 Atlas CopCo. test platform (a), electric torque wrench controller (b), test specimen (c), clamp condition (d), nut-driven torque application (e).

The clamped-end is shown in Figure 5.6 which the torque is applied from. Torque is applied at 5 RPM of constant angular velocity. Test results are given in Table 5.3. It must be noted that these results are not usable due to the relative motion between both [the bolt under head]- [washer surface] and [nut seating surface] – [test machine clamp surface].

Table 5.3 Friction test results (Atlas CopCo.).

No	Torque [Nm]	Preload [kN]	Friction Coefficient	No	Torque [Nm]	Preload [kN]	Friction Coefficient
1	38.30	35.75	0.082	1	37.30	33.87	0.085
2	38.00	35.95	0.081	2	38.00	36.01	0.081
3	36.60	35.05	0.080	3	36.90	34.17	0.083
4	36.90	32.99	0.087	4	37.70	36.58	0.078
5	37.40	34.92	0.082	5	28.70	25.62	0.087
			0.082				0.083

It can clearly be seen from the Figure 5.7 (a-b and c) that an inevitable relative motion took place slightly between flat bolt under-head surface and the flat washer surface.



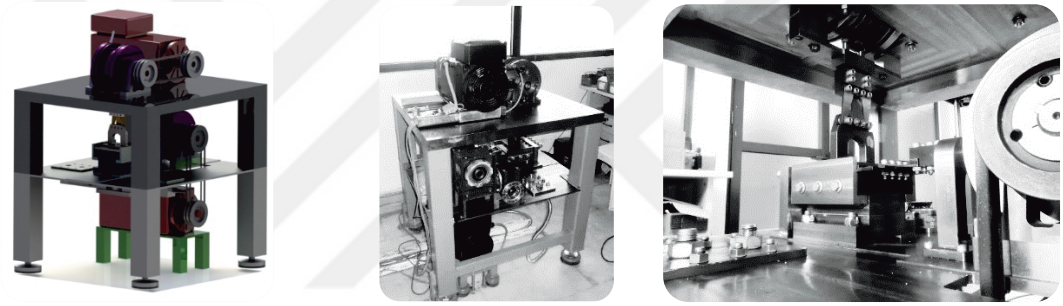
(a) (b) (c) (d) (e)

Figure 5.7 Surface conditions after experiments; flat under-head (AtlasCopCo) (a), nut seating surface (AtlasCopCo) (b), washer (c), serrated bolt under-head before test (d), serrated bolt under-head after test (e).

It is clear that this relative motion reduces the total friction coefficient which is calculated during tightening process. Because the software assumes that only one body is active for motion during tightening process, and that is the bolt or the nut, not both of them.

5.1.2 Transverse Vibration Tests

Vibration tests are performed by using the bi-axial vibration testing machine (Figure 5.8) which is developed under a TUBITAK-TEYDEB 1511 scientific project that is protected with a *Utility Model* since 2015. This Utility model is a property of Norm Fasteners Co.



(a) (b) (c)

Figure 5.8 Bi-axial vibration testing machine.

Vibration mechanism relies on the eccentric sinusoidal motion of a cam drum which is directly connected to the electric motors. Clamp load is read by two couple of load-cells as shown in Figure 5.9. Slip distance is configured by adjusting the eccentricity of the cam shaft and transmitted thru follower bearing as in the Figure 5.10 (right). Vibration test parameters are shown in Table 5.4.

Table 5.4 Vibration test parameters.

Fastener Identity	M8x1.25x50 (10.9)
Coating	Delta Protekt® KL100 - VH301.1 GZ
Washer Hardness [HV]	380
Friction Coefficient	0.13 Flat / 0.14 Serrated
Clamp Length [mm]	30
Preload [kN]	14.3
Relative Transverse Displacement [mm]	0.45
Frequency [Hz]	5

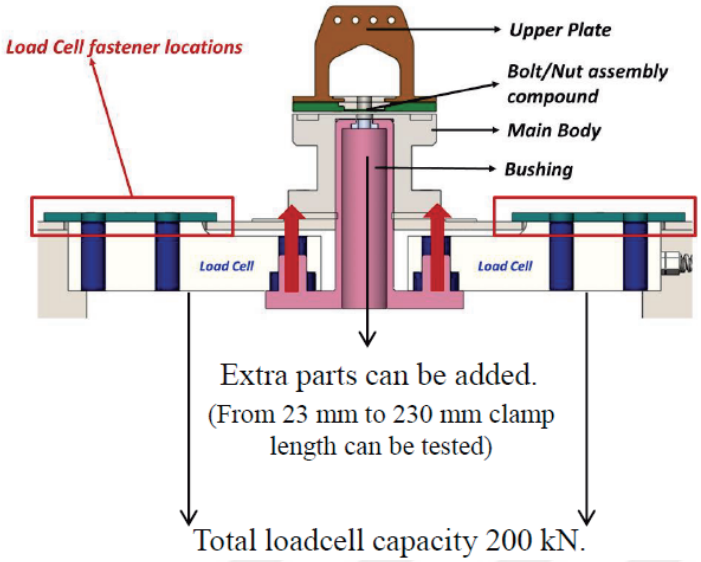


Figure 5.9 Load-cell and vibration mechanism.

Load-cells are placed at equal distance from the central axis of the bolt specimens. Load-cells report to the computer and a Java-based software collects data from both load-cells, motor and the laser distance measurement device thru communication ports.

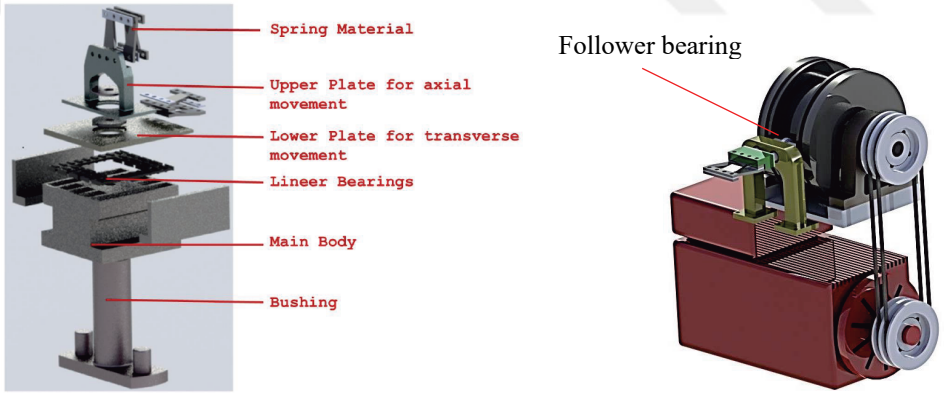


Figure 5.10 Clamp and transverse loading mechanism.

Transverse displacement is acquired via follower bearing which has an exact eccentricity that set to the *'Transverse Displacement'*. An exploded view of the clamping mechanism is depicted in Figure 5.10.

A total of 10 specimens are tested for transverse vibration. Tests are continued up to 2000 cycles.

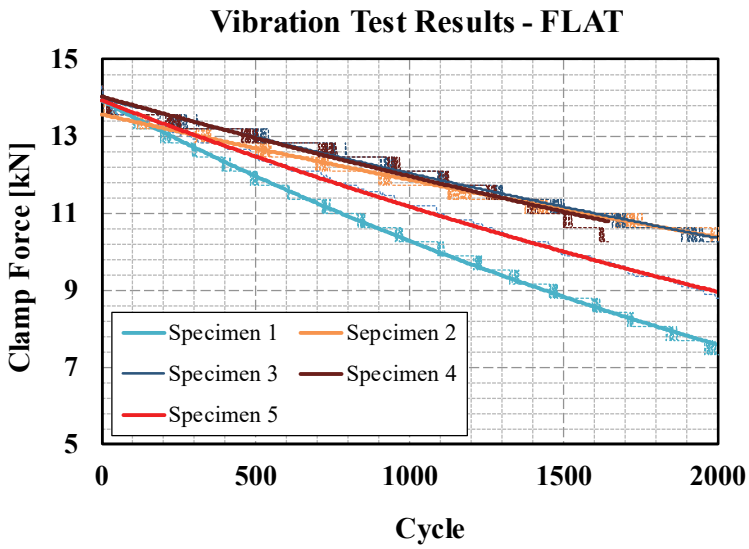


Figure 5.11 Vibration test results (flat under-head form).

Flat under-head form has lost min. 4.1 kN to max. 6.8 kN of its clamp force at 2000 cycles (Figure 5.11). Serrated under-head form has lost min. 0.7 kN to max. 3.2 kN of its clamp load (Figure 5.12).

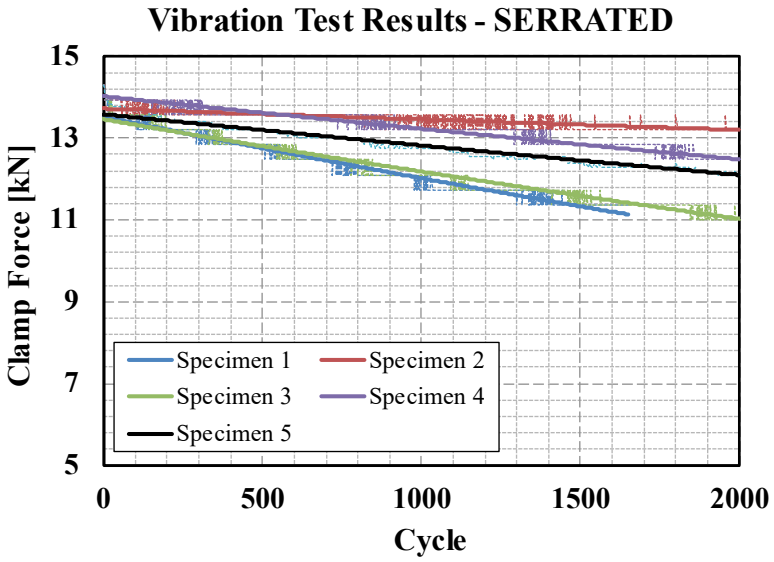


Figure 5.12 Vibration results (serrated under-head form).

Mean values of the results that given in Figure 5.11-12, belongs to the flat and serrated under-head forms, are plotted in Figure 5.13.

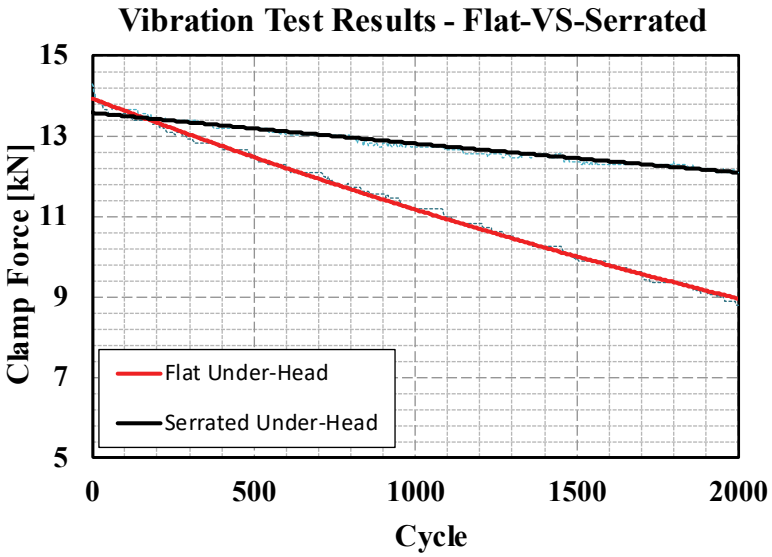
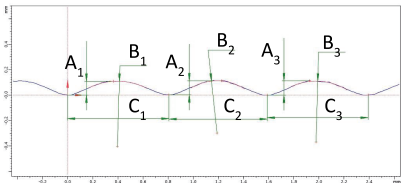


Figure 5.13 Vibration results (mean values of flat vs serrated).

According to the Figure 5.13, it can be clearly seen that serrated under-head form is more sustainable than the flat one.

5.1.3 Penetration Depth

Penetration depth is measured before and after tests. Long-distance measurements such as bolt under-head rib profile measurements are done via *Mahr Perthometer* device. Results are given in Figure 5.14. Small protrusions and carvings are measured with more sophisticated and accurate device: *Mitutoyo SJ-401* surface roughness measurement device. Results are given in Figure 5.16.



Friction [Schatz]

	Spec.	A			B			C			MEAN		
	No	A_1	A_2	A_3	B_1	B_2	B_3	C_1	C_2	C_3	A	B	C
1	A-01	0.11	0.11	0.11	0.51	0.41	0.48	0.81	0.78	0.80	0.11	0.47	0.80
2	A-02	0.13	0.11	0.12	0.44	0.41	0.44	0.79	0.79	0.78	0.12	0.43	0.79
3	A-03	0.13	0.12	0.11	0.40	0.39	0.47	0.81	0.76	0.82	0.12	0.42	0.79
4	A-04	0.12	0.12	0.12	0.52	0.44	0.55	0.79	0.78	0.83	0.12	0.51	0.80
5	A-05	0.15	0.11	0.12	0.51	0.48	0.45	0.85	0.79	0.78	0.13	0.48	0.81
	MEAN	0.13	0.11	0.12	0.48	0.43	0.48	0.81	0.78	0.80	0.12	0.46	0.80

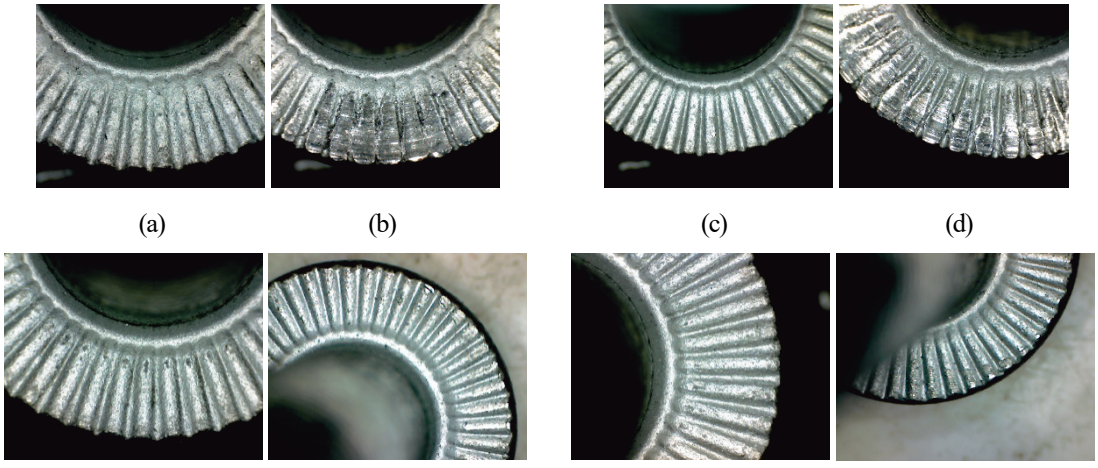
Vibration

	A			B			C			MEAN		
Spec. No	A_1	A_2	A_3	B_1	B_2	B_3	C_1	C_2	C_3	A	B	C
6	0.13	0.12	0.13	0.55	0.51	0.45	0.83	0.80	0.82	0.13	0.50	0.81
7	0.14	0.13	0.13	0.63	0.52	0.47	0.89	0.82	0.80	0.13	0.54	0.84
8	0.13	0.14	0.13	0.49	0.47	0.46	0.81	0.81	0.86	0.13	0.47	0.83
9	0.14	0.12	0.13	0.53	0.57	0.57	0.86	0.82	0.80	0.13	0.56	0.83
10	0.13	0.14	0.16	0.43	0.48	0.49	0.82	0.83	0.92	0.15	0.47	0.86
MEAN	0.13	0.13	0.14	0.53	0.51	0.49	0.84	0.82	0.84	0.13	0.51	0.83

Friction [AtlasCopCo]

	A			B			C			MEAN		
Spec. No	A_1	A_2	A_3	B_1	B_2	B_3	C_1	C_2	C_3	A	B	C
11	0.12	0.13	0.12	0.41	0.41	0.46	0.85	0.79	0.79	0.12	0.43	0.81
12	0.14	0.13800.134		0.62	0.48	0.48	0.82	0.82	0.80	0.14	0.53	0.81
13	0.13	0.14	0.13	0.45	0.40	0.51	0.79	0.80	0.86	0.13	0.46	0.82
14	0.15	0.13	0.12	0.56	0.51	0.47	0.90	0.82	0.78	0.13	0.51	0.83
15	0.12	0.12	0.12	0.55	0.41	0.45	0.78	0.78	0.79	0.12	0.47	0.78
MEAN	0.13	0.13	0.12	0.52	0.44	0.47	0.83	0.80	0.80	0.13	0.48	0.81

Figure 5.14 Rib depth under the head of the bolt, after friction and vibration tests; depth of ribs (A), rip radius (B), pitch of ribs (C). All measurements are taken by using Mahr Perthometer device.



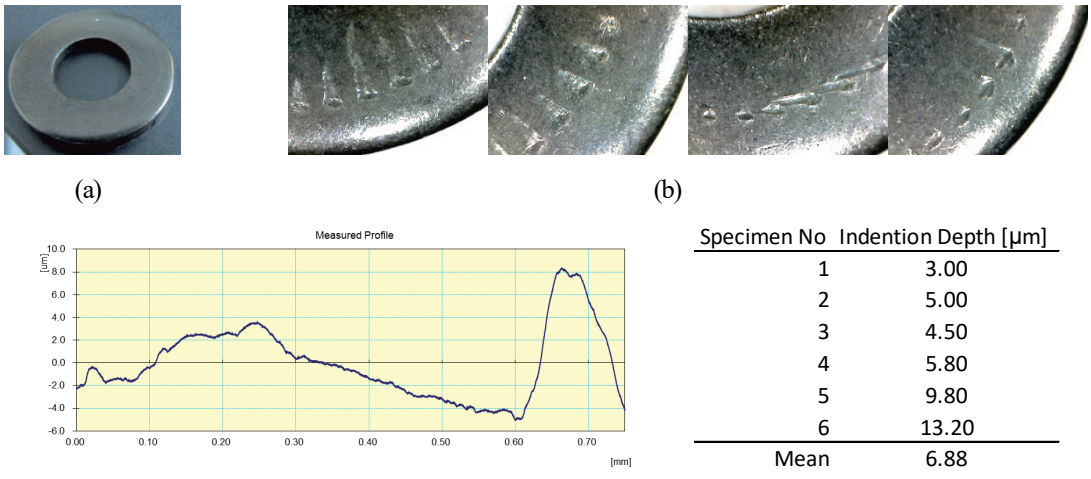
(a) (b) (c) (d)

(e) (f) (g) (h)

Figure 5.15 Rib conditions; before (Schatz) friction test (a-c), after Schatz test (b-d), before vibration test (e-g), after test (f-h).

Schatz testing machine fixes the nut and tightens bolt by rotating it around bolt axis. So, at high clamp forces, under-head serrations are deformed as shown in Figure 5.15 (a-b) and (c-d). Vibration does not cause any plastic deformation on the rib, unless there is no relative displacement between washer and bolt under-head surface.

Starches on the washer-bolt under-head interface layer is measured with surface measurement device as shown in Figure 5.16.



(a) (b)

(c)

Specimen No	Indention Depth [µm]
1	3.00
2	5.00
3	4.50
4	5.80
5	9.80
6	13.20
Mean	6.88

(d)

Figure 5.16 Indention depth after friction tests (Atlas CopCo.) measured by Mitutoyo SJ-401 surface roughness measurement device. Flat washer coupled with flat under-head bolt (a), serrated under-head bolt (b) and measurement results (c-d).

Consider the third figure from left in Figure 5.16 (b) that the embedment cavities are slipped due to the relative motion of bolt-washer under-head surface. This situation is discussed in previous sections.

5.2 Data Set & CAD Model

In this section, an adequate data set structure is constructed to be used in parametric-CAD, CAE models and in symbolic regression analysis that is based on genetic programming method.

CAD data is generated in CATIA V5 by using *'Visual Basic'* programming environment. Model is constructed under the guidance of parametric design parameters which is depicted in Figure 5.17. Macro code consists of three stages. In the first stage, design variables are read from *'data.csv'* provided by *'Design of Experiment'* study as described in previous sections. Macro code is built over a parametric template model that A, B, C and D can be replaced easily. In the second stage, these parameters are updated. In the last stage, macro-code generates STL, STP and IGS files of those are fully compatible with Simufact® Forming GP CAD interface. Build-in CADFix® detects and fixes open-surface and stitching problems during the import stage of simulations. STL mesh models are generated and refined in *'STL Rapid Prototyping'* module in CATIA V5 (Figure 5.19). Refinement is carried out by selecting the minimum edge length, and that is about 0.3 to 0.6 mm's.

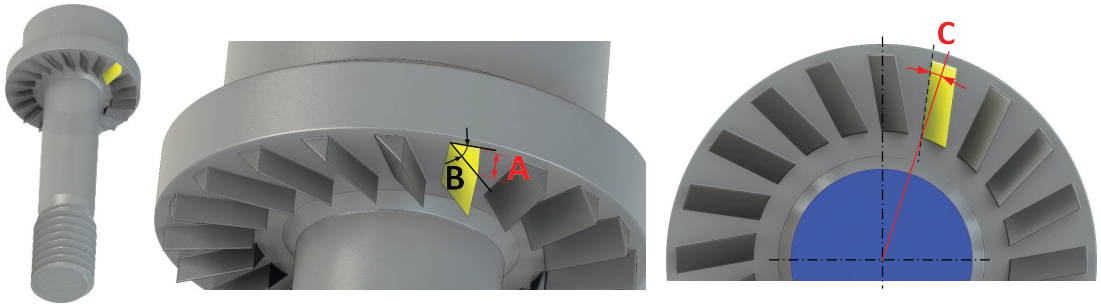


Figure 5.17 Parametric CAD model.

Depending on the model depicted in Figure 5.17 there are 4 parameters are used in the simulation and estimation models. Parameters and objective criteria are given in Table 5.5.

Table 5.5 Design variables.

Code	Input variable	Code	Output variables*
A	Depth of a rib (mm)	*CL*	Clamp loss (kN)
B	Flank angle of a rib (deg)	*FSBH*	$F_{shear\ at\ bolt\ head}$ (kN)
C	Inclination angle of a rib (deg)	*FSNS*	$F_{shear\ at\ nut\ surface}$ (kN)
D	Number of ribs	*FSMI*	$F_{shear\ (min)}$ (kN)
		FSMA	$F_{shear\ (max)}$ (kN)
		RSDLH	Relative slip distance to the left hand side (mm)
		RSDRH	Relative slip distance to the right hand side (mm)
		RMAS	Relative maximum slip distance (position at the end of the cycle) (mm)
		RMAS_M	Relative maximum slip distance (magnitude) (mm)
		DZ_P	Z Displacement up to preload or penetration index (larger value penetrates most) (mm)

** Output variables are analyzed individually.*

DOE study relies on full-factorial design modeling technique. According to this technique, at least two or more parameters with at least two or more levels that belong to each parameter, are bounded together in various combinations. Montgomery (2013) can be searched for more information about this issue. Each parameter *(input variables)* is investigated in 4 levels. In this case, a total of 256 design versions are generated. Full factorial design table is given in Table 5.7.

Pre-design study is carried out to select feasible limits for each factors and levels. Particularly, maximum value of parameter *'D'* is limited because of overlapping ribs with each other. Overlapping situation causes to lose control over the *'Depth of a rib'* or so-called parameter 'A' that is given in Figure 5.18. Similarly, larger depth of ribs cause several mesh and penetration problems in numerical simulations (FEA-CAE). Also, flank and inclination angle could cause overlapping problems. Therefore, all of these 4 parameters are defined in a feasible range to get flawless results from numerical finite elements analyzes.

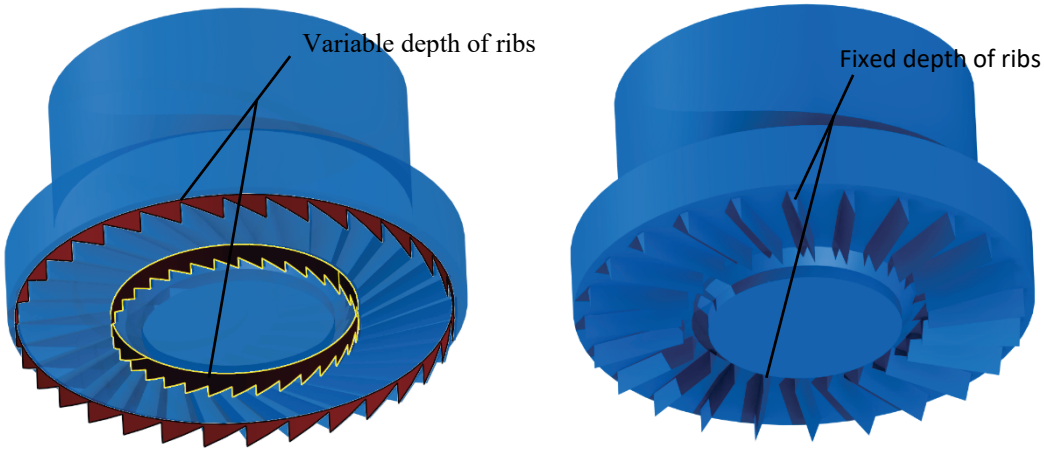


Figure 5.18 Overlapping issue for *large-number-of-ribs* case.

Factors and limits are given in Table 5.6. According to this table all possible combinations generated in CAD interface as inputs for FEA-simulations.

Table 5.6 Parameters and their limits.

	A	B	C	D
1	0.25	45	0.00	12
2	0.50	55	7.50	16
3	0.75	65	15.00	20
4	1.00	75	20.00	24

While gathering results from FEA studies, some design versions had been resulted in failures due to re-meshing and convergence problems, hence these 152 faulty design versions are filtered and eliminated from data set. Filtered design table is given in Table 5.7 with 104 various designs.

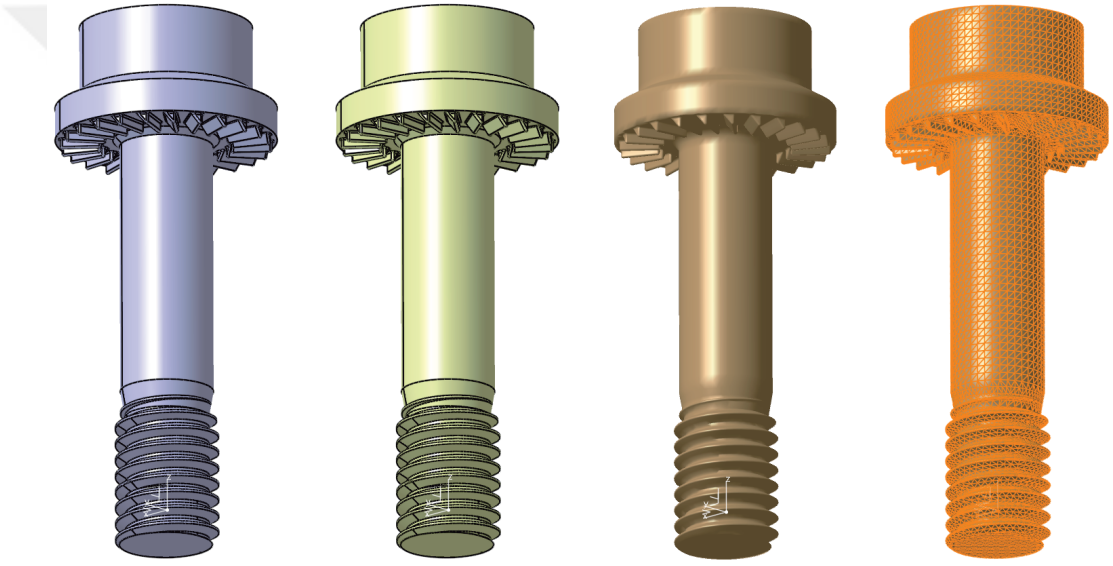
Table 5.7 Full factorial *(filtered)* experimental design table 4^4-152 (continuing ..)

	A	B	C	D		A	B	C	D		A	B	C	D
										69	0.75	75	15.00	24
										70	0.25	65	0.00	20
1	0.25	45	0.00	12	35	0.75	75	20.00	16	71	0.25	65	7.50	24
2	1.00	65	7.50	20	36	0.50	45	7.50	24	72	0.75	45	0.00	12
3	0.75	45	15.00	16	37	0.50	55	0.00	16	73	1.00	75	20.00	16
4	0.50	45	7.50	16	38	0.50	65	15.00	16	74	1.00	75	15.00	16
5	1.00	45	20.00	20	39	0.25	55	0.00	12	75	0.75	55	20.00	16
6	0.25	75	20.00	20	40	0.75	75	0.00	16	76	0.50	55	0.00	24
7	0.50	55	20.00	20	41	1.00	55	7.50	16	77	0.25	45	15.00	20
8	0.50	55	15.00	24	42	0.50	65	20.00	24	78	0.25	55	7.50	16
9	0.50	75	0.00	20	43	0.50	65	15.00	12	79	0.25	45	0.00	24
10	1.00	65	15.00	20	44	0.75	75	7.50	12	80	1.00	75	0.00	24
11	0.25	75	7.50	16	45	1.00	65	7.50	16	81	0.75	65	20.00	20
12	0.75	45	15.00	24	46	0.25	45	15.00	12	82	1.00	45	0.00	20
13	0.75	55	15.00	12	47	0.25	75	7.50	12	83	0.25	75	15.00	20
14	0.75	45	0.00	24	48	1.00	65	20.00	20	84	0.25	55	20.00	12
15	0.75	55	20.00	24	49	0.50	45	20.00	16	85	0.50	75	0.00	24
16	0.25	55	20.00	24	50	0.50	45	20.00	12	86	0.75	45	7.50	20
17	0.25	55	7.50	12	51	1.00	55	0.00	12	87	0.25	65	7.50	20
18	0.50	65	7.50	12	52	0.25	65	20.00	20	88	0.25	55	20.00	20
19	1.00	65	0.00	16	53	1.00	75	7.50	12	89	1.00	75	15.00	12
20	1.00	75	20.00	24	54	0.75	45	20.00	16	90	1.00	45	7.50	12
21	0.75	75	20.00	20	55	0.25	65	15.00	20	91	0.50	55	0.00	12
22	0.50	65	7.50	16	56	0.50	45	15.00	24	92	0.50	65	20.00	12
23	0.25	55	15.00	24	57	0.75	65	15.00	16	93	0.25	65	15.00	24
24	0.75	65	15.00	24	58	0.50	55	15.00	16	94	0.75	45	0.00	20
25	0.75	65	0.00	20	59	0.50	45	0.00	16	95	0.25	55	15.00	12

Table 5.7 Full factorial *(filtered)* experimental design table 4^4-152 (.. end)

26	0.25	45	20.00	16	60	0.25	75	20.00	16	96	0.50	75	20.00	16
27	0.25	65	7.50	16	61	0.50	45	15.00	20	97	0.50	65	15.00	20
28	0.25	75	15.00	16	62	0.75	45	20.00	12	98	1.00	45	15.00	12
29	0.50	45	15.00	16	63	0.75	65	7.50	24	99	0.50	55	7.50	16
30	0.50	75	7.50	20	64	0.25	65	0.00	16	100	0.50	55	7.50	24
31	1.00	55	7.50	12	65	1.00	75	0.00	12	101	1.00	45	20.00	24
32	1.00	45	20.00	16	66	1.00	55	0.00	24	102	0.50	65	0.00	20
33	0.50	65	20.00	16	67	0.75	55	15.00	24	103	1.00	45	15.00	24
34	0.25	55	0.00	16	68	0.75	55	20.00	20	104	0.75	75	7.50	24

These 104 design variations are transferred into the FEA simulation software via *simulation input file generator* code that is written in *Visual Basic* programming platform.



(a) (b) (c) (d)

Figure 5.19 CATIA CAD design stages: solid body (a), surface model (b), STL model (c), STL tetrahedral mesh that is used directly as a finite element initial mesh (d).

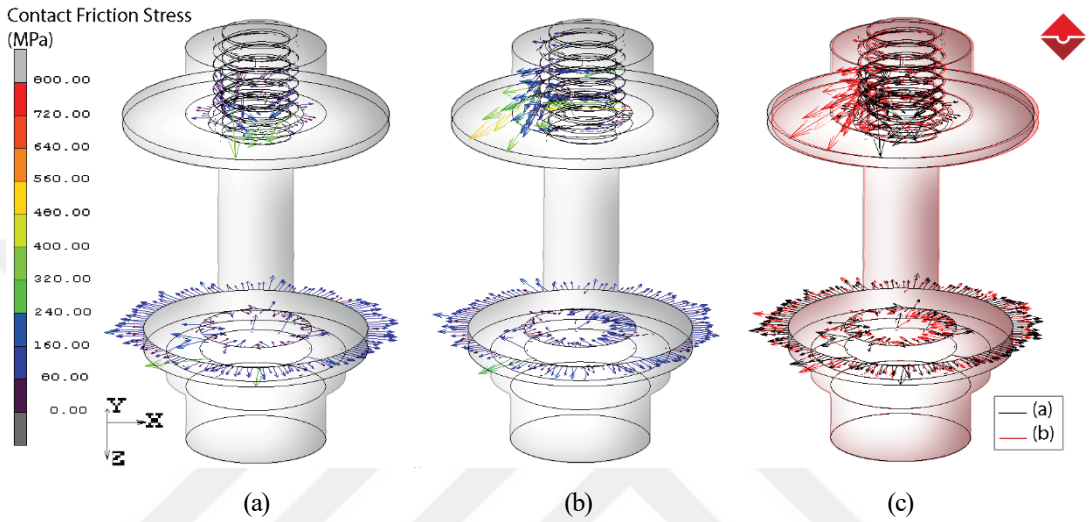
5.3 Simulation Model

Simulation studies are carried out based on the core model which is derived in Chapter Three. Two subroutine codes are generated thru *Excel VBA* environment.

First macro code generates a *'Preprocessor Procedure'* for Simufact® Forming GP interface. The file with *'.proc'* extension uses a template file that created in this thesis for the purpose of this study. Template model is optimized for fastest simulation CPU

time and optimized for flawless output criteria generation. Procedure file generates *'.mud'* files for simulation program inputs. Procedure file does not generate initial meshes. This approach speeds up model generation procedure.

Second macro code collects data from simulation results. The following outputs are extracted from simulation results:



(a) (b) (c)

Figure 5.20 Contact Friction Stress: preload (a), displaced in the +x direction (b), overlapped (c).

- F_{shear} at bolt head (kN): Friction force between the bolt head and the washer.
- F_{shear} min (kN): Minimum overall shear force in the assembly.
- F_{shear} max (kN): Maximum overall shear force in the assembly.
- Clamp Loss (kN): This is the loss of Preload value. In other words, clamp loss equals to the difference of the Z load at Figure 3.4 (b) and Figure 3.4 (f).
- Relative slip distance to the left-hand side (mm): This is the pure relative distance in the – x direction (see Figure 3.3 & Figure 3.5):

$$\delta_{Left} = \delta_{NutPlate(-x)} - \delta_{Nut(-x)} - \delta_{Bolt-head(-x)} \tag{5.6}$$

- Relative slip distance to the right-hand side (mm): This is the pure relative distance in the + x direction (see Figure 3.3 & Figure 3.5):

$$\delta_{Right} = \delta_{NutPlate(+x)} - \delta_{Nut(+x)} - \delta_{Bolt-head(x)} \tag{5.7}$$

- Relative maximum slip distance (position at the end of the cycle) (mm): This is the position of the bolt under-head at the end of the cycle relative to the initial position.

- Relative maximum slip distance (magnitude) (mm): This is the maximum elastic deflection where complete slip begins. This value is calculated in an excel macro code.

  The calculation triggered if $|\delta_{Bolt\ head}| > 0$ [OR] $|\delta_{Nut\ Plate} - \delta_{Nut}| > 0$.

  Maximum slip distance is calculated as given in (5.8):

$$\delta_{slip,\max} = \left|\delta_{NutPlate} - \delta_{Nut} - \delta_{Bolt-head}\right| \tag{5.8}$$

- Z displacement up to preload or penetration index (larger value penetrates most) (mm): This parameter indicates the penetration depth of serrations inside the washer body. One can consider that penetration indicates geometrical and mechanical locking-state, hence the more serrations penetrate, the more self-locking condition is ensured. This situation is expressed in Figure 5.21:

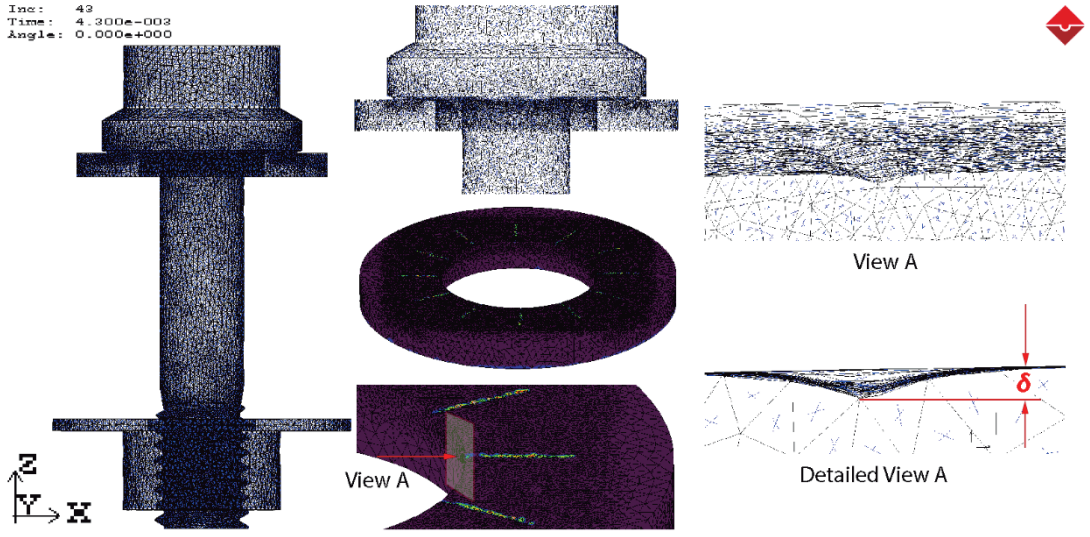


Figure 5.21 Penetration Index (δ).

- Preload (kN): Preload value is read at the last increment of *'Preload'* load case. Preload is read from the *'Rigid Plane'* that is bonded with elastic-plastic *'Washer'* as mentioned in previous sections (see Figure 3.3).

Penetration depth and contact pressure distribution are significant parameters which provides self-loosening resistance to the joint (Figure 5.22). Serrated under-head form withstands relative transverse displacements against complete-slip.

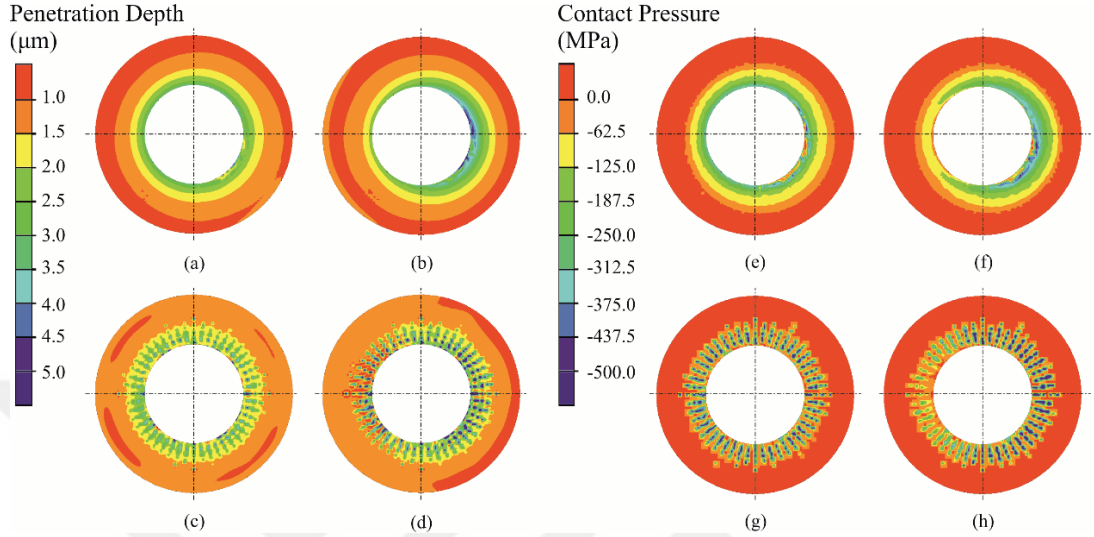


Figure 5.22 Penetration depth (z distance) and contact pressure distribution for flat and serrated under-head forms. flat - $\delta x = 0$ (a-e), flat - $\delta x = 5$ mm (b-f), serrated - $\delta x = 0$ mm (c-g), serrated - $\delta x = 5$ mm (d-h).

In the Figure 5.23-24, clamping load-case and vibration load-case are depicted. Similar to Figure 5.22 (g), serrated under-head form provides more homogeneous pressure distribution than the flat one in Figure 5.22 (e).

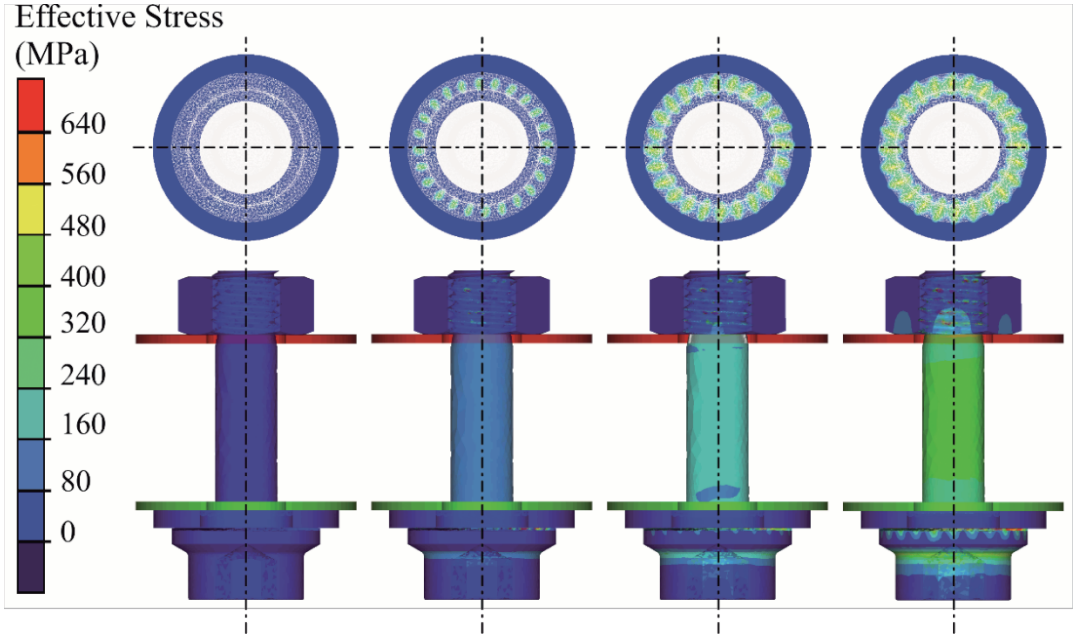


Figure 5.23 Clamp load-case for serrated under-head form.

Figure 5.24 reveals the relative motion more precisely. Nut-end of the bolt travels with nut-plate, but in the case of a slip-stick condition, initial state in Figure 5.24 (a) deviates from the final state in the Figure 5.24 (d). This situation results in that central axes of the bolt and the nut do not match exactly as seen in the Figure 5.24 (d).

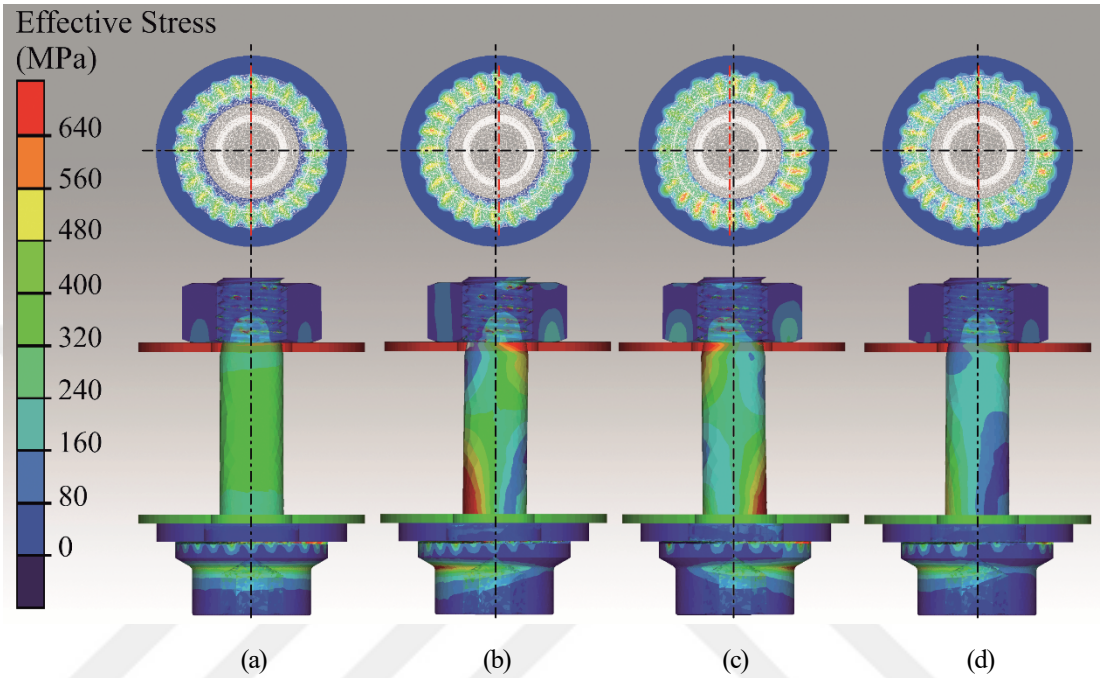


Figure 5.24 Transverse displacement of serrated under-head form (vibration load-case) $\delta x = 0$ (a), $\delta x = +5$ mm (b), $\delta x = -5$ mm (c), $\delta x = 0$ (d).

Another output criterion is the transverse displacement and the shear force history.

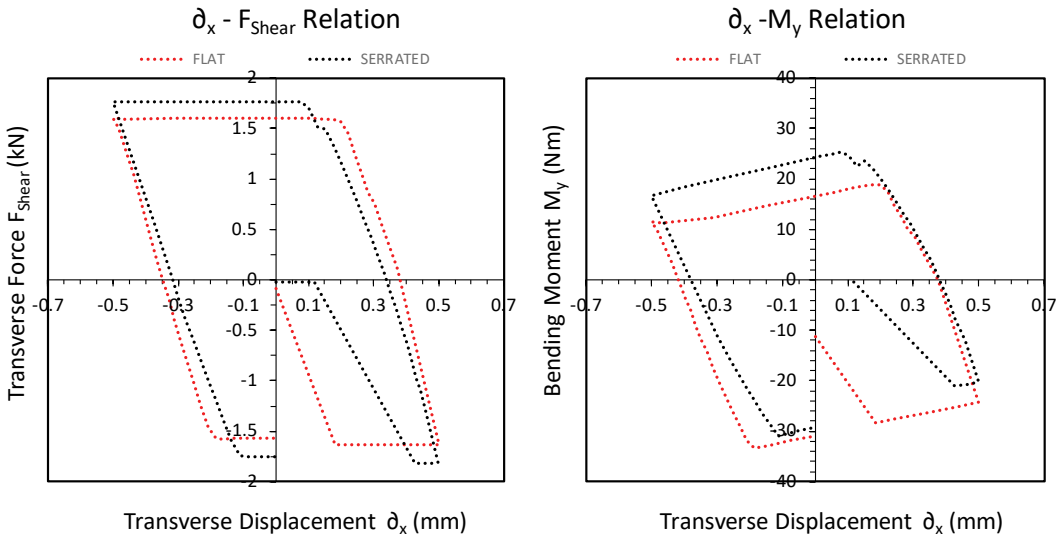


Figure 5.25 Flat and serrated comparison.

Figure 5.25 shows the slip conditions of flat and serrated under-head forms. It can be seen that serrated bolt slips at higher transverse displacements than flat one. So, bending moment in serrated bolt is higher than flat bolt.

5.4 Genetic Programming Model

In this section, Eureqa® commercial software is used for genetic programming computational work. Genetic programming code searches for a function that maps 4 main inputs, *A, B, C* and *D* in order to represent 10 output criteria.

$$y = f(A, B, C, D) \tag{5.9}$$

where *A, B, C* and *D* are the '*depth of a rib', 'flank angle of a rib', 'inclination angle of a rib', 'number of ribs'. 'y'* is the output criterion that the complete lists of these parameters are given in Table 5.5 and 5.7.

The purpose is to find a relationship from a set of data given in Table 5.8. Hence, the problem is: given a set of labeled feature vectors (data points), find a mathematical model that explains the data.

Table 5.8 Output criteria (1-20).

No	F_{Shear} at Bolt Head (kN)	F_{Shear} at Nut Surface (kN)	F_{Shear} (min) (kN)	F_{Shear} (max) (kN)	Clamp Loss (kN)	Relative Slip Distance to the Left Hand Side (mm)	Relative Slip Distance to the Right Hand Side (mm)	Relative Maximum Slip Distance (position at the end of the cycle) (mm)	Relative Maximum Slip Distance (magnitude) (mm)	Z Displacement UpTo Preload or Penetration Index (larger value penetrates most) (mm)
1	1.937020	1.727227	1.727227	1.937020	3.759949	-0.117761	0.203582	0.178861	0.178861	0.213964
2	1.892500	1.889745	1.889745	1.892500	2.317117	-0.154575	0.201251	0.187623	0.187623	0.175973
3	1.870793	1.760555	1.760555	1.870793	4.404179	-0.119602	0.213198	0.180499	0.180499	0.178791
4	2.482976	1.876028	1.876028	2.482976	3.673239	-0.225189	0.196273	0.158380	0.158380	0.179115
5	1.840258	1.799061	1.799061	1.840258	1.517685	-0.158851	0.207280	0.199782	0.199782	0.169859
6	1.938984	1.918841	1.918841	1.938984	4.017508	-0.148877	0.202912	0.159649	0.159649	0.169982
7	1.948173	1.931917	1.931917	1.948173	2.136574	-0.150874	0.203671	0.190184	0.190184	0.175084
8	1.935636	1.764758	1.764758	1.935636	1.895368	-0.147944	0.190883	0.169837	0.169837	0.179769
9	2.074978	1.893820	1.893820	2.074978	3.886571	-0.179674	0.202300	0.162178	0.162178	0.167329
10	2.460680	1.765535	1.765535	2.460680	3.335899	-0.105518	0.263218	0.183876	0.183876	0.171074
11	2.595158	1.714660	1.714660	2.595158	4.743890	-0.132497	0.298853	0.179253	0.179253	0.173666
12	1.890695	1.868463	1.868463	1.890695	2.215105	-0.145041	0.183805	0.174263	0.174263	0.164202
13	2.334618	1.555055	1.555055	2.334618	6.571353	-0.126354	0.272548	0.157972	0.157972	0.176866
14	2.018057	1.864516	1.864516	2.018057	1.893841	-0.134879	0.214942	0.214942	0.214942	0.164854
15	1.939432	1.915680	1.915680	1.939432	2.046455	-0.159535	0.191212	0.179827	0.179827	0.170316
16	1.931385	1.856104	1.856104	1.931385	1.717784	-0.148979	0.203494	0.203494	0.203494	0.171689
17	2.387492	1.659798	1.659798	2.387492	4.573649	-0.088426	0.280043	0.206871	0.206871	0.197279
18	2.105731	1.532160	1.532160	2.105731	4.941246	-0.099549	0.255730	0.184942	0.184942	0.178115
19	1.647545	1.633378	1.633378	1.647545	4.495858	-0.128004	0.183554	0.156140	0.156140	0.166875
20	1.820819	1.775898	1.775898	1.820819	3.814940	-0.154443	0.197775	0.152452	0.152452	0.167351

Table 5.8 Output criteria (21-84)

No	F_{Shear} at Bolt Head (kN)	F_{Shear} at Nut Surface (kN)	F_{Shear} (min) (kN)	F_{Shear} (max) (kN)	Clamp Loss (kN)	Relative Slip Distance to the Left Hand Side (mm)	Relative Slip Distance to the Right Hand Side (mm)	Relative Maximum Slip Distance (position at the end of the cycle) (mm)	Relative Maximum Slip Distance (magnitude) (mm)	Z Displacement UpTo Preload or Penetration Index (larger value penetrates most) (mm)
21	1.882624	1.885539	1.882624	1.885539	2.536386	-0.154325	0.198516	0.189109	0.189109	0.170587
22	1.906253	1.886046	1.886046	1.906253	3.895480	-0.148468	0.203240	0.166510	0.166510	0.177456
23	1.961431	1.873643	1.873643	1.961431	2.026366	-0.156870	0.183641	0.167614	0.167614	0.172504
24	1.872010	1.772138	1.772138	1.872010	2.777170	-0.133115	0.194355	0.179199	0.179199	0.169586
25	2.141557	1.870830	1.870830	2.141557	2.226924	-0.141416	0.241876	0.241876	0.241876	0.172887
26	1.786060	1.722482	1.722482	1.786060	3.049778	-0.111355	0.202019	0.182237	0.182237	0.171835
27	1.822488	1.725058	1.725058	1.822488	2.231602	-0.122539	0.201799	0.190582	0.190582	0.178567
28	1.830277	1.722648	1.722648	1.830277	3.087011	-0.175738	0.190765	0.150108	0.150108	0.175797
29	2.425605	1.667298	1.667298	2.425605	2.979299	-0.115614	0.269541	0.213534	0.213534	0.171384
30	1.815877	1.755813	1.755813	1.815877	2.542231	-0.156262	0.199018	0.175677	0.175677	0.174292
31	1.688705	1.564851	1.564851	1.688705	6.011191	-0.145284	0.186709	0.133159	0.133159	0.185616
32	1.758644	1.668910	1.668910	1.758644	3.733145	-0.107318	0.204325	0.183213	0.183213	0.169981
33	1.841328	1.699845	1.699845	1.841328	3.333395	-0.176923	0.186989	0.141668	0.141668	0.172293
34	1.782339	1.702723	1.702723	1.782339	2.565884	-0.140873	0.174036	0.160893	0.160893	0.177804
35	1.753967	1.687658	1.687658	1.753967	2.584273	-0.134433	0.198744	0.184121	0.184121	0.168408
36	1.849767	1.787579	1.787579	1.849767	2.225994	-0.119132	0.212987	0.204306	0.204306	0.173166
37	1.736929	1.676834	1.676834	1.736929	2.769183	-0.128395	0.189105	0.180451	0.180451	0.175772
38	1.771250	1.718685	1.718685	1.771250	2.384645	-0.146834	0.178218	0.170464	0.170464	0.172910
39	1.723001	1.594882	1.594882	1.723001	4.657407	-0.090898	0.204965	0.163702	0.163702	0.181556
40	2.282937	1.632359	1.632359	2.282937	4.413345	-0.082423	0.264222	0.191961	0.191961	0.170405
41	2.166950	1.561961	1.561961	2.166950	4.841284	-0.074050	0.243756	0.171193	0.171193	0.167990
42	1.848139	1.784880	1.784880	1.848139	1.663241	-0.125295	0.204954	0.201100	0.201100	0.172823
43	2.167969	1.637611	1.637611	2.167969	4.905472	-0.057995	0.276902	0.184741	0.184741	0.186364
44	2.023272	1.513800	1.513800	2.023272	5.910655	-0.052030	0.247078	0.176037	0.176037	0.183434
45	1.806642	1.684446	1.684446	1.806642	2.841983	-0.136841	0.208780	0.208780	0.208780	0.171100
46	1.812740	1.668898	1.668898	1.812740	2.907322	-0.132510	0.185753	0.157482	0.157482	0.179313
47	1.731398	1.592432	1.592432	1.731398	4.637358	-0.162365	0.195009	0.129367	0.129367	0.182579
48	1.824988	1.754838	1.754838	1.824988	1.927277	-0.134402	0.204300	0.185113	0.185113	0.175302
49	1.754517	1.710451	1.710451	1.754517	3.335742	-0.150196	0.200094	0.160560	0.160560	0.170817
50	1.744789	1.625975	1.625975	1.744789	4.274262	-0.090807	0.194240	0.176318	0.176318	0.182911
51	1.700273	1.588542	1.588542	1.700273	5.564811	-0.123986	0.196780	0.127195	0.127195	0.188288
52	1.824999	1.770326	1.770326	1.824999	1.823534	-0.191195	0.140705	0.137149	0.137149	0.172454
53	1.563230	1.546249	1.546249	1.563230	5.347293	-0.108095	0.204559	0.166123	0.166123	0.183876
54	1.736812	1.691195	1.691195	1.736812	3.361970	-0.103415	0.210829	0.205271	0.205271	0.167566
55	1.864612	1.768113	1.768113	1.864612	2.293724	-0.190253	0.142984	0.108992	0.108992	0.171632
56	2.028020	1.785554	1.785554	2.028020	1.915528	-0.188079	0.189811	0.159718	0.159718	0.172308
57	1.766547	1.714718	1.714718	1.766547	3.835503	-0.163859	0.199932	0.144172	0.144172	0.171665
58	1.789955	1.681334	1.681334	1.789955	3.840920	-0.107653	0.210872	0.178769	0.178769	0.176320
59	1.731055	1.691156	1.691156	1.731055	2.391484	-0.178023	0.138121	0.130483	0.130483	0.171092
60	2.666893	1.727213	1.727213	2.666893	2.867569	-0.120788	0.282707	0.167313	0.167313	0.173879
61	1.850811	1.751935	1.751935	1.850811	2.483192	-0.169325	0.168162	0.139974	0.139974	0.176048
62	1.647687	1.530778	1.530778	1.647687	5.533825	-0.064925	0.194013	0.173595	0.173595	0.179745
63	1.868692	1.783187	1.783187	1.868692	1.692499	-0.144523	0.195939	0.177787	0.177787	0.174526
64	1.877767	1.732353	1.732353	1.877767	2.847572	-0.086943	0.209888	0.185957	0.185957	0.177848
65	2.211369	1.550987	1.550987	2.211369	5.692103	-0.102088	0.265586	0.165831	0.165831	0.184164
66	1.865185	1.738713	1.738713	1.865185	2.228958	-0.152408	0.193038	0.193038	0.193038	0.159281
67	1.959638	1.767615	1.767615	1.959638	1.928154	-0.184875	0.172155	0.171135	0.171135	0.164183
68	2.075495	1.733017	1.733017	2.075495	2.302583	-0.187756	0.183683	0.165330	0.165330	0.166742
69	1.865950	1.782257	1.782257	1.865950	1.679510	-0.149739	0.201225	0.201225	0.201225	0.170785
70	1.855427	1.760662	1.760662	1.855427	2.228473	-0.127236	0.195643	0.181594	0.181594	0.173854
71	1.851759	1.797839	1.797839	1.851759	1.502003	-0.152314	0.185990	0.170015	0.170015	0.169326
72	2.139207	1.593653	1.593653	2.139207	4.977802	-0.078220	0.267368	0.185422	0.185422	0.182609
73	1.778162	1.677366	1.677366	1.778162	4.386207	-0.153227	0.214454	0.174280	0.174280	0.168185
74	2.027961	1.602878	1.602878	2.027961	5.078294	-0.187538	0.214186	0.158393	0.158393	0.169097
75	1.745063	1.691087	1.691087	1.745063	3.182520	-0.166485	0.187814	0.161923	0.161923	0.172516
76	1.811658	1.760171	1.760171	1.811658	1.985047	-0.149049	0.185589	0.176155	0.176155	0.168477
77	1.863572	1.761514	1.761514	1.863572	2.031438	-0.131029	0.195197	0.195197	0.195197	0.174133
78	1.878495	1.708976	1.708976	1.878495	2.749275	-0.121242	0.200473	0.193230	0.193230	0.179998
79	2.278323	1.707355	1.707355	2.278323	4.466380	-0.117219	0.256010	0.173651	0.173651	0.169069
80	2.124262	1.888181	1.888181	2.124262	1.760786	-0.166816	0.228705	0.228705	0.228705	0.167726
81	1.961990	1.887102	1.887102	1.961990	2.301779	-0.146315	0.204120	0.189959	0.189959	0.172338
82	1.844149	1.742033	1.742033	1.844149	1.992811	-0.145090	0.197458	0.175099	0.175099	0.178715
83	1.834222	1.761223	1.761223	1.834222	1.817933	-0.190823	0.147623	0.147623	0.147623	0.170783
84	1.671925	1.630155	1.630155	1.671925	5.376767	-0.096331	0.198890	0.162248	0.162248	0.181897

Table 5.8 Output criteria (85-104)

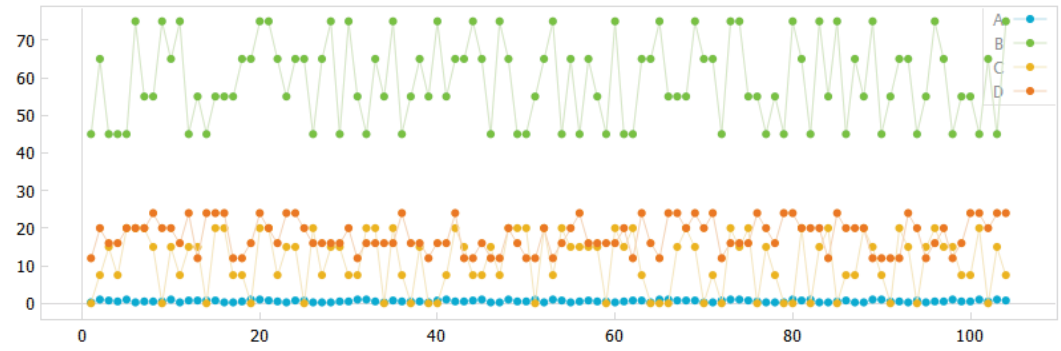
No	F_{Shear} at Bolt Head (kN)	F_{Shear} at Nut Surface (kN)	F_{Shear} (min) (kN)	F_{Shear} (max) (kN)	Clamp Loss (kN)	Relative Slip Distance to the Left Hand Side (mm)	Relative Slip Distance to the Right Hand Side (mm)	Relative Maximum Slip Distance (position at the end of the cycle) (mm)	Relative Maximum Slip Distance (magnitude) (mm)	Z Displacement UpTo Preload or Penetration Index (larger value penetrates most) (mm)
85	1.867157	1.781969	1.781969	1.867157	1.829757	-0.147926	0.222259	0.222259	0.222259	0.169549
86	1.862911	1.748335	1.748335	1.862911	2.098062	-0.144479	0.188083	0.174179	0.174179	0.177983
87	1.858568	1.753672	1.753672	1.858568	2.441648	-0.147709	0.190548	0.147996	0.147996	0.173124
88	1.886762	1.758053	1.758053	1.886762	1.818367	-0.170639	0.149567	0.142809	0.142809	0.177581
89	2.209533	1.544809	1.544809	2.209533	5.869363	-0.059619	0.268259	0.180374	0.180374	0.183066
90	2.108380	1.537303	1.537303	2.108380	5.093166	-0.056336	0.261932	0.194112	0.194112	0.181100
91	1.823636	1.599896	1.599896	1.823636	4.421969	-0.088287	0.189418	0.161526	0.161526	0.187489
92	1.753585	1.652560	1.652560	1.753585	3.000682	-0.138739	0.183209	0.161981	0.161981	0.184388
93	2.355041	2.236805	2.236805	2.355041	1.694731	-0.244905	0.238557	0.158002	0.158002	0.173524
94	1.869636	1.758239	1.758239	1.869636	1.828104	-0.145148	0.191547	0.186386	0.186386	0.175678
95	1.944401	1.614429	1.614429	1.944401	6.006560	-0.026612	0.243196	0.184370	0.184370	0.182186
96	1.756775	1.691978	1.691978	1.756775	3.384286	-0.162165	0.194751	0.152492	0.152492	0.170466
97	1.858545	1.743546	1.743546	1.858545	2.112747	-0.140682	0.191050	0.176492	0.176492	0.176782
98	2.065750	1.573863	1.573863	2.065750	5.910631	-0.138842	0.242041	0.161855	0.161855	0.176625
99	1.745389	1.706127	1.706127	1.745389	4.085024	-0.124466	0.190185	0.172780	0.172780	0.171397
100	1.836144	1.831977	1.831977	1.836144	2.952835	-0.131770	0.197096	0.182880	0.182880	0.173988
101	2.265562	1.757526	1.757526	2.265562	2.421552	-0.134552	0.246963	0.246963	0.246963	0.170919
102	1.870605	1.770103	1.770103	1.870605	1.794046	-0.116524	0.212820	0.212222	0.212222	0.175250
103	1.823714	1.775339	1.775339	1.823714	1.841269	-0.134728	0.198824	0.196976	0.196976	0.172274
104	1.882029	1.772732	1.772732	1.882029	1.813207	-0.164858	0.199013	0.182183	0.182183	0.171568

Mathematical building blocks (operators such as addition, negation, and multiplication) which they are used in genetic programming preparatory steps are given in Table 5.9. Building blocks can be simple, moderately complex, or highly complex. To maintain the simplicity of the final solutions, simple and moderately complex operators are selected. Due to the nature of problem that the data is almost non-linear, trigonometric, inverse trigonometric, exponential, and squashing function building blocks are chosen to capture the complexity and dynamics of data. Table 5.9 represents the building blocks selected for the analysis, comprising: basic operators with complexity coefficients of 1 or 2, such as constant, input variable, addition, subtraction, multiplication, and division; trigonometric operators with complexity coefficients of 3 or 4, such as sine, cosine and tangent; exponential operators with complexity coefficients of 4, such as exponents; squashing functions with complexity coefficients of 4, such as logistic functions as a common sigmonoid squashing function returning $1/(1+e^{-x})$, hyperbolic tangent, and error function as the integral of the normal distribution that returns a value between -1 and +1; and inverse trigonometric operators with complexity coefficients of 4, such as arcsine, arccosine and arctangent.

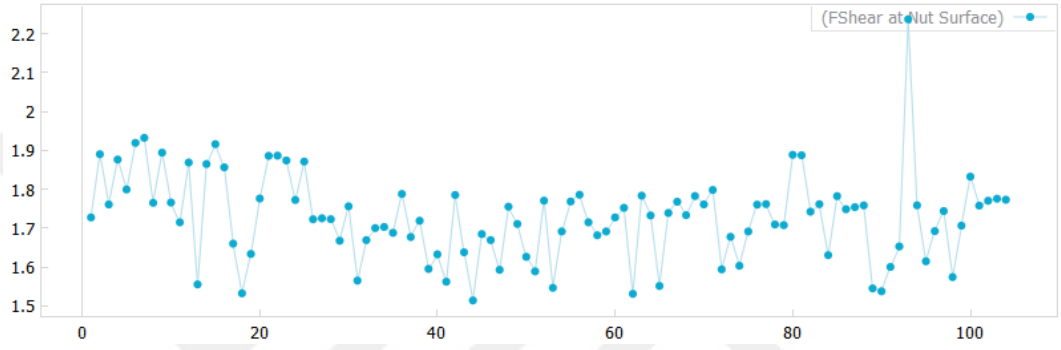
Table 5.9 Eureqa® Mathematical building block.

Mathematical Building Block			
Building block (operator)	Formula	Sign	Complexity
Arithmetic			
Constant	c		1
Input variable	x		1
Addition	x + y or add(x,y)	+	1
Subtraction	x - y or sub(x,y)	-	1
Multiplication	x * y or mul(x,y)	×	1
Division	x / y or div(x,y)	÷	2
Trigonometic			
Sine	sin(x)	sin	3
Cosine	cos(x)	cos	3
Tangent	tan(x)	tan	4
Exponential			
Exponential	exp(x)	e^x	4
Squashing Functions			
Logistic Function	logistic(x)	logistic	4
Hyperbolic Tangent	tanh(x)	tanh	4
Error Function	erf(x)	erf	4
Inverse Trigonometric			
Arcsine	asin(x)	asin	4
Arccosine	acos(x)	acos	4
Arctangent	atan(x)	atan	4

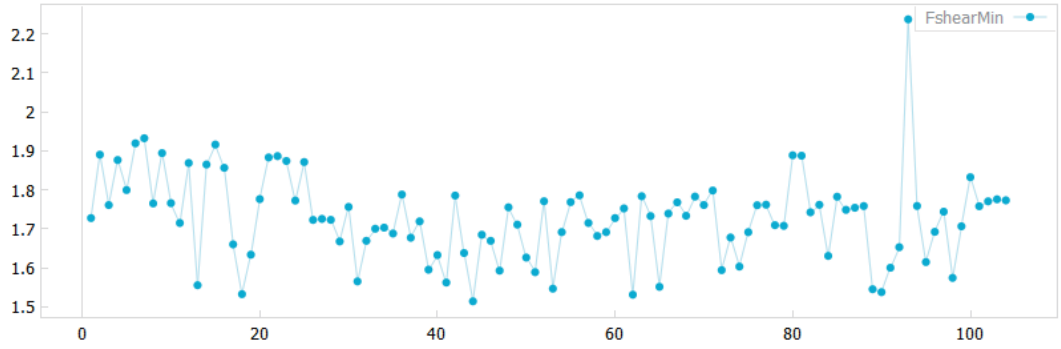
Figure 5.26 presents the distribution of the input data *(A, B, C* and *D)* and output data *($F_{shear\ at\ bolt\ head}$ (kN) [FSBH], $F_{shear\ at\ nut\ surface}$ (kN) [FSNS], $F_{shear\ (min)}$ (kN) [FSMI], $F_{shear\ (max)}$ (kN) [FSMA], clamp loss (kN) [CL], relative slip distance to the left-hand side (mm) [RSDLH], relative slip distance to the right-hand side (mm) [RSDRH], relative maximum slip distance (position at the end of the cycle) (mm) [RMAS], relative maximum slip distance (magnitude) (mm) [RMAS_M], Z displacement up to preload or penetration index (larger value penetrates most) (mm) [DZ_P]).* The data includes participants' (*FSBH*, *FSNS, FSMI, FSMA, CL, RSDLH, RSDRH, RMAS, RMAS_M* and *DZ_P*), as a function of depth of a rip *(A)*, flank angle of a rip *(B)*, inclination angle of a rip *(C)* and number of rip *(D)* on the measures.



(a)

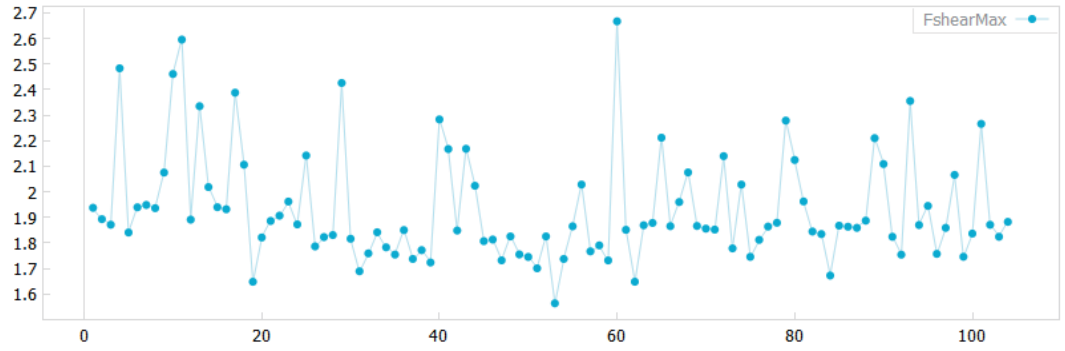


(b)

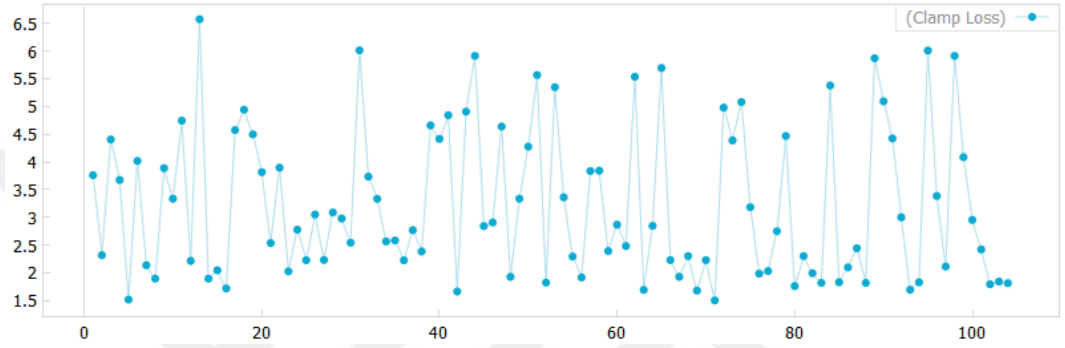


(c)

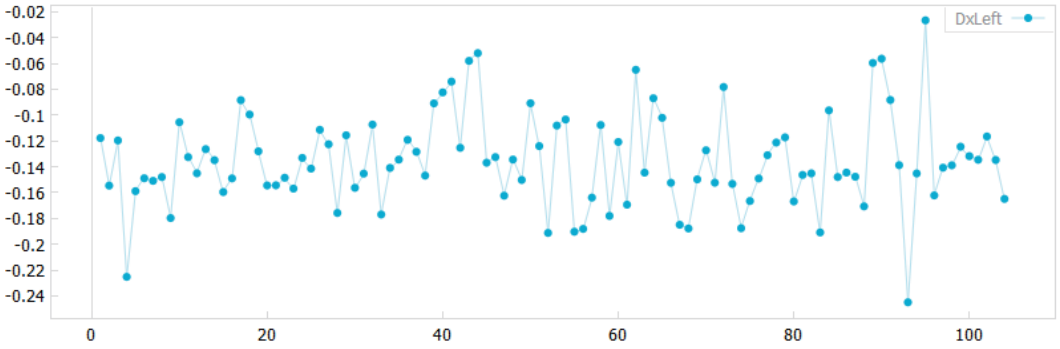
Figure 5.26 Distribution of the input data (a) (A, B, C and D) and output data (b, c, d, e, f, g, h, I ,j and k) (Fshear at bolt head (kN) [FSBH], Fshear at nut surface (kN) [FSNS], Fshear (min) (kN) [FSMI], Fshear (max) (kN) [FSMA], clamp loss (kN) [CL], relative slip distance to the left-hand side (mm) [RSDLH], relative slip distance to the right-hand side (mm) [RSDRH], relative maximum slip distance (position at the end of the cycle) (mm) [RMAS], relative maximum slip distance (magnitude) (mm) [RMAS_M], Z displacement up to preload or penetration index (larger value penetrates most) (mm) [DZ_P]) – *Continuing* ..



(d)

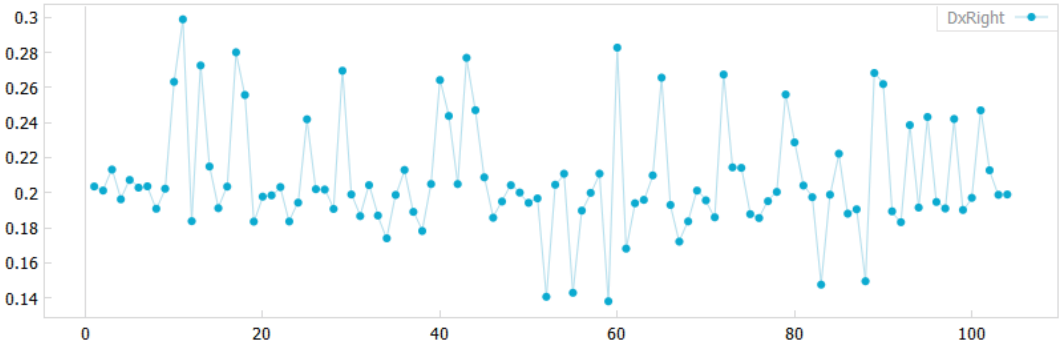


(e)

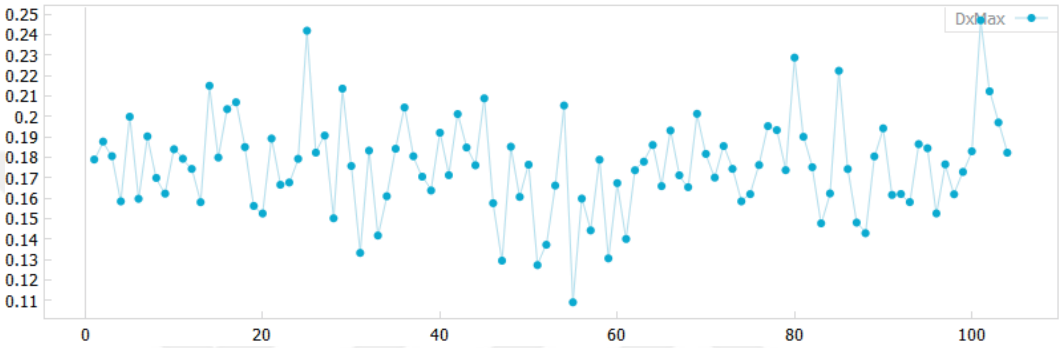


(f)

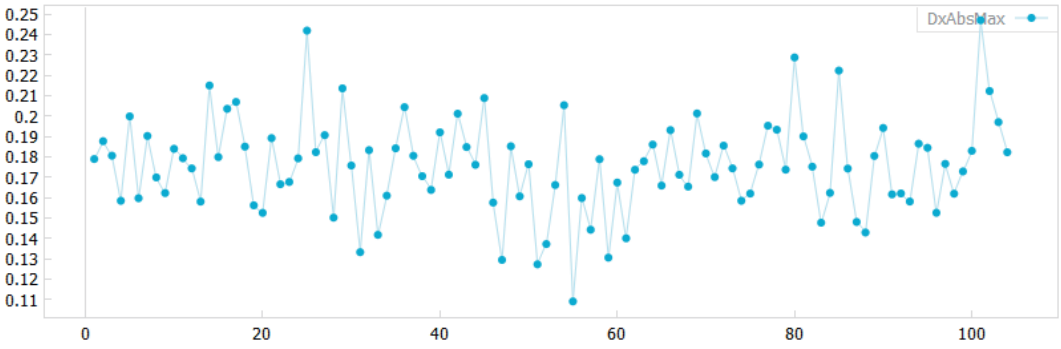
Figure 5.26 Distribution of the input data (a) (A, B, C and D) and output data (b, c, d, e, f, g, h, I ,j and k) (Fshear at bolt head (kN) [FSBH], Fshear at nut surface (kN) [FSNS], Fshear (min) (kN) [FSMI], Fshear (max) (kN) [FSMA], clamp loss (kN) [CL], relative slip distance to the left-hand side (mm) [RSDLH], relative slip distance to the right-hand side (mm) [RSDRH], relative maximum slip distance (position at the end of the cycle) (mm) [RMAS], relative maximum slip distance (magnitude) (mm) [RMAS_M], Z displacement up to preload or penetration index (larger value penetrates most) (mm) [DZ_P]) – *Continuing* ..



(g)

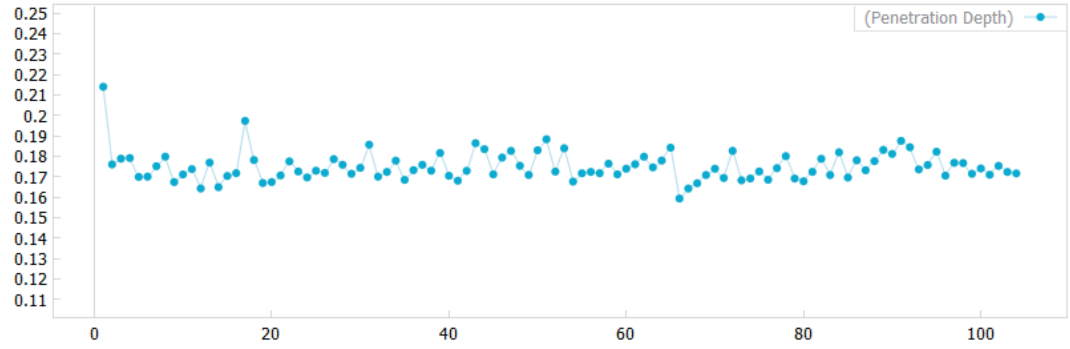


(h)

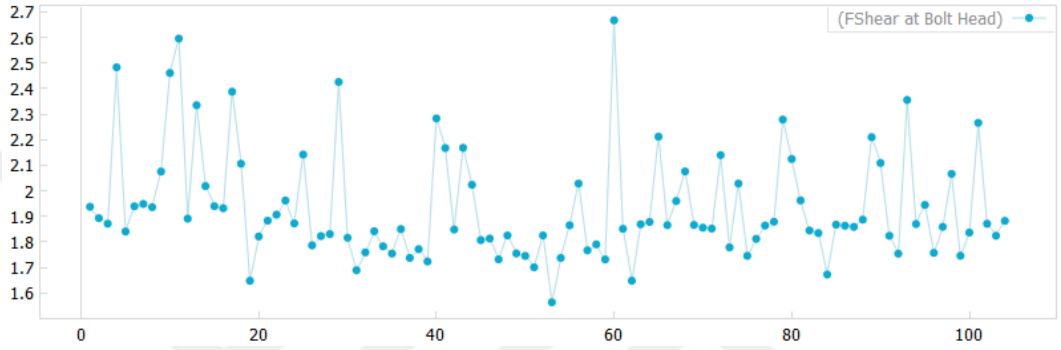


(i)

Figure 5.26 Distribution of the input data (a) (A, B, C and D) and output data (b, c, d, e, f, g, h, I ,j and k) (Fshear at bolt head (kN) [FSBH], Fshear at nut surface (kN) [FSNS], Fshear (min) (kN) [FSMI], Fshear (max) (kN) [FSMA], clamp loss (kN) [CL], relative slip distance to the left-hand side (mm) [RSDLH], relative slip distance to the right-hand side (mm) [RSDRH], relative maximum slip distance (position at the end of the cycle) (mm) [RMAS], relative maximum slip distance (magnitude) (mm) [RMAS_M], Z displacement up to preload or penetration index (larger value penetrates most) (mm) [DZ_P]) – *Continuing* ..



(j)



(k)

Figure 5.26 Distribution of the input data (a) (A, B, C and D) and output data (b, c, d, e, f, g, h, I ,j and k) (Fshear at bolt head (kN) [FSBH], Fshear at nut surface (kN) [FSNS], Fshear (min) (kN) [FSMI], Fshear (max) (kN) [FSMA], clamp loss (kN) [CL], relative slip distance to the left-hand side (mm) [RSDLH], relative slip distance to the right-hand side (mm) [RSDRH], relative maximum slip distance (position at the end of the cycle) (mm) [RMAS], relative maximum slip distance (magnitude) (mm) [RMAS_M], Z displacement up to preload or penetration index (larger value penetrates most) (mm) [DZ_P])

The examples are split into two groups for training and validation. The training set is created by randomly choosing samples from the all dataset. The data was divided into a training batch (50 %; n = 52) and a validation batch (50 %; n = 52).

Following the selection of generated solutions, multiple fit statistics were used for examining the performance of these solutions, including R^2, *CC, ME, MSE* and *MAE*.

Maximum Error (ME) minimizes the single highest error of the residuals. Use to minimize the worst-case error or to force algorithm to model a small residual feature.

$$MAE = \frac{1}{N}\sum_{i=1}^{N}\left|y - f\left(x\right)\right| \tag{5.10}$$

Mean Absolute Error (MAE) is given in Equation (5.10) which minimizes the mean of the absolute value of residual errors, *mean(abs(error))*. Assumes noise follows a double exponential distribution.

$$MSE = \frac{1}{N}\sum_{i=1}^{N}\left(y - f\left(x\right)\right)^2 \tag{5.11}$$

Mean Squared Error (MSE) is given Equation (5.11) which minimizes the mean of the squared residual errors. Assumes noise follows a normal distribution.

$$R^2 = 1 - \frac{SS_{res}}{SS_{tot}} \tag{5.12}$$

R^2 Goodness of Fit is given in Equation (5.12) which maximizes the R^2 explained variance, similar to the squared error but normalized by the scale of the output values. SS_{tot} in Equation (5.12) is proportional to the total variance, and SS_{res} is the residual sum of squares (proportional to the unexplained variance).

$$CC = \frac{1}{n-1}\sum_{i=1}^{n}\left(\frac{f\left(x_i\right) - \overline{f\left(x\right)}}{S_{f(x)}}\right)\left(\frac{y_i - \overline{y}}{s_y}\right) \tag{5.13}$$

Correlation Coefficient (CC) is given Equation (5.13) which maximizes the correlation coefficient, normalized covariance. Scale and offset invariant, models the "shape" of the data.

It should be considered that, in genetic programming-based symbolic regression analysis, 50 % of the data was used for model building (training) and 50 % for validation. Regression coefficients, R^2, and adjusted R^2 (which is R^2 adjusted for the number of input variables) were estimated. Estimation models are given in Table 5.10 according to the output variables in Table 5.5.

Models in Table 5.10 are evaluated according to performance measurement criteria *(R^2, CC, ME, MSE, MAE)*. Estimation model results show that there is no correlation

between *FSBH, FSMA, RSDLH, RSDRH, RMAS* and *RMAS_H* with simulation results; hence these objective criteria are omitted and they will not be moved to the next stage. For instance, *FSMA* estimation model gives -0.10791198, 0.18484035, 0.88747891, 0.047127566 and 0.12934219 for R^2, *CC, ME, MSE* and *MAE*, respectively. Therefore, this model is not a useful expression to represent simulation data. Consider that, a negative R^2 is not a mathematical impossibility or the sign of a computer bug. It simply means that the chosen model (with its constraints) fits the data really poorly. So, negative R^2 values eliminated.

The other finding from Table 5.10 is that high complexity is necessarily yield good fit to the data. More detailed results are given in Appendices A.8-9.

Table 5.10 Estimation models for 10 objective criteria.

	Model	R^2	CC	ME	MSE	MAE	# Coeff	Complexity
1	CL = 13.1144548753172 + 2.57156972739084*A + 0.0223030048889321*D^2 - 0.9983011903294*D - 0.111687838749917*A*D	0.80106165	0.9003398	1.9614491	0.35456609	0.41168271	5	21
2	FSBH = 1.85254486558692 + cos(D)*atan(0.107438415792173*A)	-0.07385194	0.115426	0.84006431	0.04568399	0.13420762	2	14
3	FSNS = 1.93349847878302 + (-3.20991978682081)/(D - 3.634495177150 26*A)	0.76436241	0.8913699	0.13786291	0.00226533	0.02954258	3	10
4	FSMI = 1.1629783894278 + 0.052886833989 1198*D + (-0.926701055686821)*A/D - 0.00108220512298542*D^2	0.76490859	0.891607	0.13572715	0.00225574	0.03068353	4	18
5	FSMA = 1.84132278172034 + 3.13665359273573e-5*D*C^2 - 3.13665359273573e-5*C^3 - 0.0156312465683464*tan(0.00991801639548852*D*C^2)	-0.10791198	0.1848404	0.88747891	0.04712757	0.12934219	5	31
6	RSDLH = 0.161255950008727 + 0.000569583125417103*D^2 - 0.000551164805971398*B - 0.025303140187375*D	0.39940403	0.6545316	0.06066588	0.00063813	0.01911375	4	15
7	RSDRH = 0.217155133349173 + 0.000248865955790457*A*B - 0.00141964074658196*D	0.088074076	0.4434962	0.08359988	0.00093805	0.02064791	3	11
8	RMAS = 0.163268737570535 + 0.00130740215691619*A*D - 0.000203149947100449*C	0.18112278	0.4745325	0.05899623	0.00052104	0.01726554	3	11
9	RMAS_M = 0.161562130840227 + 0.00129667472476335*A*D	0.15808181	0.4370418	0.06086375	0.0005357	0.01748976	2	7
10	DZ_P = 0.40025561536118 + 0.0019652657906894*D^2 + 2.42697538327258e-5*A*C*D - 0.0366274855397272*D - 3.49284543619726e-5*D^3 - 2.77227322561448e-5*A*C^2 - 0.000148033686839244*D*A^2	0.65878158	0.8335841	0.01386611	1.6101E-05	0.00301873	7	43

R2: Goodness of fit CC: Correaliton coefficient ME: Maximum error MSE: Mean squared error MAE: Mean absolute error # Coeff: Number of coefficients

In this table, it can be seen that *FSNS, FSMI and DZ_P* have higher R^2 values over 0.50; however, it is not recommended the models with R^2 values below 0.70 to be used for final formulation. In this table, *CL* come to front with a value over 0.80. *CL* estimation model gives the most accurate results; therefore, it can be used for representing simulation model. This estimation model can be used as an approximate formulation to calculate loosening rate of bolted joints under transverse vibrational loading conditions. Furthermore, *CL* estimation model is improved by eliminating some of outliers from the data set and performance measurement criteria is elevated to a more precise level of detail.

Table 5.11 Filtered data set with *Clamp Loss* results (2 outliers are omitted).

	A	B	C	D	*CL*		A	B	C	D	*CL*		A	B	C	D	*CL*
1	0.25	45	0.00	12	3.759949	35	0.75	75	20.00	16	2.584273	69	0.75	75	15.00	24	1.67951
2	1.00	65	7.50	20	2.317117	36	0.50	45	7.50	24	2.225994	70	0.25	65	0.00	20	2.228473
3	0.75	45	15.00	16	4.404179	37	0.50	55	0.00	16	2.769183	71	0.25	65	7.50	24	1.502003
4	0.50	45	7.50	16	3.673239	38	0.50	65	15.00	16	2.384645	72	0.75	45	0.00	12	4.977802
5	1.00	45	20.00	20	1.517685	39	0.25	55	0.00	12	4.657407	73	1.00	75	20.00	16	4.386207
6	0.25	75	20.00	20	4.017508	40	0.75	75	0.00	16	4.413345	74	1.00	75	15.00	16	5.078294
7	0.50	55	20.00	20	2.136574	41	1.00	55	7.50	16	4.841284	75	0.75	55	20.00	16	3.18252
8	0.50	55	15.00	24	1.895368	42	0.50	65	20.00	24	1.663241	76	0.50	55	0.00	24	1.985047
9	0.50	75	0.00	20	3.886571	43	0.50	65	15.00	12	4.905472	77	0.25	45	15.00	20	2.031438
10	1.00	65	15.00	20	3.335899	44	0.75	75	7.50	12	5.910655	78	0.25	55	7.50	16	2.749275
11	0.25	75	7.50	16	4.74389	45	1.00	65	7.50	16	2.841983	79	1.00	75	0.00	24	1.760786
12	0.75	45	15.00	24	2.215105	46	0.25	45	15.00	12	2.907322	80	0.75	65	20.00	20	2.301779
13	0.75	55	15.00	12	6.571353	47	0.25	75	7.50	12	4.637358	81	1.00	45	0.00	20	1.992811
14	0.75	45	0.00	24	1.893841	48	1.00	65	20.00	20	1.927277	82	0.25	75	15.00	20	1.817933
15	0.75	55	20.00	24	2.046455	49	0.50	45	20.00	16	3.335742	83	0.25	55	20.00	12	5.376767
16	0.25	55	20.00	24	1.717784	50	0.50	45	20.00	12	4.274262	84	0.50	75	0.00	24	1.829757
17	0.25	55	7.50	12	4.573649	51	1.00	55	0.00	12	5.564811	85	0.75	45	7.50	20	2.098062
18	0.50	65	7.50	12	4.941246	52	0.25	65	20.00	20	1.823534	86	0.25	65	7.50	20	2.441648
19	1.00	65	0.00	16	4.495858	53	1.00	75	7.50	12	5.347293	87	0.25	55	20.00	20	1.818367
20	1.00	75	20.00	24	3.81494	54	0.75	45	20.00	16	3.36197	88	1.00	75	15.00	12	5.869363
21	0.75	75	20.00	20	2.536386	55	0.25	65	15.00	20	2.293724	89	1.00	45	7.50	12	5.093166
22	0.50	65	7.50	16	3.89548	56	0.50	45	15.00	24	1.915528	90	0.50	55	0.00	12	4.421969
23	0.25	55	15.00	24	2.026366	57	0.75	65	15.00	16	3.835503	91	0.25	65	15.00	24	1.694731
24	0.75	65	15.00	24	2.77717	58	0.50	55	15.00	16	3.84092	92	0.75	45	0.00	20	1.828104
25	0.75	65	0.00	20	2.226924	59	0.50	45	0.00	16	2.391484	93	0.25	55	15.00	12	6.00656
26	0.25	45	20.00	16	3.049778	60	0.25	75	20.00	16	2.867569	94	0.50	75	20.00	16	3.384286
27	0.25	65	7.50	16	2.231602	61	0.50	45	15.00	20	2.483192	95	0.50	65	15.00	20	2.112747
28	0.25	75	15.00	16	3.087011	62	0.75	45	20.00	12	5.533825	96	1.00	45	15.00	12	5.910631
29	0.50	45	15.00	16	2.979299	63	0.75	65	7.50	24	1.692499	97	0.50	55	7.50	16	4.085024
30	0.50	75	7.50	20	2.542231	64	0.25	65	0.00	16	2.847572	98	0.50	55	7.50	24	2.952835
31	1.00	55	7.50	12	6.011191	65	1.00	75	0.00	12	5.692103	99	1.00	45	20.00	24	2.421552
32	1.00	45	20.00	16	3.733145	66	1.00	55	0.00	24	2.228958	100	0.50	65	0.00	20	1.794046
33	0.50	65	20.00	16	3.333395	67	0.75	55	15.00	24	1.928154	101	1.00	45	15.00	24	1.841269
34	0.25	55	0.00	16	2.565884	68	0.75	55	20.00	20	2.302583	102	0.75	75	7.50	24	1.813207

New operators are added, and some are neglected in genetic programming study. New building block consists of basic *Constant, Input Variable, Addition, Subtraction, Multiplication* and *Division* operators; trigonometric *Sine, Cosine* and *Tangent* operators, squashing *Gaussian Function* which is a bell-shaped squashing function. returns e^{-x^2}, *Hyperbolic Tangent* and *Error Function* operators, history *Weighted Moving Average* (returns the arithmetically weighted average value of the last num_rows values of the x variable) and *Modified Moving Average* (returns the modified average value of the last num_rows values of the x variable) operators. New estimation models are generated by using this block. Results are given in Table 5.12.

$$wma = \frac{m\theta_n + (m-1)\theta_{n-1} + ... + 2\theta_{n-(m+2)} + \theta_{(n-m+1)}}{n} \tag{5.14}$$

$$mma = mma_{m-1} + \frac{1}{n}(\theta_t - mma_{m-1}) \tag{5.15}$$

WMA and *MMA* are given in Equations (5.14-15), where *m* is the sequence number value, n is the total number of values, θ is the function value and θ_t is the current value.

Table 5.12 Improved estimation models with 2 outliers omitted.

Solution	R^2	CC	ME	MSE	MAE	# Coeff.	Complexity
(Clamp Loss) = 14.4849237291263 + 0.0129714769244243*A*B + 0.024835172561152*D^2 + 1.31079836962997*sin(0.452395618373651*C*B^3 *wma(A, 3))^2*wma(A, 3) - 1.14791940409032*D	0.87792072	0.93702931	1.6018783	0.21103337	0.34894358	7	63
(Clamp Loss) = 14.5031152036735 + 0.0129714769244243*A*B + 0.024835172561152*D^2 + 1.31843671079776*sin(0.452395618373651*C*B^3 *wma(A, 3))^2*wma(A, 3) - 1.14791940409032*D	0.87783826	0.93703387	1.6066639	0.21117592	0.34846005	7	60
(Clamp Loss) = 14.5515243214882 + 0.0136200507706455*A*B + 0.024835172561152*D^2 + sin(0.452395618373651*C*B^3*wma(A, 3))^2*wma(A, 3) - 1.14791940409032*D	0.8746401	0.93526387	1.6469819	0.21670445	0.35811819	6	58
(Clamp Loss) = 0.128380310290418 + 0.0131423430309544*A*B + 596.374556646578/D^2 + 1.32954505818352*sin(0.452395618373651*C*B^3 *wma(A, 3))^2*wma(A, 3)	0.87143127	0.93351489	1.574646	0.22225142	0.36637486	6	57
(Clamp Loss) = 13.7428773002727 + 0.0176376759066811*A*B + 0.022872369852119*D^2 + 0.784664869167064*sin(0.452395618373651*C*B^ 3*wma(A, 3))^2 - 1.07752576814462*D	0.87119258	0.93340233	1.4622911	0.22266403	0.36299919	7	55

Model, observed vs. predicted, outputs vs row and error/complexity pareto diagrams are given for 5 best *Clamp Loss* prediction models in Figure 5.27.

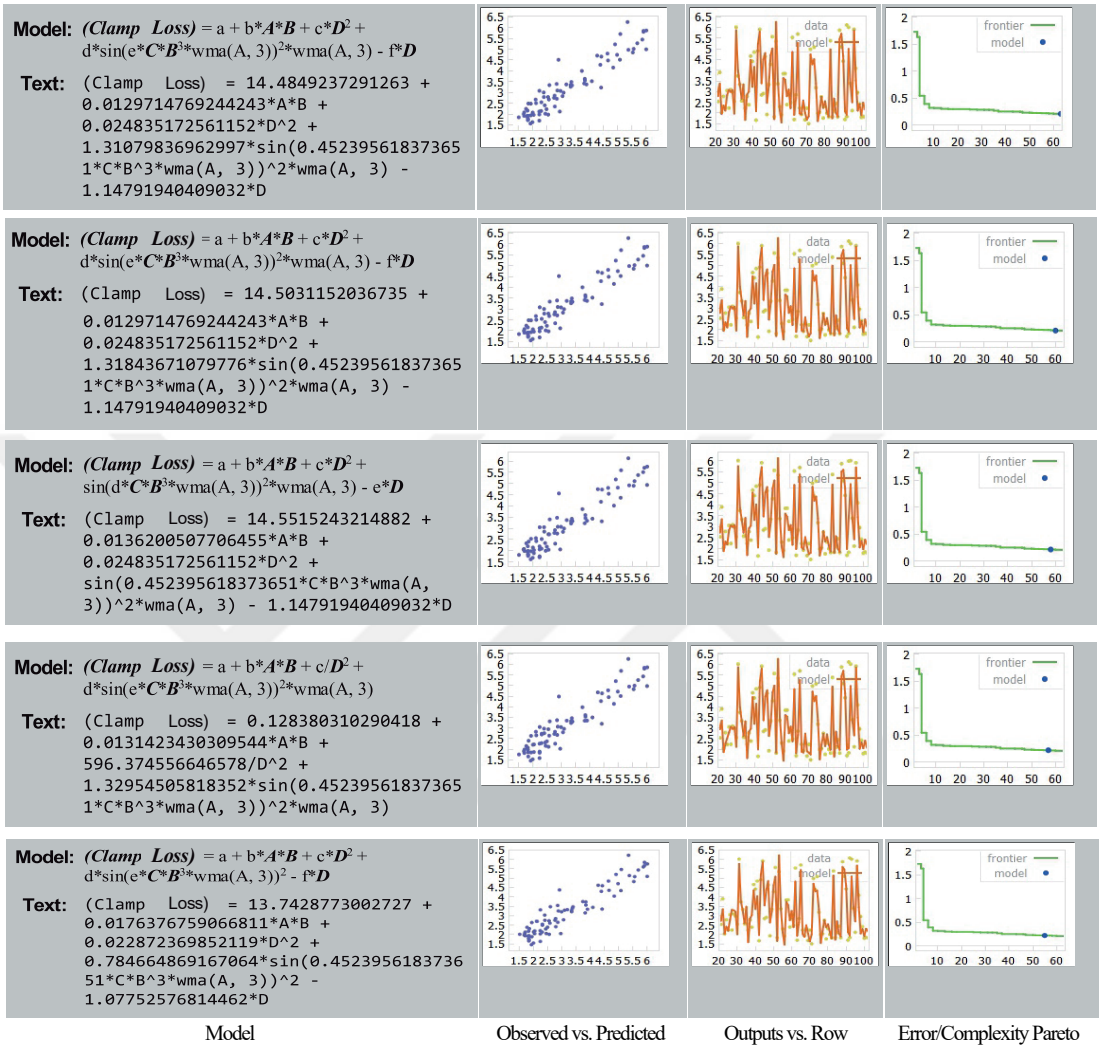


Figure 5.27 Improved and detailed estimation models for CL without outliers.

Sensitivity indicates effect of input and output variables on objective function result. Let us to say z is an objective function of $x,y,..$ as in the Equation 5.16:

$$z = f(x, y, ..) \tag{5.16}$$

Sensitivity can be expressed as the influence metrics of x on z are defined in Equation 5.17:

$$Sensitivity = \overline{\left|\frac{\partial z}{\partial_x}\right|} \cdot \frac{\sigma(x)}{\sigma(z)} \tag{5.17}$$

where $\frac{\partial_z}{\partial_x}$ is the partial derivative of z with respect to x, $\sigma(x)$is the standard deviation of x, in the input data, $\sigma(z)$ is the standard deviation of z, $|x|$ denotes the absolute value of x and $\bar{x}$ denotes the mean of x.

% Positive is the likelihood that increasing this variable will increase the target variable. If % Positive = 60 %, then 60 % of the time increases in this variable lead to increases in the target variable (but the remaining 40 % of the time it either decreases it or has no impact). If % Positive = 0 %, increases in this variable will not increase the target variable. The percent of data points where:

$$\frac{\partial_z}{\partial_x} < 0 \tag{5.18}$$

$$PositiveMagnitude = \left|\frac{\partial_z}{\partial_x}\right| \cdot \frac{\sigma(x)}{\sigma(z)} \rightarrow \frac{\partial_z}{\partial_x} > 0 \tag{5.19}$$

An increase in *Positive Magnitude* (Equation 5.19) leads to increases in the target variable, this is generally how big the positive impact is.

$$\frac{\partial_z}{\partial_x} > 0 \tag{5.20}$$

$$NegativeMagnitude = \left|\frac{\partial_z}{\partial_x}\right| \cdot \frac{\sigma(x)}{\sigma(z)} \rightarrow \frac{\partial_z}{\partial_x} < 0 \tag{5.21}$$

% Negative is the likelihood that increasing this variable will decrease the target variable. If % Negative = 70 %, then 70 % of the time increases in this variable lead to decreases in the target variable (but the remaining 30 % of the time it either increases it or has no impact). If % Negative = 0 %, increases in this variable will not decrease the target variable.

An increase in *Negative Magnitude* leads to decreases in the target variable, this is generally how big the negative impact is. Detailed report is given in Table 5.13.

Table 5.13 Sensitivity analysis report.

Variable Sensitivity

(Clamp Loss) = 14.48 + 0.01297*A*B + 0.02484*D² + 1.311*sin(0.4524*C*B³wma(A, 3))²wma(A, 3) - 1.148*D

Variable	Sensitivity	% Positive	Positive Magnitude	% Negative	Negative Magnitude
D	0.7288	0%	0	100%	0.7288
A	0.23761	100%	0.23761	0%	0
C	0.11173	33%	0.28303	67%	0.026079
B	0.056507	100%	0.056507	0%	0

(Clamp Loss) = 0.1284 + 0.01314*A*B + 596.4/D² + 1.33*sin(0.4524*C*B³wma(A, 3))²wma(A, 3)

Variable	Sensitivity	% Positive	Positive Magnitude	% Negative	Negative Magnitude
D	0.75858	0%	0	100%	0.75858
A	0.24586	100%	0.24586	0%	0
C	0.11569	33%	0.29305	67%	0.027002
B	0.058442	100%	0.058442	0%	0

(Clamp Loss) = 14.5 + 0.01297*A*B + 0.02484*D² + 1.318*sin(0.4524*C*B³wma(A, 3))²wma(A, 3) - 1.148*D

Variable	Sensitivity	% Positive	Positive Magnitude	% Negative	Negative Magnitude
D	0.72835	0%	0	100%	0.72835
A	0.23804	100%	0.23804	0%	0
C	0.11231	33%	0.28451	67%	0.026215
B	0.056472	100%	0.056472	0%	0

(Clamp Loss) = 13.74 + 0.01764*A*B + 0.02287*D² + 0.7847*sin(0.4524*C*B³wma(A, 3))² - 1.078*D

Variable	Sensitivity	% Positive	Positive Magnitude	% Negative	Negative Magnitude
D	0.74133	0%	0	100%	0.74133
A	0.20418	100%	0.20418	0%	0
C	0.11082	67%	0.14013	33%	0.052197
B	0.075454	100%	0.075454	0%	0

(Clamp Loss) = 14.55 + 0.01362*A*B + 0.02484*D² + sin(0.4524*C*B³wma(A, 3))²wma(A, 3) - 1.148*D

Variable	Sensitivity	% Positive	Positive Magnitude	% Negative	Negative Magnitude
D	0.7451	0%	0	100%	0.7451
A	0.22628	100%	0.22628	0%	0
C	0.087144	33%	0.22075	67%	0.020341
B	0.060617	100%	0.060617	0%	0

A detailed and fine-tuned genetic programming study is resulted with the best estimation model that is given Equation 5.22.

$$CL = 14.48 + 0.01297 \cdot A \cdot B + 0.02484 \cdot D^2 + 1.311 \cdot \sin\left(0.4524 \cdot C \cdot B^3 wma\left(A,3\right)\right)^2 \cdot wma\left(A,3\right) - 1.148 \cdot D \tag{5.22}$$

Best results have the most accurate R^2 value (0.8779207) in the whole study. *Correlation coefficient* is 0.9370293, *ME* is 1.601878, *MSE* value is 0.2110334, *MAE* is 0.34894358 with *complexity* value of 63. Comparison plot is given in Figure 5.28.

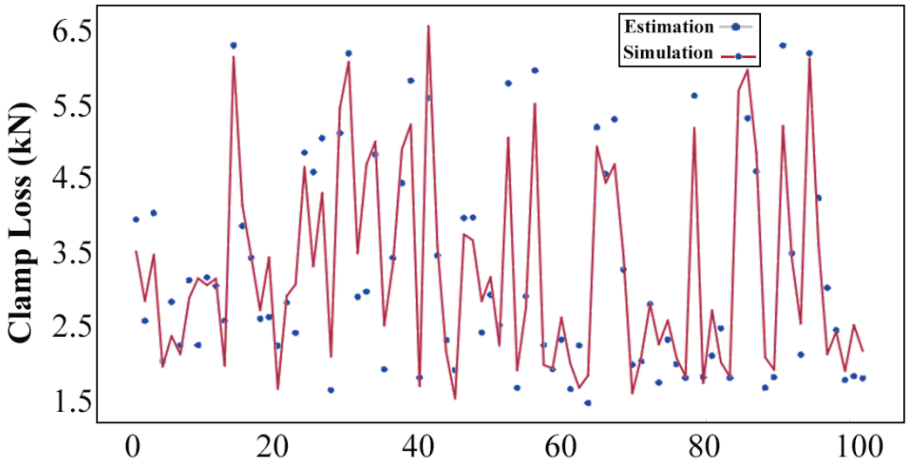


Figure 5.28 Simulation results vs estimation results.

Table 5.14 Simulation results and the estimated model results.

					RESULT							RESULT	
No	**A**	**B**	**C**	**D**	**Simulation**	**Estimated**	**No**	**A**	**B**	**C**	**D**	**Simulation**	**Estimated**
1	0.25	45	0.00	12	3.75995	nan	52	0.25	65	20.00	20	1.82353	1.69341
2	1.00	65	7.50	20	2.31712	nan	53	1.00	75	7.50	12	5.34729	6.24130
3	0.75	45	15.00	16	4.40418	3.87467	54	0.75	45	20.00	16	3.36197	3.46471
4	0.50	45	7.50	16	3.67324	2.83553	55	0.25	65	15.00	20	2.29372	2.11957
5	1.00	45	20.00	20	1.51768	2.17954	56	0.50	45	15.00	24	1.91553	1.53179
6	0.25	75	20.00	20	4.01751	1.81670	57	0.75	65	15.00	16	3.83550	3.61029
7	0.50	55	20.00	20	2.13657	2.29164	58	0.50	55	15.00	16	3.84092	3.53571
8	0.50	55	15.00	24	1.89537	2.19013	59	0.50	45	0.00	16	2.39148	2.76788
9	0.50	75	0.00	20	3.88657	1.94704	60	0.25	75	20.00	16	2.86757	3.07125
10	1.00	65	15.00	20	3.33590	3.02600	61	0.50	45	15.00	20	2.48319	2.20250
11	0.25	75	7.50	16	4.74389	3.18172	62	0.75	45	20.00	12	5.53383	4.83407
12	0.75	45	15.00	24	2.21510	2.48189	63	0.75	65	7.50	24	1.69250	1.88663
13	0.75	55	15.00	12	6.57135	5.45366	64	0.25	65	0.00	16	2.84757	2.68680
14	0.75	45	0.00	24	1.89384	1.67770	65	1.00	75	0.00	12	5.69210	5.25902
15	0.75	55	20.00	24	2.04645	1.77696	66	1.00	55	0.00	24	2.22896	1.95335
16	0.25	55	20.00	24	1.71778	1.89260	67	0.75	55	15.00	24	1.92815	1.91246
17	0.25	55	7.50	12	4.57365	4.57658	68	0.75	55	20.00	20	2.30258	2.55600
18	0.50	65	7.50	12	4.94125	5.07452	69	0.75	75	15.00	24	1.67951	1.97280
19	1.00	65	0.00	16	4.49586	3.31916	70	0.25	65	0.00	20	2.22847	1.67139
20	1.00	75	20.00	24	3.81494	3.38688	71	0.25	65	7.50	24	1.50200	1.82033
21	0.75	75	20.00	20	2.53639	2.76609	72	0.75	45	0.00	12	4.97780	4.72394
22	0.50	65	7.50	16	3.89548	3.35313	73	1.00	75	20.00	16	4.38621	4.25841
23	0.25	55	15.00	24	2.02637	1.93278	74	1.00	75	15.00	16	5.07829	4.49390
24	0.75	65	15.00	24	2.77717	2.32046	75	0.75	55	20.00	16	3.18252	3.35119
25	0.75	65	0.00	20	2.22692	2.09296	76	0.50	55	0.00	24	1.98505	1.59663
26	0.25	45	20.00	16	3.04978	2.80921	77	0.25	45	15.00	20	2.03144	2.05657
27	0.25	65	7.50	16	2.23160	3.05643	78	0.25	55	7.50	16	2.74927	2.73115
28	0.25	75	15.00	16	3.08701	2.97038	79	1.00	75	0.00	24	1.76079	2.21278
29	0.50	45	15.00	16	2.97930	3.05061	80	0.75	65	20.00	20	2.30178	2.52188
30	0.50	75	7.50	20	2.54223	1.94995	81	1.00	45	0.00	20	1.99281	2.04432
31	1.00	55	7.50	12	6.01119	5.85019	82	0.25	75	15.00	20	1.81793	1.81636
32	1.00	45	20.00	16	3.73314	3.97464	83	0.25	55	20.00	12	5.37677	4.95582
33	0.50	65	20.00	16	3.33339	3.32651	84	0.50	75	0.00	24	1.82976	1.72635
34	0.25	55	0.00	16	2.56588	2.65438	85	0.75	45	7.50	20	2.09806	2.64685
35	0.75	75	20.00	16	2.58427	3.31854	86	0.25	65	7.50	20	2.44165	1.99246
36	0.50	45	7.50	24	2.22599	1.65273	87	0.25	55	20.00	20	1.81837	1.81096
37	0.50	55	0.00	16	2.76918	2.83273	88	1.00	75	15.00	12	5.86936	5.43086
38	0.50	65	15.00	16	2.38464	2.97925	89	1.00	45	7.50	12	5.09317	5.68653
39	0.25	55	0.00	12	4.65741	4.46451	90	0.50	55	0.00	12	4.42197	4.64287
40	0.75	75	0.00	16	4.41334	3.20566	91	0.25	65	15.00	24	1.69473	2.04864
41	1.00	55	7.50	16	4.84128	4.13088	92	0.75	45	0.00	20	1.82810	1.89839
42	0.50	65	20.00	24	1.66324	2.06043	93	0.25	55	15.00	12	6.00656	4.97902
43	0.50	65	15.00	12	4.90547	5.20964	94	0.50	75	20.00	16	3.38429	3.30825
44	0.75	75	7.50	12	5.91066	5.78956	95	0.50	65	15.00	20	2.11275	2.48011
45	1.00	65	7.50	16	2.84198	3.37257	96	1.00	45	15.00	12	5.91063	5.83074
46	0.25	45	15.00	12	2.90732	4.49543	97	0.50	55	7.50	16	4.08502	3.49933
47	0.25	75	7.50	12	4.63736	4.78220	98	0.50	55	7.50	24	2.95283	2.08751
48	1.00	65	20.00	20	1.92728	2.45615	99	1.00	45	20.00	24	2.42155	2.37454
49	0.50	45	20.00	16	3.33574	3.24314	100	0.50	65	0.00	20	1.79405	1.88218
50	0.50	45	20.00	12	4.27426	4.68814	101	1.00	45	15.00	24	1.84127	2.45732
51	1.00	55	0.00	12	5.56481	4.99959	102	0.75	75	7.50	24	1.81321	2.13144

Estimation model is evaluated by using *A, B, C, D* and *clamp loss* is calculated. Then, estimation results are compared with simulation results that is given in Table 5.14. Reasonable results are achieved with the best model in the Equation 5.22.

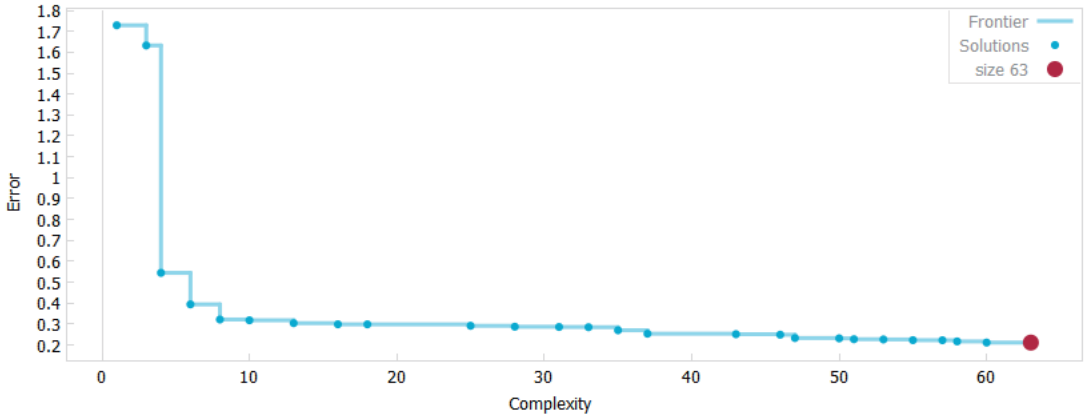


Figure 5.29 Eureqa®: Accuracy-complexity for predicting modelling of Clamp Loss

Error value is minimized and best estimation model is acquired in 63 iterations by using Eureqa® software. Accuracy vs Complexity plot is given in Figure 5.29.

CHAPTER SIX
CONCLUSION

In this thesis, industry's one of the most disturbing problem, anti-loosening of fasteners under transverse vibrations, is modeled, simulated and estimated by using *FEA* and *genetic programming* method. Some of the results can be concluded to shine a light to the researchers in the field:

- *Preload* or the *Clamp Load* is the crucial parameter to decrease loosening rate in the assembly. *Loosening rate* decreases when *Preload* is increased.

- *Under-head (bearing) and thread friction coefficients, clamp length, stiffness of the joint members, relative transverse displacement* are also important where they affect the *loosening rate.* Simply, increasing *bearing fiction* results in a decrease in *clamping load* for a certain torque value. Hence, if designers would decide to increase *friction coefficient*, they have to consider increasing tightening torque to achieve *clamping force* or *preload*.

- *Loosening rate* can be decreased by modifying seating surface of contact elements. One can change the adjacent thread surface, nut seating surface or the bolt under-head surface. Likely, designers should consider adding a *special washer* into the assembly to overcome *clamp loss* problem, nevertheless, adding an additional component brings up some other problems such as wear, fatigue or functional incongruities.

- Adding a pattern under the head of the bolt should be an effective way to eliminate *clamp loss* providing that it must be a simple and cost efficient design.

- FEA modelling method is able to simulate loosening phenomenon of the bolted joints under transverse loading conditions. FEA method can reveal the pressure distribution between contact layers and it can map asymmetrical displacement of each nodal element between contact layers.

- Partial slip at bearing surface and thread surface can be separately investigated, similarly, complete and stick-slip conditions can be clearly understood with FEA method.

- When experimental and simulation model results are merged, vibration analysis can be carried out under computational environment. However, it should take too much CPU time.

- Although yet certain that FEA method is capable of revealing hidden mysteries in the field, it is not feasible to do an optimization study with tremendous number of simulations. It is because each of simulations take 45 to 75 minutes to complete on a contemporary desktop workstation PC.

- It is more feasible to build and educate a code by using *genetic programming* method or to use a software package which is already made it before.

In this study, *genetic programming*-based *(GP-based) symbolic regression (SR)* is used for estimating *loosening rate*. A highly accurate model is generated with this method. Ten output criteria which they are obtained via simulation results, are used in the *estimation model* generation stage. Only the *Clamp Loss* function has been provided a meaningful result representing *loosening rate* properly from the rest of the output criteria. Significant parameters in the process are also detected with this *GP-based SR* method. Through the *estimation model* stated in this study, loosening behavior of under-head forms, having various geometries which consist of different parameter combinations, can be computed in shorter CPU times than the conventional finite elements simulation model. Thus, thousands of different under-head geometries could be analyzed faster than ever; then, results could be extracted easily. *GP-based SR* method is applied thru Eureqa® software. This method has not been used for estimating the loosening behavior of fasteners operating under transverse vibrational conditions, before. This thesis serves as a basis with this regard.

REFERENCES

Abrahart, R. J., & See, L.M. (Eds.) (2014). *Geocomputation*. CRC Press: Boca Raton.

Aryadoust, V. (2015). Application of evolutionary algorithm-based symbolic regression to language assessment: Toward nonlinear modeling. *Psychological Test and Assessment Modeling, 57*(3), 301.

Bhattacharya, A., Sen, A., & Das, S. (2010). An investigation on the anti-loosening characteristics of threaded fasteners under vibratory conditions. *Mechanism and Machine Theory, 45*(8), 1215-1225.

Blume, D. (1969). Wann müssen Schrauben gesichert werden? *Verbindungstechnik*(1), 6.

Blume, D., & Illgner, K. (1988). Schrauben Vademecum. Neuss: Bauer & Schaurte Karcher.

Bojarczuka, C. C., Lopesa, H. S., Freitasb, A. A., & Michalkiewiczc, E. L. (2004). A constrained-syntax genetic programming system for discovering classification rules: application to medical data sets. *Artificial Intelligence in Medicine, 30*, 27-48.

Bommisetty, K., & Narayanan, K. (2014). Three-dimensional finite element analysis of bolted joint with helical thread connection. *Proceedings of the ASME 2014 Gas Turbine India Conference*.

Cevik, A., Arslan, M. H., & Köroğlu, M. A. (2010). Genetic-programming-based modeling of RC beam torsional strength. *KSCE Journal of Civil Engineering, 14*(3), 371-384.

Chipperfield, A. (1997). Introduction to genetic algorithms. In A. M. S. Zalzala, & P. J. Fleming (Eds.). *Genetic Algorithms in engineering systems, London: The Institution of Electrical Engineers*, 1-41.

Cramer, N. L. (1985). A representation for the adaptive generation of simple sequential programs. *Paper presented at the Proceedings of the First International Conference on Genetic Algorithms.*

Deb, K. (1996). Genetic algorithms for function optimization, in Genetic Algorithms and Soft Computing. *Eds. Herrera, F. & Verdegay, J L., Physica – Verlag, Heidelberg.*, 3-19.

Dinger, G. (2015). Design of multi-bolted joints to prevent self-loosening failure. *Proceedings of the Institution of Mechanical Engineers, Part C: Journal of Mechanical Engineering Science, 230*(15), 2564-2578.

Dinger, G., & Friedrich, C. (2011). Avoiding self-loosening failure of bolted joints with numerical assessment of local contact state. *Engineering Failure Analysis, 18*(8), 2188-2200.

Fernando, S., Hons, & Masi, M. (2005), Mechanisms and prevention of vibration loosening in bolted joints. *Australian Journal of Mechanical Engineering, 2,* (2) 73-92

Ferreira, C. (2002). Analyzing the founder effect in simulated evolutionary processes using gene expression programming. *Soft Computing Systems: Design, Management And Applications, IOS Pres, Netherlands*, 153-163.

Finkelston, R. J. (1972). How much shake can bolted joints take. *Machine Design, 44*, 122-125.

Fogel, D. B., & Corne, D. W. (1998). An introduction to evolutionary computation for biologists. *In D. B. Fogel (Ed.), Evolutionary computation: The Fossil Record, Piscataway.* New Jersey*: IEEE Press.,* 19-38.

Friede, R., & Lange, J. (2009). Self loosening of prestressed bolts. *Paper presented at the Nordic Steel Construction Conference NSCC2009,* Malmö.

Friede, R., & Lange, J. (2010). Loss of preload in bolted connections due to embedding and self loosening. *SDSS'Rio 2010 Stability and Ductility of Steel Structures*.

Fujioka, Y. (2008). Behavior and mechanisms of bolt self-loosening under transverse load due to vibrations of a washer along an arc. *Proceedings of IMECE2008 ASME International Mechanical Engineering Congress and Exposition, IMECE2008-66830*.

Ganeshmurthy, S., & Nassar, S. A. (2014). Finite element simulation of process control for bolt tightening in joints with nonparallel contact. *Journal of Manufacturing Science and Engineering, 136*(2), 021018-021018.

Ghugare, S. B., & Tambe, S. S. (2016) Genetic programming based high performing correlations for prediction of higher heating value of coals of different ranks and from diverse geographies. *Journal of the Energy Institute*, 1-9.

Gong, H., Liu, J., & Ding, X. (2016). Calculation of the effective bearing contact radius for precision tightening of bolted joints. *Advances in Mechanical Engineering, 8*(9).

Goodier, J. N., & Sweeney, R. J. (1945). Loosening by vibrations of threaded fastening. *Mechanical Engineering, 67*(12), 798-802.

Gruau, F. (1992). Cellular encoding of genetic neural networks. *Technical Report, 92*(21).

Guggolz, D., Manoharan, S. K., & Friedrich, C. (2015). Avoiding of self-loosening in components with multiple screw joints. *Proceedings of the ASME 2015 International Mechanical Engineering Congress and Exposition*.

Gwiazda, T. D. (2006). *Genetic algorithms reference Vol.1, Crossover for single-objective numerical optimization problems* (Vol. 1): Tomasz Gwiazda, Poland: Lomianki.

Hattori, T., Yamashita, M., Mizuno, H., & Naruse, T. (2010). Loosening and Sliding Behaviour of Bolt-Nut Fastener under Transverse Loading. *EPJ Web of Conferences, 6*, 08002.

Hess, D. P., Keifer, O. P., & Moody, C. B. (2014). Tests on loosening of aviation threaded fasteners with different washer configurations. *Journal of Failure Analysis and Prevention, 14*(5), 683-689.

Hess, D. P., & Pai, N. G. (July 8-11, 2002). Vibration induced fastener failure from localized slip. *Proceedings of the 9th International Conference on Sound and Vibration, Orlando, FL*.

Housari, B. A., & Nassar, S. A. (2007). Effect of thread and bearing friction coefficients on the vibration-induced loosening of threaded fasteners. *Journal of Vibration and Acoustics, 129*(4), 484.

Izumi, S., Yokoyama, T., Iwasaki, A., & Sakai, S. (2005). Three-dimensional finite element analysis of tightening and loosening mechanism of threaded fastener. *Engineering Failure Analysis, 12*(4), 604-615.

Izumi, S., Yokoyama, T., Kimura, M., & Sakai, S. (2009). Loosening-resistance evaluation of double-nut tightening method and spring washer by three-dimensional finite element analysis. *Engineering Failure Analysis, 16*(5), 1510-1519.

Jeong, J. H., Lee, H.-K., Park, K., & Kim, J.-B. (2015). An investigation into the anti-releasing performance of a serrated bolt. *Journal of Mechanical Science and Technology, 29*(12), 5127-5132.

Jung, S.-P., Park, T.-W., Yoon, J.-W., Jun, K.-J., & Chung, W.-S. (2009). Design optimization of spring of a locking nut using design of experiments. *International Journal of Precision Engineering and Manufacturing, 10*(4), 77-83.

Kacprzyk, J., & Pedrycz, W. (2015). *Springer handbook of computational intelligence*. Dordrecht: Springer.

Kasei, S. (2007). A study of self-loosening of bolted joints due to repetition of small amount of slippage at bearing surface. *Journal of Advanced Mechanical Design, Systems, and Manufacturing*.

Kelly, S. G. (2012). *Mechanical vibrations : theory and applications*. Stamford: Cengage Learning.

Koza, J. R. (1990). Genetic programming: A paradigm for genetically breeding populations of computer programs to solve problems. *Technical Report STAN-CS-90-1314. Stanford University, Stanford, CA.*

Kumar, R. (2013). Causes and prevention of loosening in prestressed bolts. *Mechanica Confab, 2,* (4) 11-16

Marshall, M. B., Zainal, I., & Lewis, R. (2011). Influence of the interfacial pressure distribution on loosening of bolted joints. *Strain, 47*, 65-78.

Mayer, M. H., & Gaul, L. (2007). Segment-to-segment contact elements for modelling joint interfaces in finite element analysis. *Mechanical Systems and Signal Processing, 21*(2), 724-734.

McRee, R. K. (2010). Symbolic regression using nearest neighbor indexing. *Paper Presented at the Proceedings of the 12th Annual Conference Companion on Genetic and Evolutionary Computation.*

Milfelner, M., Kopac, J., Cus, F., & Zuperl, U. (2005). Genetic equation for the cutting force in ball-end milling. *Journal of Materials Processing Technology, 164*, 1554-1560.

Montgomery, D. C. (2013). *Statistical quality control: a modern introduction*: Hoboken, New Jersey: *Wiley.*

Nassar, S. A., & Housari, B. A. (2006). Effect of thread pitch and initial tension on the self-loosening of threaded fasteners. *Journal of Pressure Vessel Technology, 128*(4), 590.

Nassar, S. A., & Yang, X. (2009). A mathematical model for vibration-induced loosening of preloaded threaded fasteners. *Journal of Vibration and Acoustics, 131*(2), 021009.

Nastran, M., & Balic, J. (2002). Prediction of metal wire behavior using genetic programming. *Journal of Materials Processing Technology, 122*(2), 368-373.

Ouyang, H., Oldfield, M. J., & Mottershead, J. E. (2006). Experimental and theoretical studies of a bolted joint excited by a torsional dynamic load. *International Journal of Mechanical Sciences, 48*(12), 1447-1455.

Pai, N. G., & Hess, D. P. (2002a). Experimental study of loosening of threaded fasteners due to dynamic shear loads. *Journal of Sound and Vibration, 253*(3), 585-602.

Pai, N. G., & Hess, D. P. (2002b). Three-dimensional finite element analysis of threaded fastener loosening due to dynamic shear load. *Engineering Failure Analysis, 9*(4), 383-402.

Patel, T. M., & Bhatt, N. M. (2016). Development of a Mathematical Model of VMS for Automotive Structural Member using FEA-RSM Hybrid Modeling. *Procedia Technology, 23*, 98-105.

Reiff, J. D. (2005). A Procedure for Calculation of Torque Specifications for Bolted Joints with Prevailing Torque. *Journal of ASTM International*.

Sakai, T. (2011). Mechanism for a Bolt and Nut Self Loosening under Repeated Bolt Axial Tensile Load. *Journal of Solid Mechanics and Materials Engineering Failure Analysis*.

Sanclemente, J. A., & Hess, D. P. (2007). Parametric study of threaded fastener loosening due to cyclic transverse loads. *Engineering Failure Analysis, 14*(1), 239-249.

Schmidt, M., & Lipson, H. (2007). Comparison of tree and graph encodings as function of problem complexity. *Paper Presented at the Proceedings of the 9th Annual Conference on Genetic and Evolutionary Computation.*

Schmidt, M. D., & Lipson, H. (2008). Coevolution of fitness predictors. *IEEE Transactions on Evolutionary Computation, 12*(6), 736-749.

Schmidt, M. D., Vallabhajosyula, R. R., Jenkins, J. W., Hood, J. E., Soni, A. S., Wikswo, J. P., & Lipson, H. (2011). Automated refinement and inference of analytical models for metabolic networks. *Physical Biology, 8*, 1478–3975.

Shoji, Y., & Sawa, T. (2011). Self-loosening of Nuts due to External Load. *SIMULIA Customer Conference*.

Takac, A. (2002). Cellular genetic programming algorithm applied to classification task. *Institute of Informatics, Faculty of Mathematics, Physics and Informatics Comenius University, Brastislava, Slovakia*.

Telcioğlu, M. B. (2002). *Montaj hattı dengeleme problemlerinin genetik algoritma teknigi kullanılarak çözülmesi ve bilgisayar programı uygulaması pegasus yazılımı.* Yüksek Lisans Tezi, Erciyes Üniversitesi, Erciyes.

Telcioğlu, M. B. (2007). *Veri madenciliğinde genetik programlama temelli yeni bir sınıflandırma yaklaşımı ve uygulaması.*Yüksek Lisans Tezi, Erciyes Üniversitesi, Erciyes.

Teller, A., & Veloso, M. (1996). *PADO: A new learning architecture for object recognition.* Oxford University Pres, 81-116.

Wang, W., Wang, Q., Zheng, S., Liu, X., & Liu, H. (2014). Research on self-loosening mechanism of bolted joints under transversal vibration. *Proceedings of the ASME 2014 International Mechanical Engineering Congress and Exposition*.

Wu, Z., & Nassar, S. A. (2014). Effect of underhead design configuration on bolt behavior under shear loads. *Proceedings of the ASME 2015 Pressure Vessels and Piping Conference*.

Yang, X., & Nassar, S. (2010). Vibration-induced loosening performance of preloaded threaded fasteners. *Proceedings of the ASME 2010 Pressure Vessels & Piping Division / K-PVP Conference*.

Yokoyama, T. (2008). Loosening resistance evaluation of double-nut tightening method, spring washers, and conical spring washers; finite element study. *Proceedings of PVP2008 ASME Pressure Vessels and Piping Division Conference*.

Yokoyama, T., Izumii, S., & Sakai, S. (2009). Analytical modeling of the transverse load-displacement relation of a bolted joint with consideration of the mechanical behavior on contact surfaces. *Proceedings of the ASME 2009 Pressure Vessels and Piping Division Conference*.

Yokoyama, T., Olsson, M., Izumi, S., & Sakai, S. (2012). Investigation into the self-loosening behavior of bolted joint subjected to rotational loading. *Engineering Failure Analysis, 23*, 35-43.

Zhang, L., Goh, C. C., & Kunnan, A. J. (2014). Analysis of test takers' metacognitive and cognitive strategy use and EFL reading test performance: A multi-sample SEM approach. *Language Assessment Quarterly, 11*(1), 76-102.

Zhu, L., Hong, J., & Jiang, X. (2016). On controlling preload and estimating anti-loosening performance in threaded fasteners based on accurate contact modeling. *Tribology International, 95*, 181-191.

APPENDICES

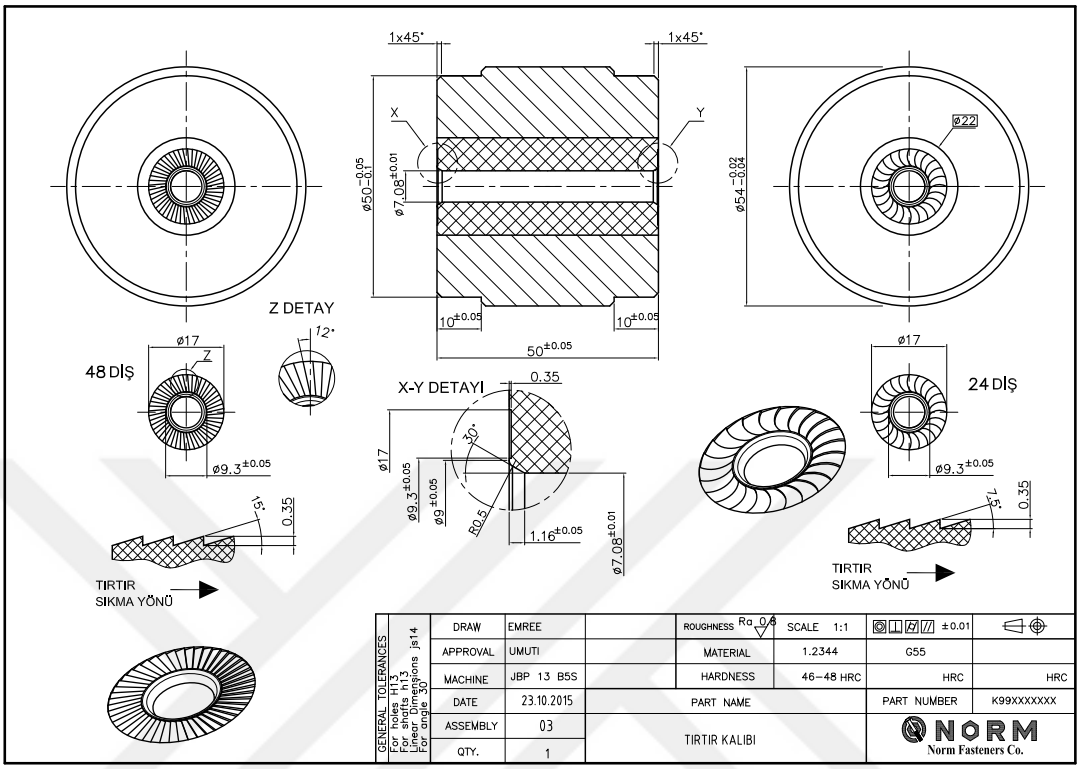


Figure A.1 Form 01 & Form 02.

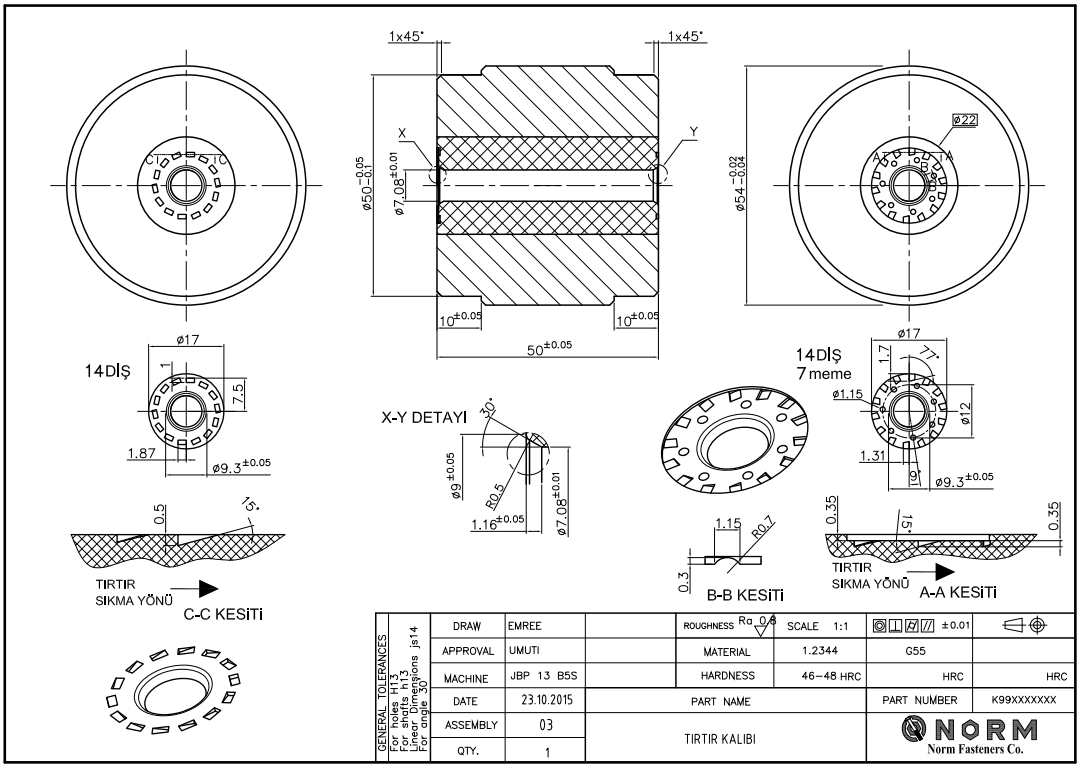


Figure A.2 Form 03 & Form 04

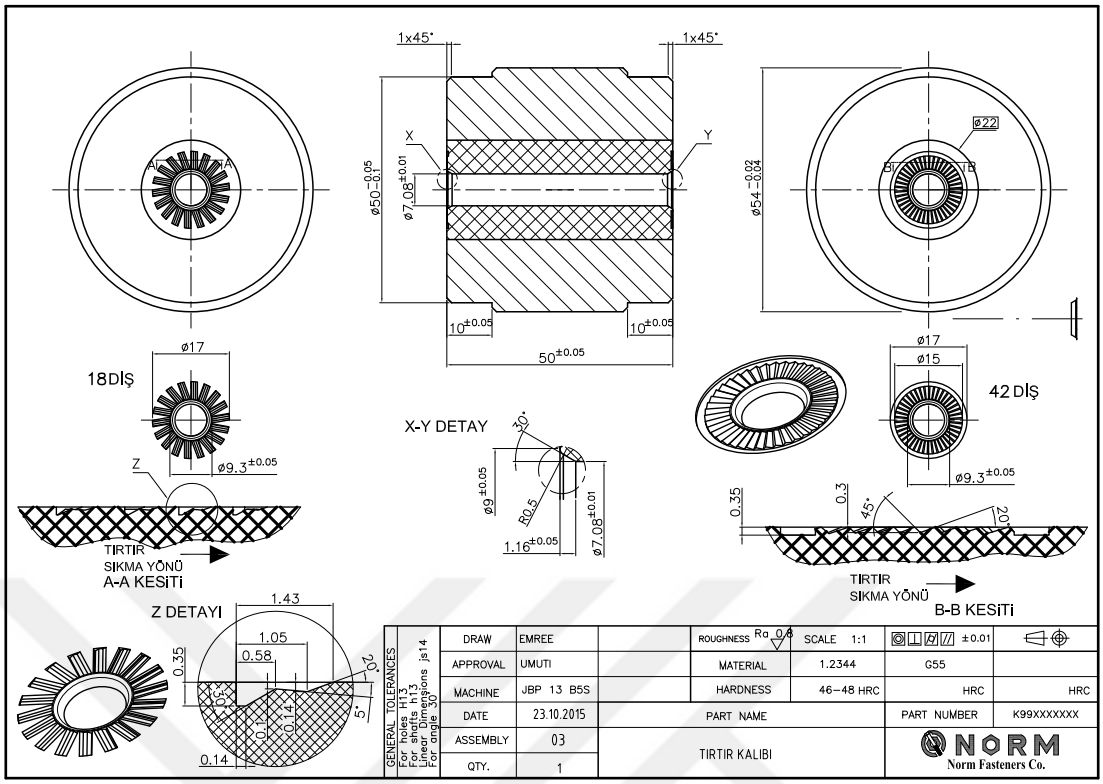


Figure A.3 Form 05 & Form 06

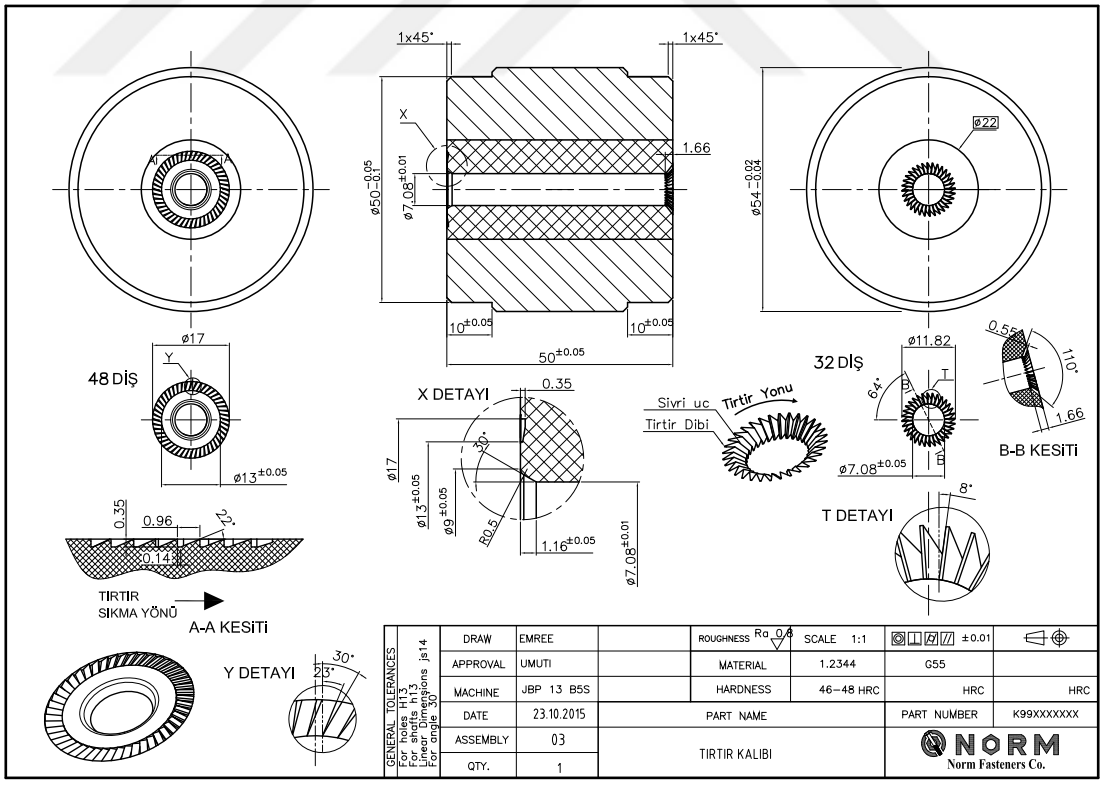


Figure A.4 Form 07 & Form 08

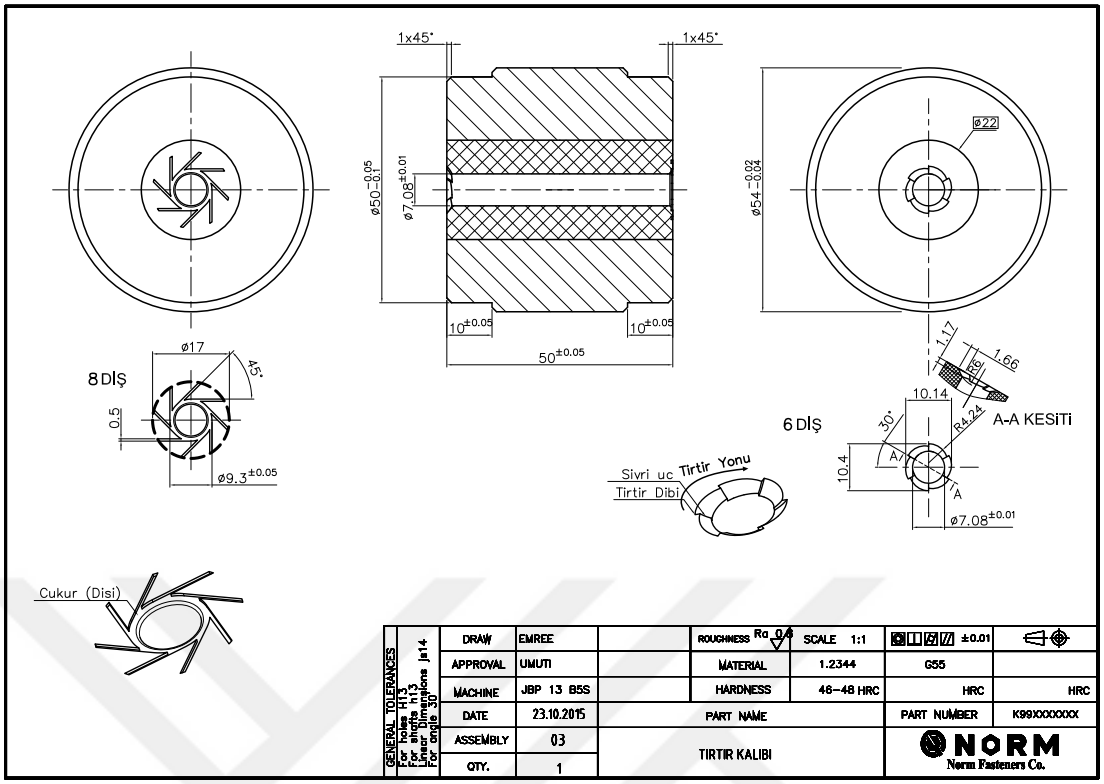


Figure A.5 Form 09 & Form 10

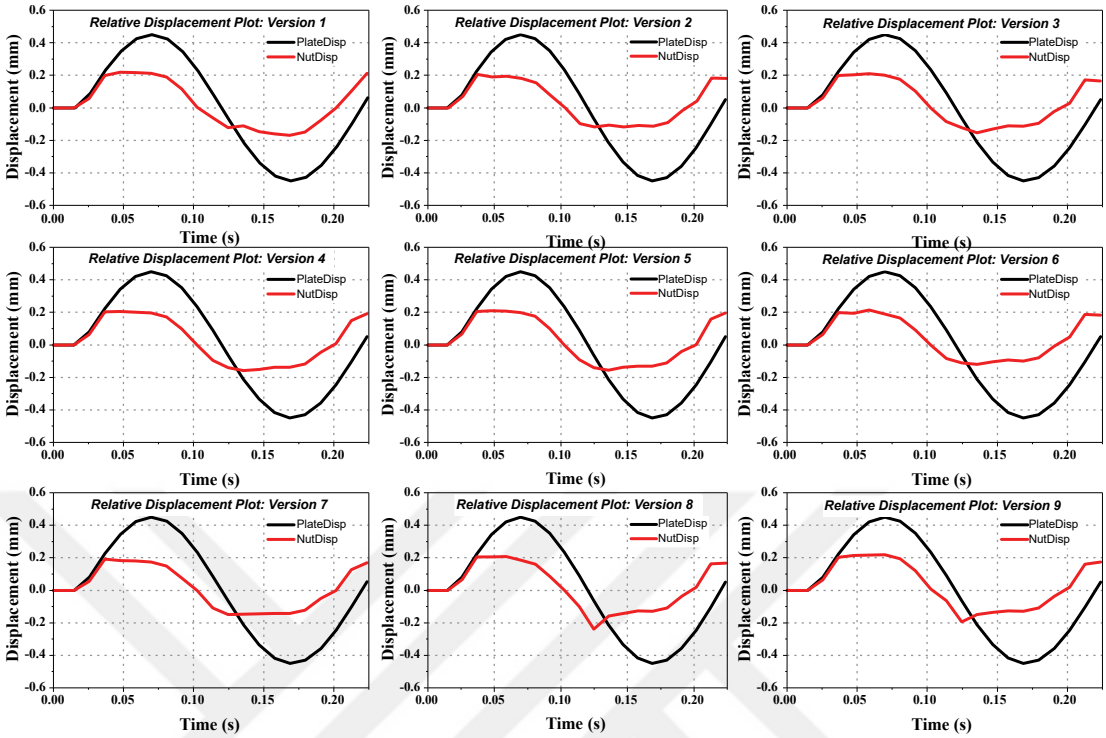


Figure A.6 Relative displacement vs Time plots ver.1-9

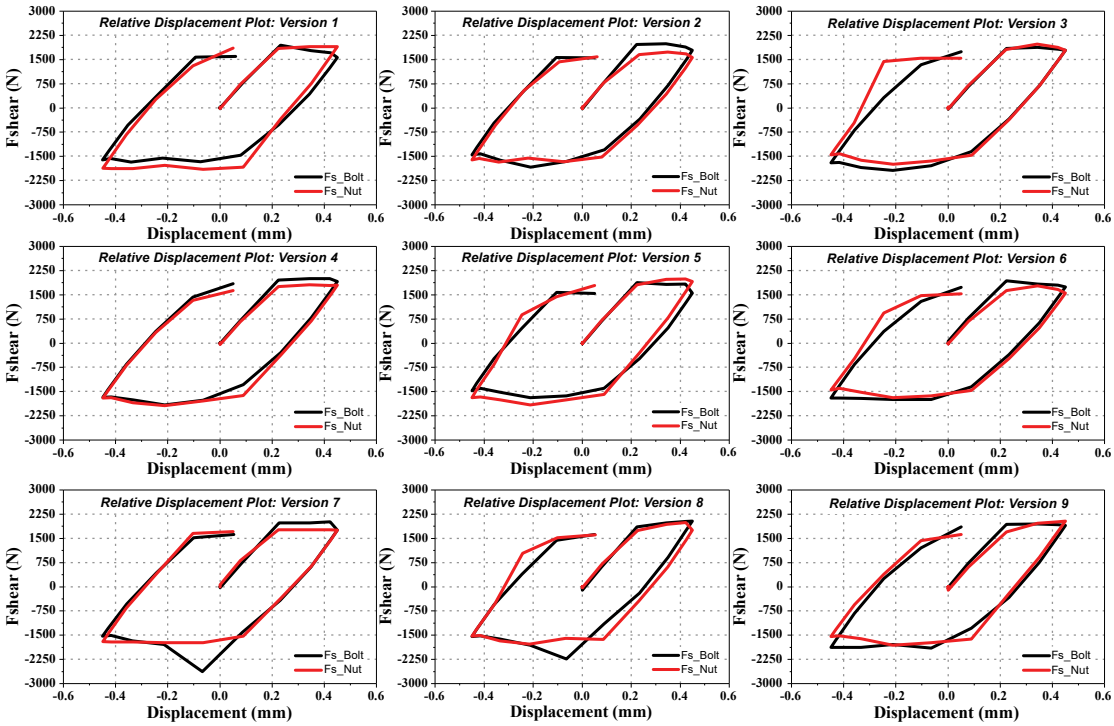


Figure A.7 Fshear vs Relative displacement plots ver.1-9

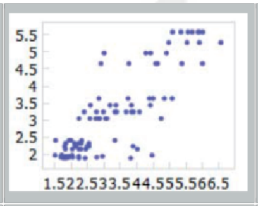
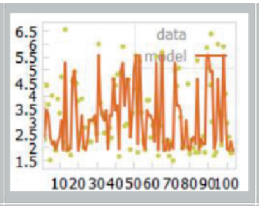
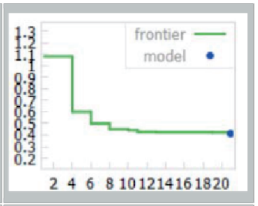
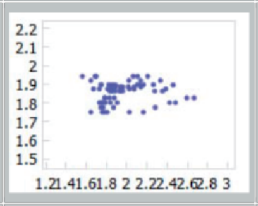
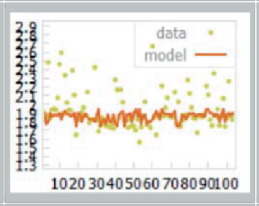
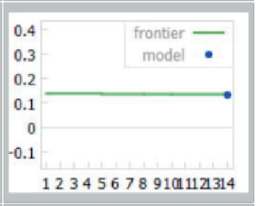
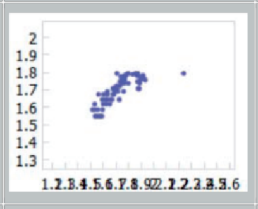
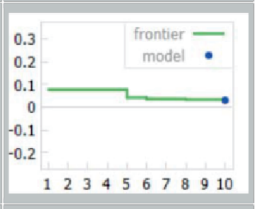
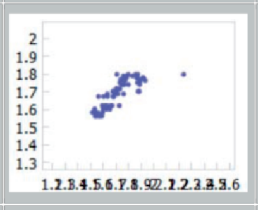
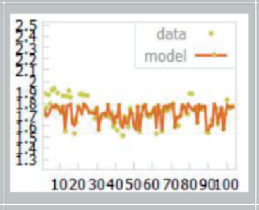
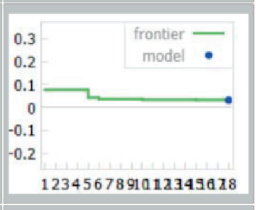
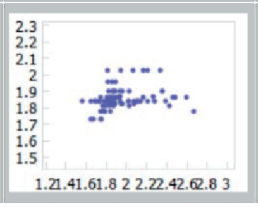
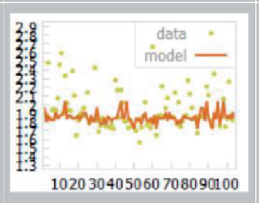
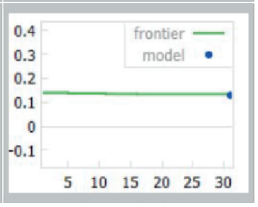
Model	Observed vs. Predicted	Outputs vs. Row	Error/Complexity Pareto
Model: $CL = a + b*A + c*D^2 - d*D - e*A*D$ **Text:** `CL = 13.1144548753172 + 2.57156972739084*A + 0.0223030048889321*D^2 0.9983011903294*D- 0.111687838749917*A*D`			
Model: $FSBH = a + \cos(D)*\text{atan}(b*A)$ **Text:** `FSBH = 1.85254486558692 + cos(D)*atan(0.107438415792173*A)`			
Model: $FSNS = a + -b/(D - c*A)$ **Text:** `FSNS = 1.93349847878302 +-3.20991978682081/(D- 3.63449517715026*A)`			
Model: $FSMI = a + b*D + -c*A/D - d*D^2$ **Text:** `FSMI = 1.1629783894278 + 0.0528868339891198*D +0.926701055686821*A/D- 0.00108220512298542*D^2`			
Model: $FSMA = a + b*D*C^2 - c*C^3 - d*\tan(e*D*C^2)$ **Text:** `FSMA = 1.84132278172034 + 3.136653592735735*D*C^2 - 3.13665359273573e5*C^3 - 0.0156312465683464*tan(0.00991801639548852*D*C^2)`			

Figure A.8 Estimation models according to the Table 5.5

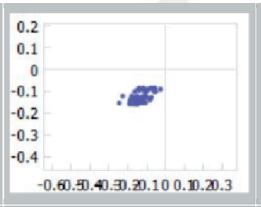
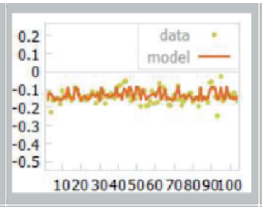
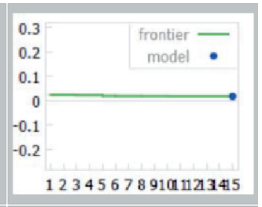
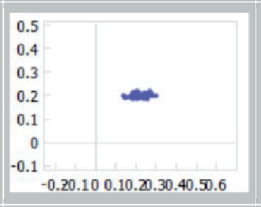
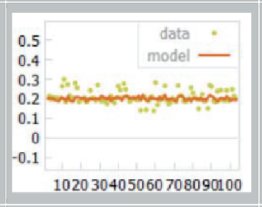
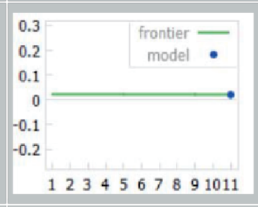
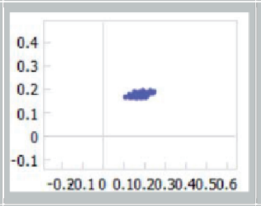
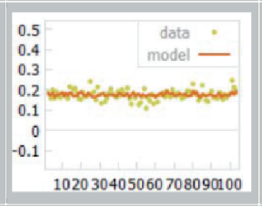
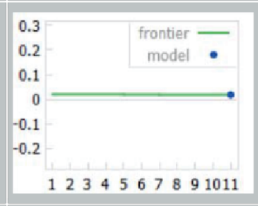
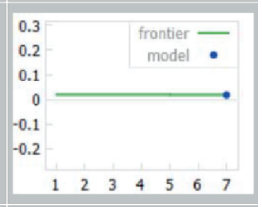
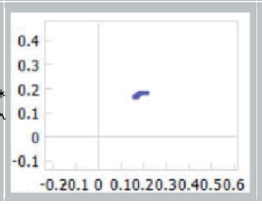
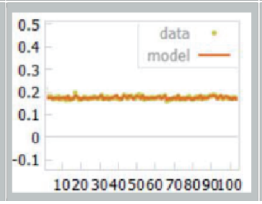
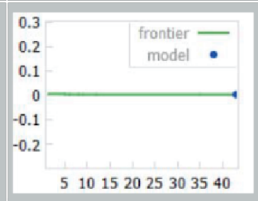
Model	Observed vs. Predicted	Outputs vs. Row	Error/Complexity Pareto
Model: $RSDLH = a + b*D^2 - c*B - d*D$ **Text:** RSDLH= 0.161255950008727 + 0.00056958312541710 3*D^20.000551164805971398*B - 0.025303140187375*D			
Model: $RSDRH = a + b*A*B - c*D$ **Text:** RSDLH = 0.217155133349173 + 0.000248865955790457*A*B0.00141964074658196*D			
Model: $RMAS = a + b*A*D - c*C$ **Text:** RMAS = 0.163268737570535 + 0.00130740215691619*A*D0.000203149947100449*C			
Model: $RMAS_M = a + b*A*D$ **Text:** RMAS_M = 0.161562130840227 + 0.00129667472476335*A*D			
Model: $DZ_P = a + b*D^2 + c*A*C*D - d*D - e*D^3 - f*A*C^2 - g*D*A^2$ **Text:** DZ_P = 0.40025561536118 + 0.0019652657906894*D^2 + 2.42697538327258e-5*A*C* - 0.0366274855397272*D - 3.49284543619726e-5*D^3 - 2.77227322561448e-5*A*C^ - 0.000148033686839244*D*A^2			

Figure A.9 Estimation models according to the Table 5.5